Supplementary Information

A biocatalytic platform for synthesis of chiral α-trifluoromethylated organoborons

Xiongyi Huang,[†§] Marc Garcia-Borràs,[†‡] Kun Miao,[§] S. B. Jennifer Kan,[§] Arjun Zutshi,[§] K. N. Houk,*[‡] and Frances H. Arnold*[§]

[§]Division of Chemistry and Chemical Engineering, California Institute of Technology, Pasadena, CA 91125

[‡]Department of Chemistry and Biochemistry, University of California, Los Angeles, CA 90095

[†] = These authors contributed equally to this work.

This PDF includes:

I. Materials and Methods

Unless otherwise noted, all chemicals and reagents were obtained from commercial suppliers (Sigma-Aldrich, VWR, Alfa Aesar, Acros, etc.) and used without further purification. Bovine serum albumin (BSA) was purchased from Sigma-Aldrich. Silica gel chromatography was carried out using AMD Silica Gel 60, 230-400 mesh. ^{1}H and ^{13}C NMR spectra were recorded on a Bruker Prodigy 400 MHz instrument (400 MHz for ^{1}H and 100 MHz for ^{13}C NMR) or a Varian 400 MHz Spectrometer (400 MHz for ^{1}H NMR), or a Varian 500 MHz Spectrometer (500 MHz for ^{1}H and 126 MHz for ^{13}C NMR). Chemical shifts (δ) are reported in ppm downfield from tetramethylsilane, using the solvent resonance as the internal standard (^{1}H NMR: $\delta = 7.26$, ^{13}C NMR: $\delta = 77.36$ for $CDCl_3$). ^{19}F NMR and ^{11}B NMR data were collected on a VARIAN 300 MHz spectrometer (101 MHz for ^{19}F NMR), a Bruker Prodigy 400 MHz instrument (128 MHz for ^{11}B NMR), or a Varian 400 MHz Spectrometer (376 MHz for ^{19}F NMR). Sonication was performed using a Qsonica Q500 sonicator. High-resolution mass spectra were obtained at the California Institute of Technology Mass Spectral Facility. Gas chromatography-mass spectrometry (GC-MS) analyses were carried out using Shimadzu GCMS-QP2010SE system and J&W HP-5ms column. Analytical chiral supercritical fluid chromatography (SFC) was performed with a JACSO 2000 series instrument using *i*-PrOH and supercritical CO_2 as the mobile phase. Chiral normal-phase HPLC analyses were performed using an Agilent 1200 series instrument with *i*-PrOH and hexanes as the mobile phase. Chiral GC was performed on an Agilent 6850 GC with FID detector using a Chirasil-DEX CB column (30.0 m × 0.25 mm) at 1.0 mL/min He carrier gas flow.

Plasmid pET22b(+) was used as a cloning vector, and cloning was performed using Gibson assembly [1]. The cytochrome *c* maturation plasmid pEC86 [2] was used as part of a two-plasmid system to express prokaryotic cytochrome *c* proteins. Cells were grown using Luria-Bertani medium or HyperBroth (AthenaES) with 100 μg/mL ampicillin and 20 μg/mL chloramphenicol ($LB_{amp/chlor}$ or $HB_{amp/chlor}$). Cells without the pEC86 plasmid were grown with 100 μg/mL ampicillin (LB_{amp} or HB_{amp}). Primer sequences are available upon request. T5 exonuclease, Phusion polymerase, and *Taq* ligase were purchased from New England Biolabs (NEB, Ipswich, MA). M9-N minimal medium (abbreviated as M9-N buffer; pH 7.4) was used as a buffering system for whole cells, lysates, and purified proteins, unless otherwise specified. M9-N buffer was used without a carbon source; it contains 47.7 mM Na_2HPO_4, 22.0 mM KH_2PO_4, 8.6 mM NaCl, 2.0 mM $MgSO_4$, and 0.1 mM $CaCl_2$.

II. General Procedures

2.1 Plasmid construction. All variants described in this paper were cloned and expressed using the pET22b(+) vector (Novagen). The gene encoding *Rma* cyt *c* (UNIPROT ID B3FQS5) was obtained as a single gBlock (IDT), codon-optimized for *E. coli*, and cloned using Gibson assembly [1] into pET22b(+) (Novagen) between restriction sites *Nde*I and *Xho*I in frame with an *N*-terminal pelB leader sequence (to ensure periplasmic localization and proper maturation; MKYLLPTAAAGLLLLAAQPAMA) and a *C*-terminal 6xHis-tag. This plasmid was co-transformed with the cytochrome *c* maturation plasmid pEC86 into *E. cloni*® EXPRESS BL21(DE3) cells (Lucigen).

2.2 Cytochrome *c* (cyt *c*) expression and the preparation of suspensions of *E. coli* cells expressing cyt *c*. 100 mL $HB_{amp/chlor}$ in a 500 mL flask was inoculated with an overnight culture (2 mL, $LB_{amp/chlor}$) of recombinant *E. cloni*® EXPRESS BL21(DE3) cells containing a pET22b(+) plasmid encoding the cytochrome *c* variant, and the pEC86 plasmid. The culture was shaken at 37 °C and 230 rpm (no humidity control) until the OD_{600} was 0.7 (approximately 3 hours). The culture was placed on ice for 30 minutes, and isopropyl β-*D*-1-thiogalactopyranoside (IPTG) and 5-aminolevulinic acid (ALA) were added to final concentrations of 20 μM and 200 μM, respectively. The incubator temperature was reduced to 21 °C, and the culture was allowed to shake for 20 hours at 160 rpm. Cells were harvested by centrifugation (4 °C, 15 min, 4,000xg), and the cell pellet was resuspended in M9-N buffer (OD_{600} = 20). The concentrations of cytochrome *c* in suspensions of *E. coli* cells are determined using the procedures described in section 2.4.

2.3 Cytochrome P450 and globin expression and the preparation of suspensions of *E. coli* cells expressing these proteins. Purified P450s and globins were prepared differently from the cytochrome *c* proteins, and described as follows. 100 mL HB_{amp} in a 500 mL flask was inoculated with an overnight culture (2 mL, LB_{amp}) of recombinant *E. cloni*® EXPRESS BL21(DE3) cells containing a pET22b(+) plasmid encoding the P450 or globin variant. The culture was shaken at 37 °C and 200 rpm (no humidity control) until the OD_{600} was 0.7 (approximately 3 hours). The culture was placed on ice for 30 minutes, and IPTG and 5-ALA were added to final concentrations of 0.5 mM and 1 mM, respectively. The incubator temperature was reduced to 21 °C, and the culture was allowed to shake for 20 hours at 160 rpm. Cells were harvested by centrifugation (4 °C, 15 min, 4,000xg), and the cell pellet was resuspended in M9-N buffer (OD_{600} = 20). The concentrations of cytochrome P450 and globins in suspensions of *E. coli* cells are determined using the procedures described in section 2.4.

2.4 Cell lysate preparation and protein concentration determination. Cell lysates were prepared as follow: The suspensions of *E. coli* cells containing expressed heme proteins obtained in section 2.2 or 2.3 were lysed by sonication (1 minute, 1 second on, 1 second off, 40% duty cycle; Qsonica Q500 sonicator). BugBuster 10X protein extraction reagent (EMD Millipore) was then added to each cell suspension. After 30 min incubation on ice, the solution was aliquoted into 2 mL microcentrifuge tubes and the cell debris was removed by centrifugation for 10 min (14,000xg, 4 °C). The supernatant was sterile filtered through a 0.45 μm cellulose acetate filter to obtain the cell lysate solution. The concentration of heme protein in cell lysate solution was determined by the hemochrome assay [3]. Briefly,

500 μL of the cell lysate was added to a cuvette. 500 μL of solution I (0.2 M NaOH, 40% (v/v) pyridine, 500 μM potassium ferricyanide) was added and the spectrum of this oxidized sample was taken from 350-680 nm. Sodium dithionite (10 μL of 0.5 M solution in 0.5 M NaOH) was added and the reduced spectrum was taken from 350-680 nm. The pyridine hemochromagen concentration was determined using its Q bands, with the following extinction coefficients: P450s and globins: 34.7 mM^{-1} cm^{-1} at 557 nm; cytochromes *c*: 30.27 mM^{-1} cm^{-1} at 550 nm.

2.5 Library construction. Cytochrome *c* site-saturation mutagenesis libraries were generated using a modified version of the 22-codon site-saturation method [4]. For each site-saturation library, oligonucleotides were ordered such that the coding strand contained the degenerate codon NDT, VHG or TGG. The reverse complements of these primers were also ordered. The three forward primers were mixed together in a 12:9:1 ratio, (NDT:VHG:TGG) and the three reverse primers were mixed similarly. Two PCRs were performed, pairing the mixture of forward primers with a pET22b(+) internal reverse primer, and the mixture of reverse primers with a pET22b(+) internal forward primer. The two PCR products were gel purified, ligated together using Gibson assembly[1], and transformed into *E. cloni*® EXPRESS BL21(DE3) cells. Primer sequences are available upon request.

2.6 Library screening in whole cells. Single colonies were picked with toothpicks off of $LB_{amp/chlor}$ agar plates, and grown in deep-well (2 mL) 96-well plates containing $LB_{amp/chlor}$ (400 μL) at 37 °C, 250 rpm shaking, and 80% relative humidity overnight. After 16 hours, 30 μL aliquots of these overnight cultures were transferred to deep-well 96-well plates containing $HB_{amp/chlor}$ (1 mL) using a 12-channel EDP3-Plus 5-50 μL pipette (Rainin). Glycerol stocks of the libraries were prepared by mixing cells in $LB_{amp/chlor}$ (100 μL) with 50% v/v glycerol (100 μL). Glycerol stocks were stored at −78 °C in 96-well microplates. Growth plates were allowed to shake for 3 hours at 37 °C, 250 rpm shaking, and 80% relative humidity. The plates were then placed on ice for 30 min. Cultures were induced by adding 10 μL of a solution, prepared in sterile deionized water, containing 2 mM isopropyl β-*D*-1-thiogalactopyranoside (IPTG) and 20 mM ALA. The incubator temperature was reduced to 20 °C, and the induced cultures were allowed to shake for 20 hours (250 rpm, no humidity control). Cells were pelleted (4,000xg, 5 min, 4 °C), resuspended in 380 μL M9-N buffer, and the plates containing the cell suspensions were transferred to an anaerobic chamber. To deep-well plates of cell suspensions were added NHC-borane substrate (10 μL per well, 400 mM in MeCN) and diazo reagent (10 μL per well, 400 mM in MeCN). The plates were sealed with aluminum sealing tape and shaken in the anaerobic chamber at 680 rpm. After 36 h, the plates were removed from the anaerobic chamber. After quenching with hexanes/ethylacetate (4:6 v/v, 0.6 mL). The plates were then sealed with sealing mats and shaken vigorously to thoroughly mix the organic and aqueous layers. The plates were centrifuged (4,000xg, 5 min) and the organic layer (200 μL) was transferred to autosampler vials with vial inserts for chiral HPLC. Variants with improved activity and enantioselectivity obtained from library screening were confirmed by small-scale biocatalytic reactions, as described in section 2.7.

2.7 Small-scale whole cell bioconversion. In an anaerobic chamber, NHC-borane (10 μL, 400 mM in MeCN) and diazo reagent (7.5 μL, 400 mM in MeCN) were added to *E. coli*

harboring *Rma* cyt *c* variant (380 μL, OD_{600} = 20) in a 2 mL crimp vial. The vial was crimp-sealed and shaken in the anaerobic chamber at 680 rpm at room temperature for 36 h. At the end of the reaction, the crimp vial was removed from the anaerobic chamber and was quenched with hexanes/ethylacetate (4:6 v/v, 0.6 mL), followed by the addition of internal standard (20 μL of 20 mM 1,2,3-trimethoxybenzene in toluene). The reaction mixture was transferred to a microcentrifuge tube, vortexed (10 seconds, 3 times), then centrifuged (14,000xg, 5 min) to completely separate the organic and aqueous layers (the vortex-centrifugation step was repeated if complete phase separation was not achieved). The organic layer (200 μL) was removed for GC-MS and chiral SFC/HPLC analysis. All biocatalytic reactions reported were performed in replicates (duplicates to quadruplicates) from at least two biological replicates. The total turnover numbers (TTNs) reported are calculated with respect to *Rma* cyt *c* expressed in *E. coli* and represent the total number of turnovers obtained from the catalyst under the stated reaction conditions.

Table S1. Preliminary experiments with heme and heme proteins

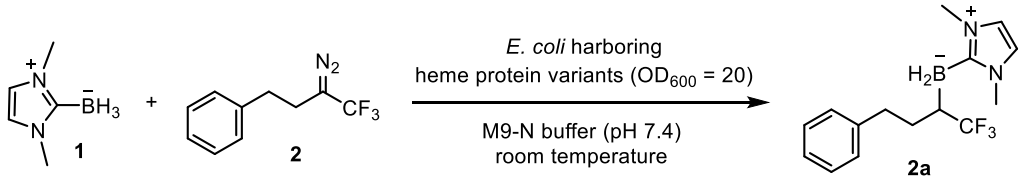

Catalyst	TTN of 2a	ee of 2a
Controls		
None	NR	N/A
Hemin	11 ± 2	0
hemin + BSA	5 ± 2	4%
E. coli cell background	trace	n.d.
Heme protein variants		
R. marinus cyt *c* BOR^{P2}[5]	27 ± 2	10%
R. marinus cyt *c* BOR^{G1}[5]	60 ± 10	33%
R. marinus cyt *c* BOR^{R1}[5]	90 ± 30	60%
Rhodothermus marinus nitric oxide dioxygenase (RmaNOD)	NR	N/A
Myoglobin	NR	N/A
P411 CHA[6]	NR	N/A
BM3 wild-type	NR	N/A

N/A – not applicable; NR – no product was detected; n.d. – not determined.

Experiments with hemin were performed using 100 μM hemin, 10 mM NHC-borane **1**, 10 mM diazo substrate **2**, 10 mM $Na_2S_2O_4$. Experiments with hemin and BSA were performed using 100 μM hemin in the presence of BSA (0.75 mg/mL) instead. Experiments to determine *E. coli* cell background reaction was performed with *E. cloni*® EXPRESS BL21(DE3) cells containing a pET22b(+) plasmid encoding halohydrin dehalogenase (HHDH) from *Agrobacterium tumefaciens* (UNIPROT ID Q93D82) instead of *Rma* cyt *c*. *A.* tumefaciens HHDH is inactive towards NHC-borane **1** and diazo **2**. Experiments were performed using *E. coli* harboring the corresponding protein (OD_{600} = 20) according to the protocol described in Section II. Reactions were performed in triplicate. TTNs reported are the average of three experiments. Within instrument detection limit, variability in e.e. was not observed.

Scheme S1. *Rma* cyt *c* variants for enantioselective synthesis of α-CF_3 organoborons **13a** with NHC borane **1** and diazo compound **13**. Reactions were performed in M9-N (pH 7.4) suspensions of *E. coli* cells expressing *Rma* cyt *c* variants (OD_{600} = 20). Standard reaction conditions were 10 mM borane substrate **1**, 7.5 mM diazo substrate **2**, room temperature under anaerobic conditions. Total turnovers (TTN) were defined as the amount of α-CF_3 organoboron product divided by the total amount of expressed *Rma* cyt *c* protein as determined by the hemochrome assay. wt refers to wild-type *Rma* cyt *c*. Single-letter abbreviations for the amino acid residues: V, Val; S, Ser; M, Met; L, Leu; D, Asp; A, Ala; Y, Tyr; I, Ile.

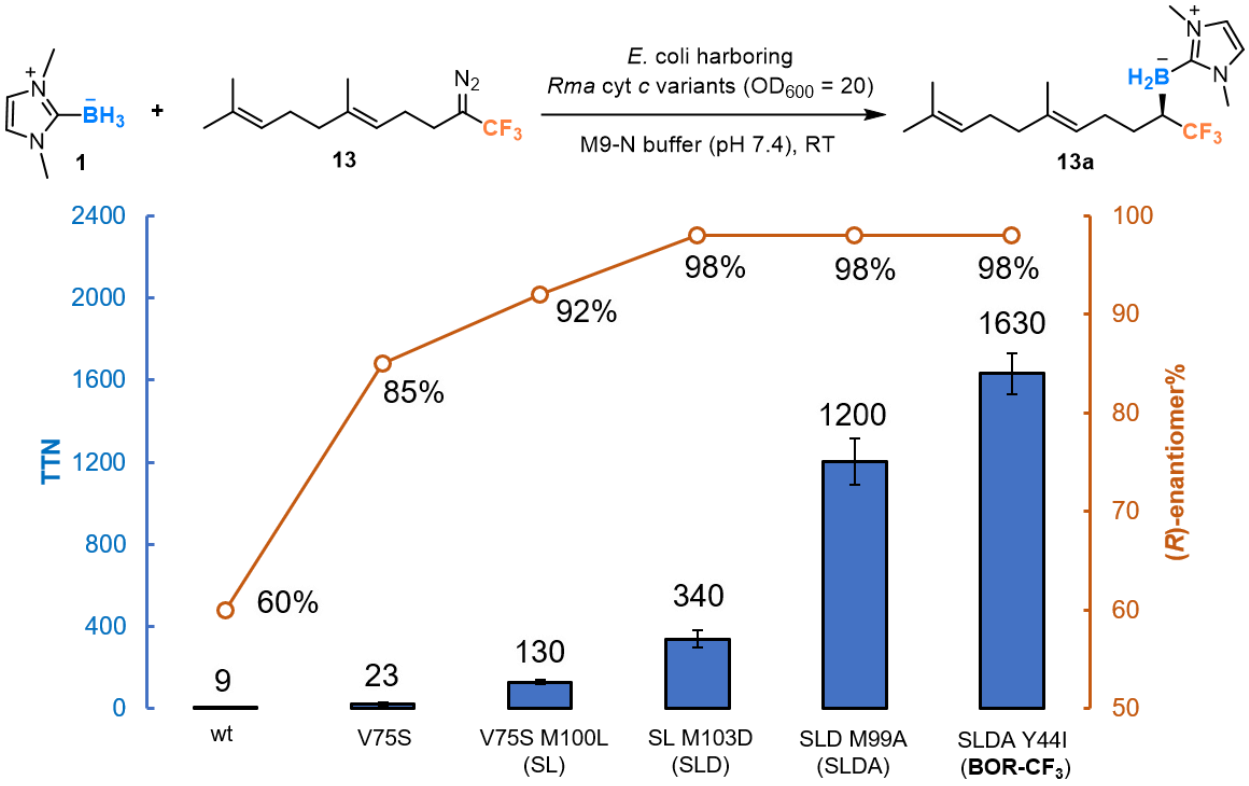

III. Trifluorodiazo Alkane Synthesis and Characterization

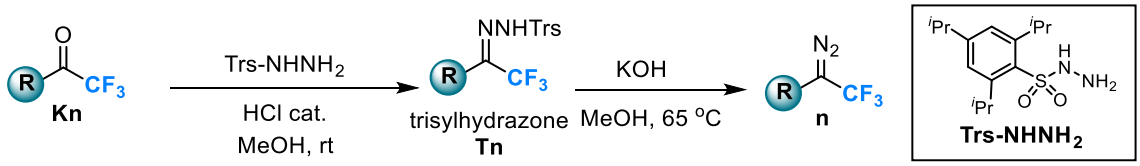

(1)

2,4,6-triisopropylbenzenesulfonylhydrazide (trisylhydrazide, Trs-$NHNH_2$) was synthesized as previously reported [7]. Ketone precursors (**K2-K12**) of diazo compounds **2-12** were synthesized from corresponding alkyl bromides following the procedure reported in ref [8], while the ketone precursor **K13** of diazo compound **13** was synthesized from geranyl bromide following the procedure in ref [9]. Trifluoroalkyl diazo compound **n** was synthesized from the corresponding trifluoromethyl ketones **Kn** and trisylhydrazide via eq. 1 with a procedure modified from ref [7]. In a typical experiment, the trifluoromethyl ketone substrate **Kn** (10 mmol) was dissolved in 10 mL methanol in a 50 mL round bottom flask followed by addition of trisylhydrazide powder (3.6 g, 12 mmol). The flask was then purged with Ar for 15 min. 200 µL of concentrated hydrochloric acid was added to the reaction solution via syringe and the reaction was allowed to stir at room temperature for 8 – 12 hours. The reaction progress was monitored by TLC and ^{19}F NMR. All trifluoromethyl ketone substrates (**Kn**) studied in this work have ^{19}F NMR resonances around -81 ppm, while the trisylhydrazone products (**Tn**) have ^{19}F NMR resonances around -70 ppm. After the majority (generally > 80%) of the trifluoromethyl ketone substrate **Kn** was converted to the trisylhydrazone **Tn** as indicated by ^{19}F NMR, KOH pellets (1.68 g, 30 mmol) were added to the reaction mixture and the flask was heated at 65 °C for 1.5 hours. The resulting reaction mixture was cooled to room temperature and diluted with 50 mL water. The solution was then extracted with 20 mL pentane for three times. The combined extract was washed two times with saturated $NaHCO_3$ solution and dried over anhydrous Na_2SO_4. After removing the solvent under reduced pressure, the resulting orange crude product was quickly purified via flash chromatography (pure pentane) on neutralized silica gel. The obtained diazo compounds were generally over 90% pure as indicated by ^{19}F and ^{1}H NMR. The main impurity was an unidentified species with ^{19}F NMR resonance around -71 ppm. The presence of this impurity in the diazo compounds will not affect the activity and enantioselectivity of our enzymatic reaction. For all trifluoroalkyl diazo compounds synthesized in this work, the ^{13}C NMR resonances that correspond to the diazo carbon were not observed, which is consistent with previous reports [10].

CAUTION: Diazo compounds are toxic and potentially explosive and should be handled with care in a well-ventilated fumehood.

(3-diazo-4,4,4-trifluorobutyl)benzene (2)

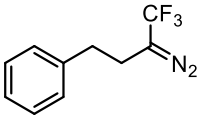

^{1}H NMR (500 MHz, $CDCl_3$) δ 7.41 – 7.32 (m, 2H), 7.30 – 7.14 (m, 3H), 2.87 (t, *J* = 7.6 Hz, 2H), 2.55 (t, *J* = 7.6 Hz, 2H); ^{13}C NMR (101 MHz, $CDCl_3$) δ 139.52, 128.72, 128.48, 126.68, 33.94, 24.03. The ^{13}C resonance corresponds to the CF_3 group was not well resolved; ^{19}F NMR (282 MHz, $CDCl_3$) δ -58.63 (s); MS (ESI) *m/z* $[M + H]^+$ calcd for $C_{10}H_{10}N_2F_3$: 215.0796, found: 215.0809.

1-chloro-4-(3-diazo-4,4,4-trifluorobutyl)benzene (3)

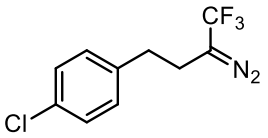

^{1}H NMR (500 MHz, $CDCl_3$) δ 7.33 – 7.29 (m, 2H), 7.16 (d, *J* = 8.2 Hz, 2H), 2.83 (t, *J* = 7.5 Hz, 2H), 2.64 – 2.44 (m, 2H); ^{13}C NMR (101 MHz, $CDCl_3$) δ 137.9, 132.5, 129.8, 128.9, 33.3, 24.0. The ^{13}C resonance corresponds to the CF_3 group was not well resolved; ^{19}F NMR (376 MHz, $CDCl_3$) δ -58.6 (s); MS (FAB) *m/z* $[M + H]^+$ calcd for $C_{10}H_9N_2F_3Cl$: 249.0406, found: 249.0397.

1-(3-diazo-4,4,4-trifluorobutyl)-3-methoxybenzene (4)

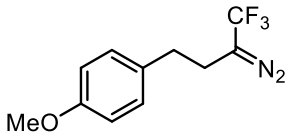

^{1}H NMR (400 MHz, $CDCl_3$) δ 7.15 – 7.09 (m, 2H), 6.87 – 6.83 (m, 2H), 3.80 (s, 3H), 2.78 (t, *J* = 7.6 Hz, 2H), 2.48 (t, *J* = 7.6 Hz, 2H); ^{13}C NMR (101 MHz, $CDCl_3$) δ 158.4, 131.6, 129.4, 127.1 (q, *J* = 267.9 Hz) 114.1, 55.3, 33.0, 24.2; ^{19}F NMR (282 MHz, $CDCl_3$) δ -58.6 (s); MS (FAB) *m/z* $[M + H]^+$ calcd for $C_{11}H_{12}ON_2F_3$: 245.0902, found: 245.0904.

4-(3-diazo-4,4,4-trifluorobutyl)-1,2-dimethoxybenzene (5)

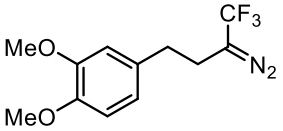

^{1}H NMR (400 MHz, $CDCl_3$) δ 6.75 (d, *J* = 8.1 Hz, 1H), 6.71 – 6.63 (m, 2H), 3.81 (s, 3H), 3.80 (s, 3H), 2.72 (t, *J* = 7.5 Hz, 2H), 2.43 (t, *J* = 7.6 Hz, 2H); ^{13}C NMR (101 MHz, $CDCl_3$) δ 149.0, 147.8, 132.1, 127.1 (q, *J* = 268.0 Hz), 120.4, 111.6, 111.4, 55.9, 55.9, 33.5, 24.2; ^{19}F NMR (282 MHz, $CDCl_3$) δ -58.8 (s); MS (ESI) *m/z* $[M + Na]^+$ calcd for $C_{12}H_{13}N_2O_2F_3Na$: 297.0827, found: 297.0810.

6-(3-diazo-4,4,4-trifluorobutyl)-2,3-dihydrobenzofuran (6)

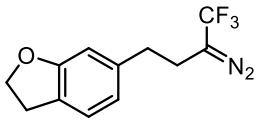

^{1}H NMR (400 MHz, $CDCl_3$) δ 7.08 – 7.03 (m, 1H), 6.98 – 6.92 (m, 1H), 6.75 (d, *J* = 8.1 Hz, 1H), 4.59 (t, *J* = 8.7 Hz, 2H), 3.21 (t, *J* = 8.7 Hz, 2H), 2.79 (t, *J* = 7.6 Hz, 2H), 2.49 (dd, *J* = 8.1, 7.0 Hz, 2H); ^{13}C NMR (101 MHz, $CDCl_3$) δ 158.9, 131.5, 128.0, 127.4, 127.1 (q, *J* = 268.0 Hz), 125.0, 71.2, 33.4, 29.7, 24.4. ^{19}F NMR (282 MHz, $CDCl_3$) δ -58.6 (s); MS (FAB) *m/z* $[M - N_2]^{\bullet+}$ calcd for $C_{12}H_{11}F_3O$: 228.0762, found: 228.0760.

(4-diazo-5,5,5-trifluoropentyl)benzene (7)

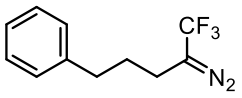

^{1}H NMR (400 MHz, $CDCl_3$) δ 7.51 – 7.12 (m, 1H), 2.74 (t, *J* = 7.6 Hz, 5H), 2.29 (t, *J* = 7.5 Hz, 2H), 1.90 (p, *J* = 7.6 Hz, 2H); ^{13}C NMR (101 MHz, $CDCl_3$) δ 140.9, 128.6, 128.4, 127.0 (q, *J* = 267.9 Hz), 126.2, 34.8, 29.0, 21.2; ^{19}F NMR (282 MHz, $CDCl_3$) δ -59.0 (s); MS (FAB) *m/z* $[M + H - N_2]^+$ calcd for $C_{11}H_{11}F_3$: 200.0813, found: 200.0814.

(5-diazo-6,6,6-trifluorohexyl)benzene (8)

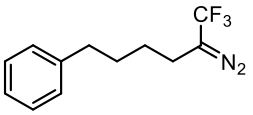

^{1}H NMR (500 MHz, $CDCl_3$) δ 7.32 (dd, *J* = 8.2, 6.8 Hz, 2H), 7.24 – 7.18 (m, 3H), 2.67 (t, *J* = 7.6 Hz, 2H), 2.27 (t, *J* = 7.5 Hz, 2H), 1.73 (tt, *J* = 9.1, 6.8 Hz, 2H), 1.64 – 1.52 (m, 2H); ^{13}C NMR

(101 MHz, $CDCl_3$) δ 141.9, 128.4, 128.4, 127.0 (q, *J* = 268.0 Hz), 125.9, 35.5, 30.4, 26.9, 21.5; ^{19}F NMR (376 MHz, $CDCl_3$) δ -58.8 (s); MS (FAB) *m/z* $[M + H]^+$ calcd for $C_{12}H_{14}N_2F_3$: 243.1109, found: 243.1097.

(2-diazo-3,3,3-trifluoropropyl)benzene (9)

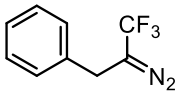

^1H NMR (300 MHz, $CDCl_3$) δ 7.46 – 7.19 (m, 5H), 3.54 (s, 2H); 13C NMR (126 MHz, $CDCl_3$) δ 135.7, 129.0, 128.4, 127.5, 27.9. The ^{13}C resonance corresponds to the CF_3 group was not well resolved; ^{19}F NMR (282 MHz, $CDCl_3$) δ -58.7; MS (FAB) *m/z* $[M + H]^+$ calcd for $C_9H_8N_2F_3$: 201.0640, found: 201.0638.

(3-diazo-4,4,4-trifluorobutyl)cyclohexane (10)

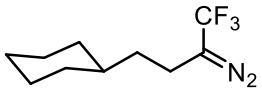

^1H NMR (500 MHz, $CDCl_3$) δ 2.29 – 2.21 (m, 2H), 1.80 – 1.66 (m, 5H), 1.47 – 1.37 (m, 2H), 1.36 – 1.14 (m, 4H), 1.02 – 0.87 (m, 2H); ^{13}C NMR (101 MHz, $CDCl_3$) δ 127.1 (q, *J* = 267.9 Hz). 36.8, 34.6, 33.0, 26.50, 26.20, 18.90; ^{19}F NMR (376 MHz, $CDCl_3$) δ -58.9; MS (ESI) *m/z* $[M + H]^+$ calcd for $C_{10}H_{16}N_2F_3$: 221.1266, found: 221.1259.

2-diazo-1,1,1-trifluorodecane (11)

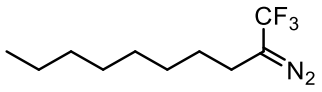

^1H NMR (500 MHz, $CDCl_3$) δ 2.23 (t, *J* = 7.5 Hz, 2H), 1.54 (p, *J* = 7.4 Hz, 2H), 1.45 – 1.21 (m, 10H), 0.91 (t, *J* = 6.8 Hz, 3H); ^{13}C NMR (101 MHz, $CDCl_3$) δ 127.1 (q, *J* = 268.0 Hz), 31.8, 29.2, 29.1, 28.7, 27.3, 22.6, 21.6, 14.1; ^{19}F NMR (282 MHz, $CDCl_3$) δ -58.9; MS (FAB) *m/z* $[(M + H) - H_2]^+$ calcd for $C_{10}H_{16}N_2F_3$: 221.1266, found: 221.1285.

2-diazo-1,1,1-trifluorodecane (12)

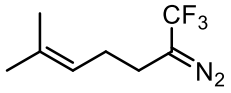

This diazo compound was purified with Biotage SNAP Ultra C18 column using water/acetonitrile (50% - 95%) eluent. The product fractions were combined, diluted with water, and extracted with pentane. The solvent of the pentane extract was carefully removed under reduced pressure to afford the volatile diazo compound **12**. ^1H NMR (500 MHz, $CDCl_3$) δ 5.20 – 5.01 (m, 1H), 2.29 – 2.20, (m, 4H), 1.73 (s, 3H), 1.65 (s, 3H); ^{13}C NMR (101 MHz, $CDCl_3$) δ 134.5, 121.8, 26.3, 25.9, 22.1, 17.8. The ^{13}C resonance corresponds to the CF_3 group was not well resolved; ^{19}F NMR (376 MHz, $CDCl_3$) δ -58.9; MS (ESI) *m/z* $[M + H]^+$ calcd for $C_8H_{12}N_2F_3$: 193.0953, found: 193.0941.

(*E*)-9-diazo-10,10,10-trifluoro-2,6-dimethyldeca-2,6-diene (13)

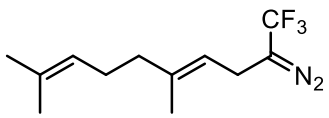

^1H NMR (400 MHz, $CDCl_3$) δ 5.20 – 5.06 (m, 2H), 2.28 (d, *J* = 3.3 Hz, 2H), 2.18 – 1.97 (m, 4H), 1.71 (d, *J* = 1.4 Hz, 3H), 1.66 (s, 3H), 1.64 (s, 3H); ^{13}C NMR (101 MHz, $CDCl_3$) δ 137.9, 131.6, 127.1 (d, *J* = 267.9 Hz), 124.0, 121.4, 39.7, 26.5, 26.1, 25.6, 22.0, 17.6, 16.0. ^{19}F NMR (282 MHz, cdcl$_3$) δ -58.9; MS (FAB) *m/z* $[M]^{\bullet+}$ calcd for $C_{12}H_{17}F_3N_2$: 246.1344, found: 246.1367.

IV. Synthesis and Characterization of Authentic Organoborane Products

Racemic standard references of organoborane products were prepared *via* Rh-catalyzed B–H insertion reactions with procedures slightly modified from a previously reported method [11]. Namely, a 4 mL vial with screw cap and PTFE septum was charged with a borane substrate (1.0 mmol, 1 equiv.) and $Rh_2(OAc)_4$ (22 mg, 5 mol%). The vial was evacuated and backfilled with Ar three times and 2 mL of anhydrous CH_2Cl_2 was added. A CH_2Cl_2 solution (1 mL) of diazo compound (1.0 mmol) was slowly added to the reaction mixture over 4 hours at room temperature. Afterwards, the reaction mixture was allowed to further react overnight. The crude reaction mixture was purified by flash chromatography using EtOAc and hexanes as eluents and afforded organoborane products. The ^{1}H NMR resonances of the B–H protons are broad (due to geminal coupling with boron) and generally in the range of 0.4 – 1.6 ppm. The ^{13}C NMR resonances of the boron-binding NHC quaternary carbons usually appear at around 170 ppm and are typically broad (due to germinal coupling with boron) and weak; these signals are sometimes not visible in the ^{13}C NMR spectra.

(1,3-dimethyl-1H-imidazol-3-ium-2-yl)(1,1,1-trifluoro-4-phenylbutan-2-yl)dihydroborate (2a)

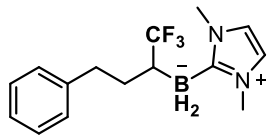

^{1}H NMR (400 MHz, $CDCl_3$) δ 7.22 – 7.14 (m, 4H), δ 7.11 – 7.03 (m, 1H), 6.71 (s, 2H), 3.62 (s, 6H), 2.73 (dddd, *J* = 50.4, 13.7, 9.8, 6.1 Hz, 2H), 2.01 – 1.84 (m, 1H), 1.80 – 1.50 (m, 2H), 1.37 – 1.05 (m, 2H); ^{13}C NMR (101 MHz, $CDCl_3$) δ 170.7, 143.8, 133.5 (q, *J* = 279.0 Hz), 128.9, 128.4, 125.6, 120.6, 36.1, 35.4, 33.1, 32.3 (q, *J* = 3.7 Hz); ^{11}B NMR (128 MHz, $CDCl_3$) δ -28.6 (t, *J* = 87.4 Hz); ^{19}F NMR (282 MHz, $CDCl_3$) δ -64.2 (d, *J* = 12.5 Hz); MS (ESI) *m/z* $[M + Na]^+$ calcd for $C_{15}H_{20}BN_2F_3Na$: 319.1569, found: 319.1567.

(4-(3-chlorophenyl)-1,1,1-trifluorobutan-2-yl)(1,3-dimethyl-1H-imidazol-3-ium-2-yl)dihydroborate (3a)

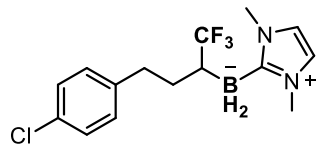

^{1}H NMR (300 MHz, $CDCl_3$) δ 7.34 – 7.17 (m, 4H), 6.85 (d, *J* = 0.7 Hz, 6H), 3.75 (d, *J* = 0.7 Hz, 2H), 2.98 – 2.70 (m, 2H), 2.09 – 0.98 (m, 5H); ^{13}C NMR (101 MHz, $CDCl_3$) δ 170.3, 142.1, 133.1 (q, *J* = 278.7 Hz), 131.0, 130.0, 128.2, 120.4, 35.8, 34.3, 32.7, 31.9; ^{11}B NMR (128 MHz, $CDCl_3$) δ -28.6 (t, *J* = 87.3 Hz); ^{19}F NMR (282 MHz, $CDCl_3$) δ -64.2 (d, *J* = 11.5 Hz); MS (ESI) *m/z* $[M + Na]^+$ calcd for $C_{15}H_{19}BN_2F_3ClNa$: 353.1180, found: 353.1195.

(1,3-dimethyl-1H-imidazol-3-ium-2-yl)(1,1,1-trifluoro-4-(3-methoxyphenyl)butan-2-yl)dihydroborate (4a)

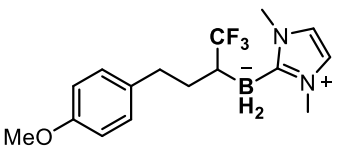

^{1}H NMR (400 MHz, $CDCl_3$) δ 7.19 – 7.12 (m, 2H), 6.84 – 6.80 (m, 2H), 6.79 (s, 2H), 3.79 (s, 3H), 3.70 (s, 6H), 2.89 – 2.59 (m, 2H), 1.96 (tt, *J* = 10.3, 5.5 Hz, 1H), 1.84 – 1.03 (m, 4H); ^{13}C NMR (101 MHz, $CDCl_3$) δ 170.7, 157.4, 135.6, 133.2 (q, *J* = 278.8 Hz), 129.4, 120.3, 113.5, 55.3, 35.8,

34.1, 32.4, 32.2 (q, J = 3.7 Hz); ^{11}B NMR (128 MHz, $CDCl_3$) δ -28.6 (t, J = 87.5 Hz); ^{19}F NMR (282 MHz, $CDCl_3$) δ -64.2 (d, J = 12.3 Hz); MS (FAB) *m/z* $[M]^{\bullet+}$ calcd for $C_{16}H_{22}BN_2OF_3$: 326.1777, found: 326.1777.

(4-(3,4-dimethoxyphenyl)-1,1,1-trifluorobutan-2-yl)(1,3-dimethyl-1H-imidazol-3-ium-2-yl)dihydroborate (5a)

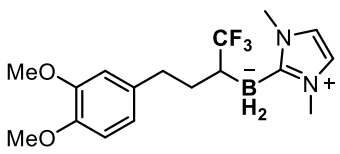

^{1}H NMR (400 MHz, $CDCl_3$) δ 6.73 (s, 2H), 6.73 – 6.70 (m, 3H), 3.80 (s, 3H), 3.79 (s, 3H), 3.64 (s, 6H), 2.69 (dddd, J = 55.9, 13.8, 9.9, 6.1 Hz, 2H), 1.91 (q, J = 12.5, 10.2 Hz, 1H), 1.73 – 1.47 (m, 2H), 1.32 – 1.03 (m, 2H); ^{13}C NMR (101 MHz, $CDCl_3$) δ 148.6, 146.8, 133.2 (d, J = 279.0 Hz), 129.1, 120.3, 120.3, 111.8, 111.0, 55.9, 55.8, 35.8, 34.6, 32.0 (d, J = 3.8 Hz); ^{11}B NMR (128 MHz, $CDCl_3$) δ -28.6 (t, J = 87.5 Hz); ^{11}B NMR (128 MHz, $CDCl_3$) δ -28.6 (t, J = 87.4 Hz); ^{19}F NMR (282 MHz, $CDCl_3$) δ -64.2 (d, J = 12.4 Hz); MS (ESI) *m/z* $[M + H - H_2]^+$ calcd for $C_{17}H_{23}BN_2O_2F_3$: 355.1805, found: 355.1832.

(4-(2,3-dihydrobenzofuran-6-yl)-1,1,1-trifluorobutan-2-yl)(1,3-dimethyl-1H-imidazol-3-ium-2-yl)dihydroborate (6a)

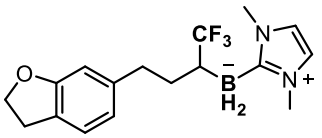

^{1}H NMR (400 MHz, $CDCl_3$) δ 7.10 – 7.05 (m, 1H), 6.97 – 6.93 (m, 1H), 6.79 (s, 2H), 6.68 (d, J = 8.1 Hz, 1H), 4.53 (t, J = 8.6 Hz, 2H), 3.71 (s, 6H), 3.22 – 3.11 (m, 2H), 2.73 (dddd, J = 54.4, 13.7, 10.0, 6.0 Hz, 2H), 2.02 – 1.88 (m, 1H), 1.84 – 1.57 (m, 2H), 1.45 – 1.00 (m, 2H); ^{13}C NMR (101 MHz, $CDCl_3$) δ 170.7, 157.9, 135.6, 133.3 (q, J = 278.8 Hz), 127.8, 126.7, 125.0, 120.3, 108.6, 71.1, 35.8, 34.5, 32.6 (q, J = 3.6 Hz), 31.9, 29.9; ^{11}B NMR (128 MHz, $CDCl_3$) δ -28.6 (t, J = 87.4 Hz); ^{19}F NMR (282 MHz, $CDCl_3$) δ -64.2 (d, J = 12.5 Hz); MS (FAB) *m/z* $[M]^{\bullet+}$ calcd for $C_{17}H_{22}BN_2OF_3$: 338.1777, found: 338.1777.

(1,3-dimethyl-1H-imidazol-3-ium-2-yl)(1,1,1-trifluoro-5-phenylpentan-2-yl)dihydroborate (7a)

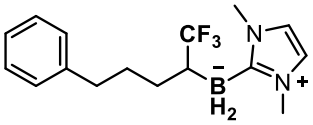

^{1}H NMR (400 MHz, $CDCl_3$) δ 7.27 – 7.00 (m, 5H), 6.71 (s, 2H), 3.64 (s, 6H), 2.54 (ddd, J = 9.0, 6.6, 2.5 Hz, 2H), 1.79 (m, 1H), 1.73 – 1.56 (m, 2H), 1.39 (m, 2H), 1.32 – 0.93 (m, 2H); ^{13}C NMR (101 MHz, $CDCl_3$) δ 170.7, 143.6, 133.6 (q, J = 279.0 Hz), 128.8, 128.5, 125.7, 120.6, 36.9, 36.1, 33.1, 31.6, 30.7 (q, J = 3.7 Hz); ^{11}B NMR (128 MHz, $CDCl_3$) δ -28.6 (t, J = 87.3 Hz); ^{19}F NMR (282 MHz, $CDCl_3$) δ -64.9 (d, J = 12.0 Hz); MS (ESI) *m/z* $[M + Na]^+$ calcd for $C_{16}H_{22}BN_2F_3Na$: 333.1726, found: 333.1736.

(1,3-dimethyl-1H-imidazol-3-ium-2-yl)(1,1,1-trifluoro-6-phenylhexan-2-yl)dihydroborate (8a)

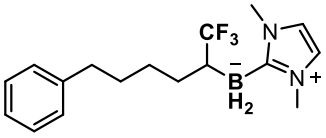

^{1}H NMR (400 MHz, $CDCl_3$) δ 7.23 – 7.17 (m, 2H), 7.16 – 7.03 (m, 3H), 6.71 (s, 2H), 3.65 (s, 6H), 2.64 – 2.48 (m, 2H), 1.73 – 0.91 (m, 9H); ^{13}C NMR (101 MHz, $CDCl_3$) δ 170.8, 143.6, 133.6 (q, J = 278.9 Hz), 128.8, 128.5, 125.8, 120.6, 36.4, 36.1, 33.2, 32.4, 30.6 (q, J = 3.7 Hz), 29.2; ^{11}B NMR

(128 MHz, $CDCl_3$) δ -28.6 (t, *J* = 87.4 Hz); ^{19}F NMR (282 MHz, $CDCl_3$) δ -64.3 (d, *J* = 12.6 Hz); MS (ESI) *m/z* $[M + Na]^+$ calcd for $C_{17}H_{24}BN_2F_3Na$: 347.1882, found: 347.1877.

(1,3-dimethyl-1H-imidazol-3-ium-2-yl)(1,1,1-trifluoro-3-phenylpropan-2-yl)dihydroborate (9a)

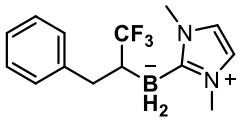

^1H NMR (400 MHz, $CDCl_3$) δ 7.17 – 7.12 (m, 4H), 7.09 – 6.99 (m, 1H), 6.65 (s, 2H), 3.52 (s, 6H), 2.95 (d, *J* = 13.5 Hz, 1H), 2.65 – 2.42 (m, 1H), 1.87 – 0.82 (m, 3H); ^{13}C NMR (101 MHz, $CDCl_3$) δ 143.5, 132.8 (q, *J* = 278.7 Hz), 129.1, 127.8, 125.2, 120.2, 36.6 (q, *J* = 4.0 Hz), 35.7; ^{11}B NMR (128 MHz, $CDCl_3$) δ -28.6 (t, *J* = 87.5 Hz); ^{19}F NMR (282 MHz, $CDCl_3$) δ -64.2 (d, *J* = 11.9 Hz); MS (ESI) *m/z* $[M + Na]^+$ calcd for $C_{14}H_{18}BN_2F_3Na$: 305.1413, found: 305.1416.

(4-cyclohexyl-1,1,1-trifluorobutan-2-yl)(1,3-dimethyl-1H-imidazol-3-ium-2-yl)dihydroborate (10a)

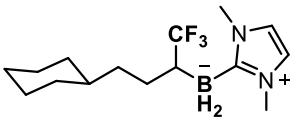

^1H NMR (400 MHz, $CDCl_3$) δ 6.80 (s, 2H), 3.75 (s, 6H), 1.81 – 1.03 (m, 16H), 0.96 – 0.80 (m, 2H); ^{13}C NMR (101 MHz, $CDCl_3$) δ 133.7 (q, *J* = 278.9 Hz), 120.6, 38.6, 37.4, 36.2, 33.9, 33.7, 28.1 (q, *J* = 3.7 Hz), 27.2, 26.9 (d, *J* = 3.2 Hz); ^{11}B NMR (128 MHz, $CDCl_3$) δ -28.6 (t, *J* = 87.4 Hz); ^{19}F NMR (282 MHz, $CDCl_3$) δ -64.4 (d, *J* = 12.4 Hz); MS (ESI) *m/z* $[M + Na]^+$ calcd for $C_{15}H_{26}BN_2F_3Na$: 325.2039, found: 325.2031.

(1,3-dimethyl-1H-imidazol-3-ium-2-yl)(1,1,1-trifluorodecan-2-yl)dihydroborate (11a)

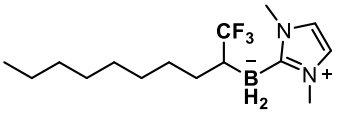

^1H NMR (400 MHz, $CDCl_3$) δ 6.80 (s, 2H), 3.75 (s, 6H), 1.75 – 1.45 (m, 3H), 1.40 – 1.13 (m, 14H), 0.93 – 0.83 (m, 3H); ^{13}C NMR (101 MHz, $CDCl_3$) δ 171.0, 133.7 (q, *J* = 278.9 Hz), 120.6, 36.2, 33.5, 32.3, 30.8 (q, *J* = 3.7 Hz), 30.5, 30.0, 29.8, 29.6, 23.0, 14.5; ^{11}B NMR (128 MHz, $CDCl_3$) δ -28.6 (t, *J* = 87.3 Hz); ^{19}F NMR (282 MHz, $CDCl_3$) δ -64.3 (d, *J* = 12.3 Hz); MS (ESI) *m/z* $[M + Na]^+$ calcd for $C_{15}H_{28}BN_2F_3Na$: 327.2195, found: 327.2178.

(1,3-dimethyl-1H-imidazol-3-ium-2-yl)(1,1,1-trifluoro-6-methylhept-5-en-2-yl)dihydroborate (12a)

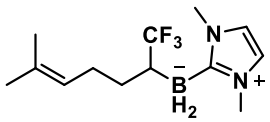

^1H NMR (400 MHz, $CDCl_3$) δ 6.80 (s, 2H), 5.14 (tp, *J* = 7.0, 1.4 Hz, 1H), 3.75 (s, 6H), 2.29 – 2.02 (m, 2H), 1.68 (s, 3H), 1.63 (s, 3H), 1.80 – 1.03 (m, 5H); ^{13}C NMR (101 MHz, $CDCl_3$) δ 133.6 (q, *J* = 278.8 Hz), 131.2, 126.0, 120.6, 36.1, 33.1, 30.8 (q, *J* = 3.6 Hz), 27.8, 26.1, 18.1; ^{11}B NMR (128 MHz, $CDCl_3$) δ -28.7 (t, *J* = 87.4 Hz); ^{19}F NMR (282 MHz, $CDCl_3$) δ -64.3 (d, *J* = 12.3 Hz); MS (ESI) *m/z* $[M + Na]^+$ calcd for $C_{13}H_{22}BN_2F_3Na$: 297.1726, found: 297.1723.

(*E*)-(1,3-dimethyl-1H-imidazol-3-ium-2-yl)(1,1,1-trifluoro-6,10-dimethylundeca-5,9-dien-2-yl)dihydroborate (13a)

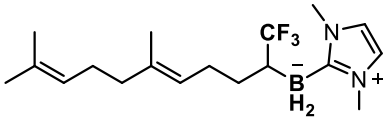

^{1}H NMR (400 MHz, $CDCl_3$) δ 6.73 (s, 2H), 5.17 – 4.96 (m, 2H), 3.66 (s, 6H), 2.20 – 2.01 (m, 2H), 2.01 – 1.85 (m, 4H), 1.65 – 1.56 (m, 3H), 1.53 (d, *J* = 8.5 Hz, 6H), 1.42 – 0.96 (m, 3H); ^{13}C NMR (101 MHz, $CDCl_3$) δ 170.2, 133.3 (q, *J* = 278.8 Hz), 134.6, 131.2, 125.5, 124.5, 120.3, 39.8, 35.8, 32.8, 30.4 (q, *J* = 3.7 Hz), 27.4, 26.8, 25.7, 17.7, 16.0; ^{11}B NMR (128 MHz, $CDCl_3$) δ -28.7 (t, *J* = 87.1 Hz); ^{19}F NMR (282 MHz, $CDCl_3$) δ -64.3 (d, *J* = 12.6 Hz); MS (FAB) *m/z* $[(M + H) – H_2]^+$ calcd for $C_{17}H_{27}BN_2F_3$: 327.2219, found: 327.2223.

V. GC-MS Standard Curves for Organoborane Products

Product formation in enzymatic reactions was quantified by GC-MS based on standard curves. To determine the standard calibration curves, stock solutions of chemically synthesized organoborane products were prepared at various concentrations (0.5 - 7 mM in 4:6 hexanes/EtOAc) with added internal standard 1,2,3-trimethoxybenzene (6.45 mM final concentration in the stock solutions). All data points represent the average of duplicate runs. The standard curves plot product concentration in mM (y-axis) against the ratio of product area to internal standard area on GC-MS (x-axis).

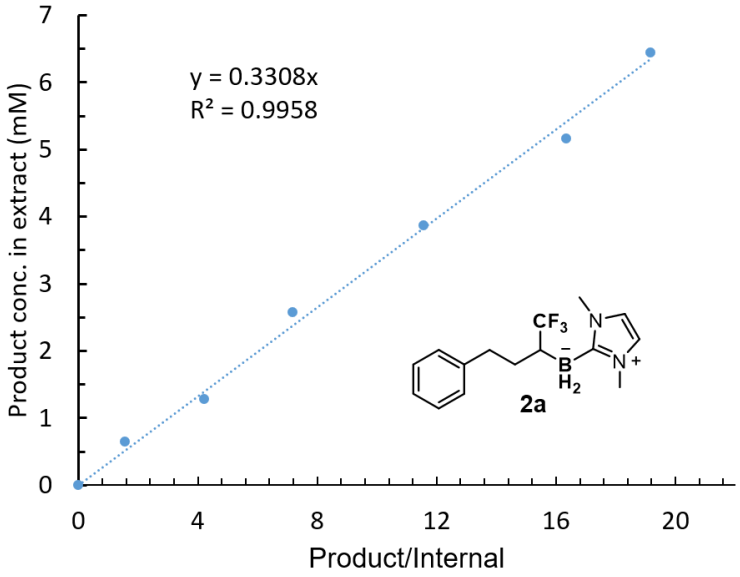

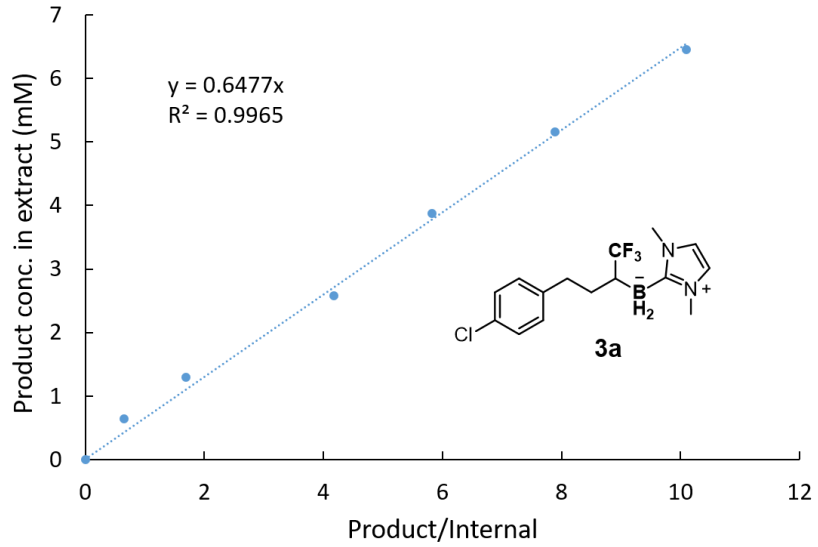
y = 0.6477x
R² = 0.9965
Product conc. in extract (mM)
Product/Internal
3a

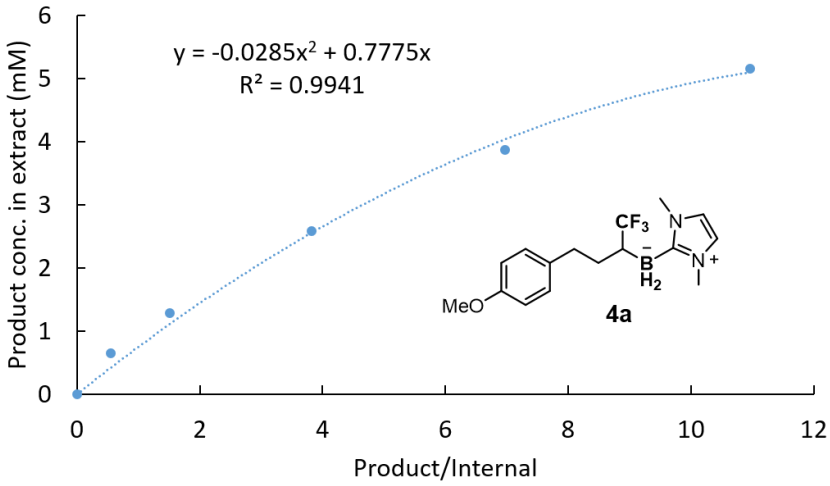
y = -0.0285x² + 0.7775x
R² = 0.9941
Product conc. in extract (mM)
Product/Internal
4a

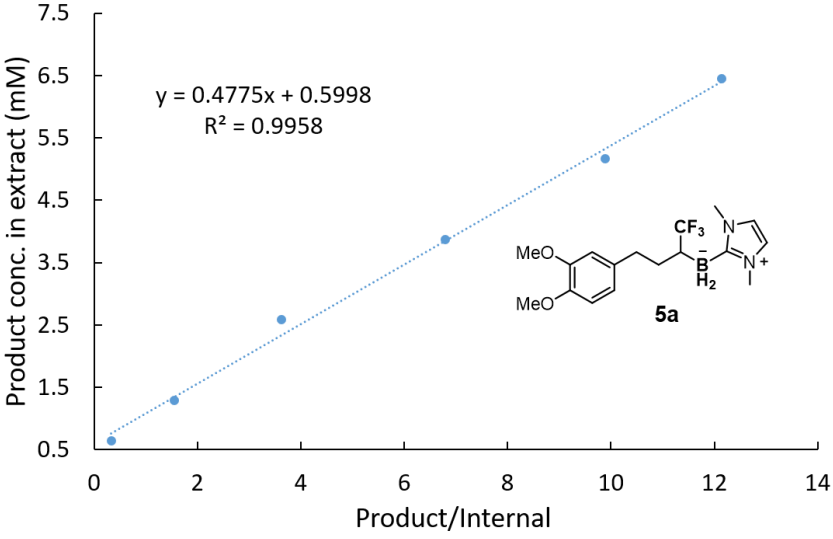
y = 0.4775x + 0.5998
R² = 0.9958
Product conc. in extract (mM)
Product/Internal
5a

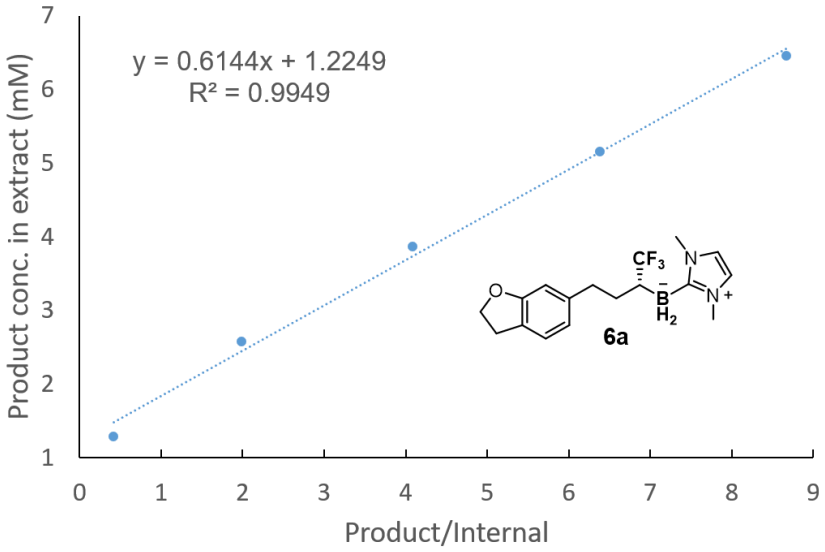
y = 0.6144x + 1.2249
R² = 0.9949
Product conc. in extract (mM)
Product/Internal
6a

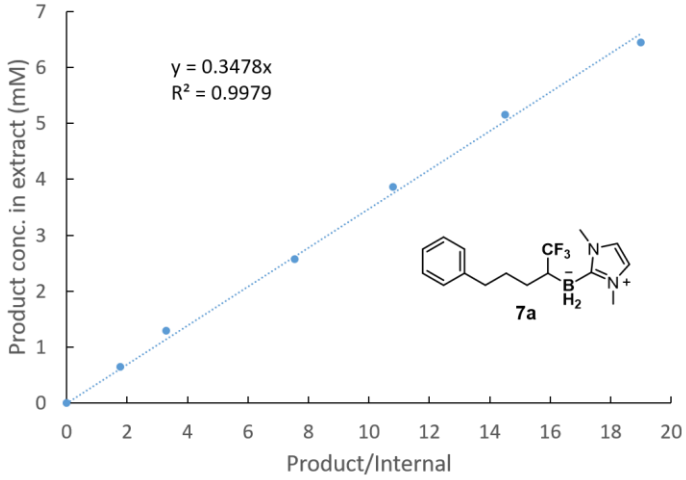
y = 0.3478x
R² = 0.9979
Product conc. in extract (mM)
Product/Internal
7a

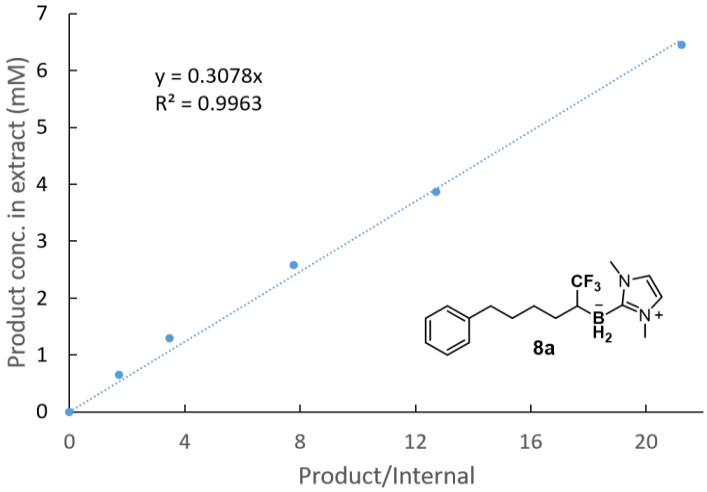
y = 0.3078x
R² = 0.9963
Product conc. in extract (mM)
Product/Internal
8a

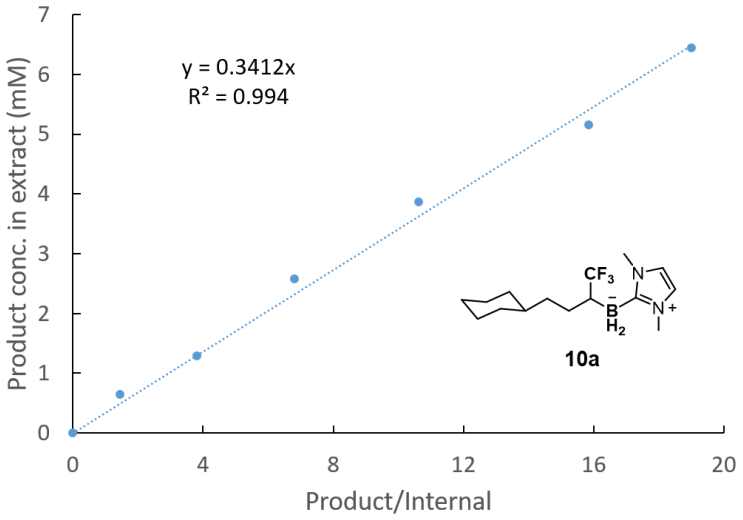
y = 0.3412x
R² = 0.994
Product conc. in extract (mM)
Product/Internal
0
1
2
3
4
5
6
7
0
4
8
12
16
20
CF3
B
H2
N
N+
10a

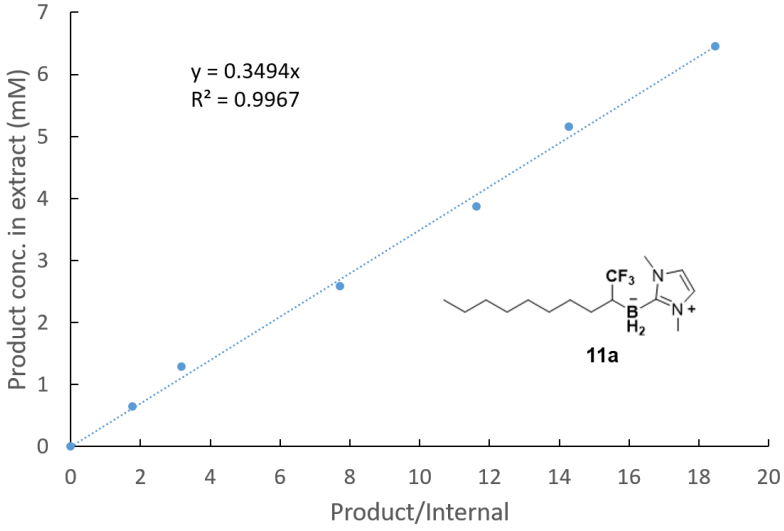
y = 0.3494x
R² = 0.9967
Product conc. in extract (mM)
Product/Internal
0
1
2
3
4
5
6
7
0
2
4
6
8
10
12
14
16
18
20
CF3
B
H2
N
N+
11a

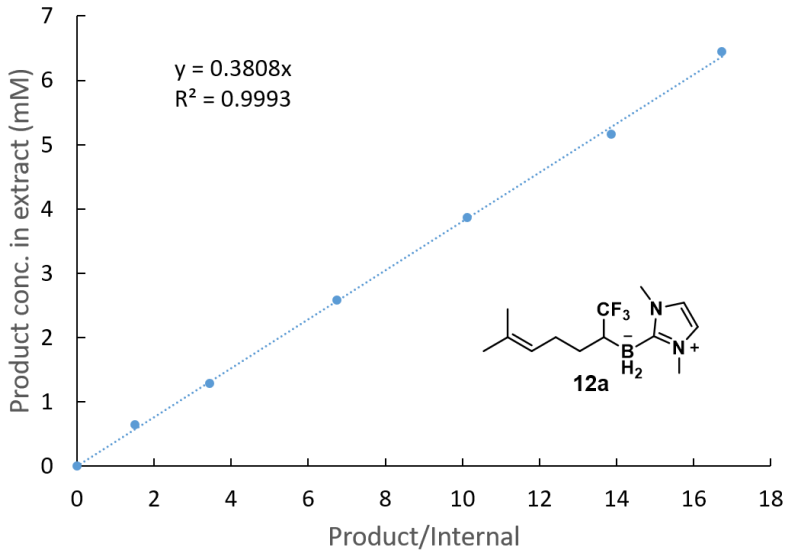

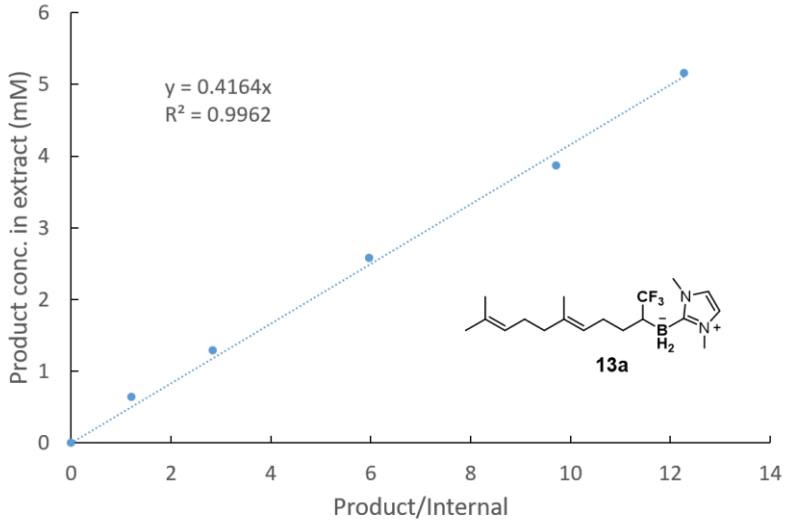

VI. Determination of Enantioselectivity

All e.r. values of enzymatically synthesized borane products were determined using chiral SFC or normal-phase chiral HPLC. The absolute configurations of enzymatically synthesized borane products **2a** were determined to be *R* by measuring the optical rotation of its derivatized alcohol (see section VIII). Absolute configurations of other organoborane products were inferred by analogy, assuming the facial selectivity of the diazo reagents from which these products were made remains the same as that of **2a**.

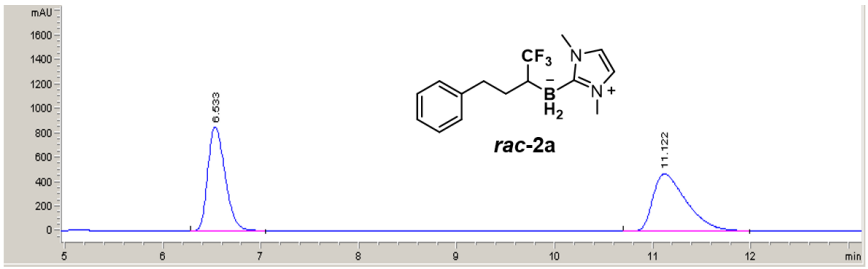

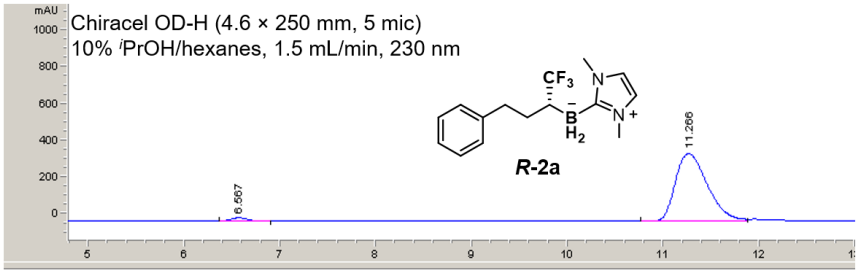

***rac*-2a**			***R*-2a**		
Retention Time (min)	Area (mAu)	Area%	Retention Time (min)	Area (mAu)	Area%
6.533	10492	49.0	6.567	230	2.6
11.122	11002	51.0	11.266	8526	97.4

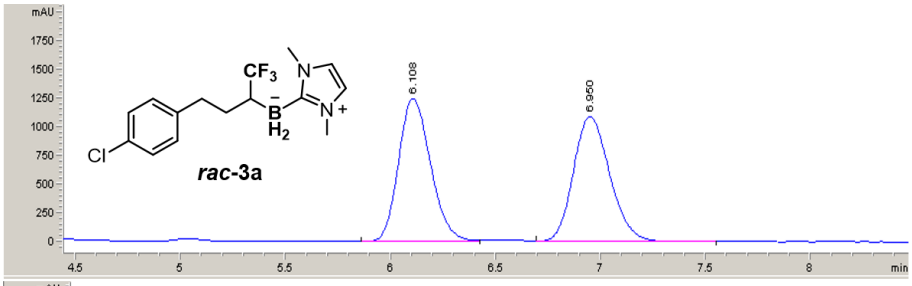

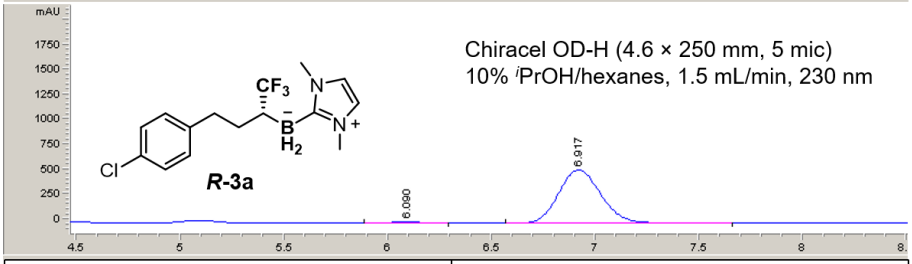

***rac*-3a**			***R*-3a**		
Retention Time (min)	Area (mAu)	Area%	Retention Time (min)	Area (mAu)	Area%
6.108	13271	50.1	6.090	204	2.6
6.95	13215	49.9	6.917	7704	97.4

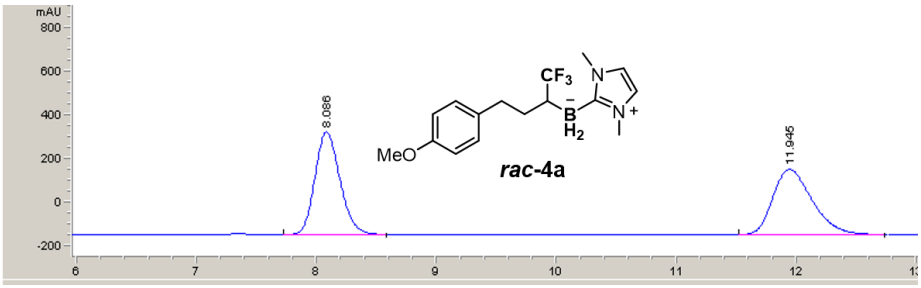

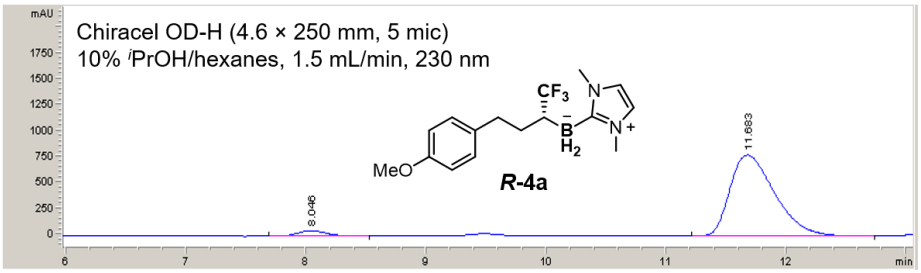

***rac*-4a**			***R*-4a**		
Retention Time (min)	Area (mAu)	Area%	Retention Time (min)	Area (mAu)	Area%
8.086	6839	50.0	8.046	956	4.5
11.945	6826	50.0	11.683	20415	95.5

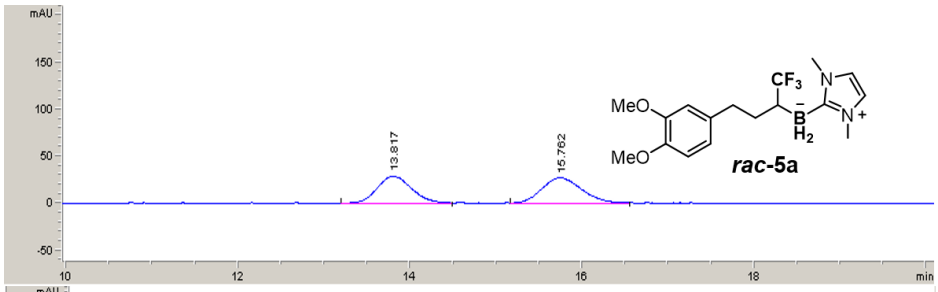

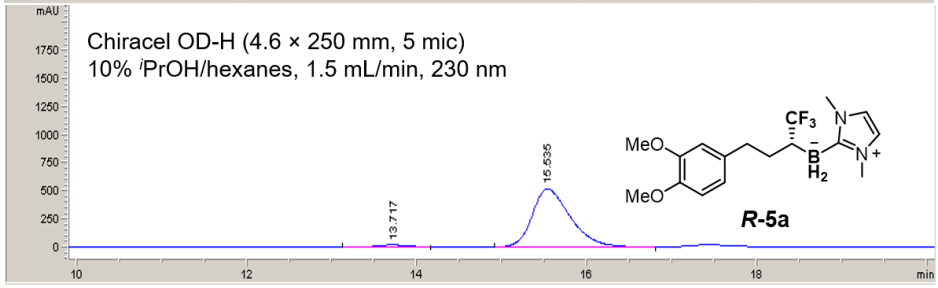

***rac*-6**			***R*-6**		
Retention Time (min)	Area (mAu)	Area%	Retention Time (min)	Area (mAu)	Area%
13.817	834	49.5	13.717	673	3.9
15.762	850	50.5	15.535	16543	96.1

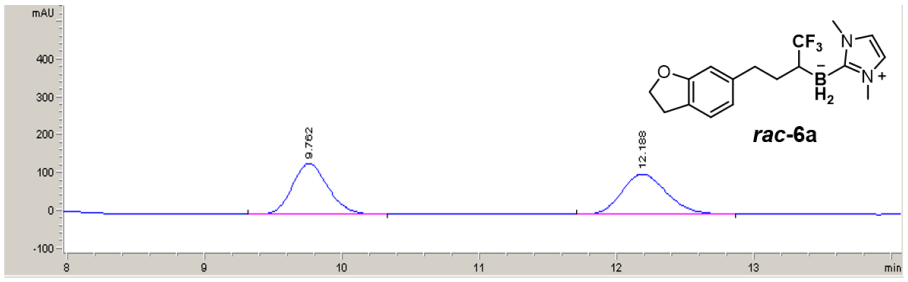

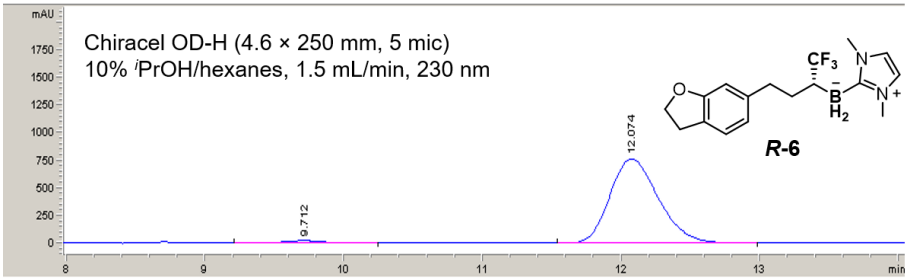

rac-7			*R*-7		
Retention Time (min)	Area (mAu)	Area%	Retention Time (min)	Area (mAu)	Area%
9.762	2443	50.0	9.712	496	2.6
12.188	2449	50.0	12.074	18630	97.4

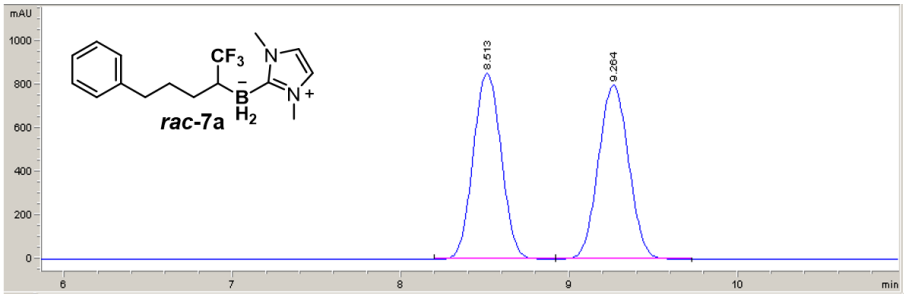

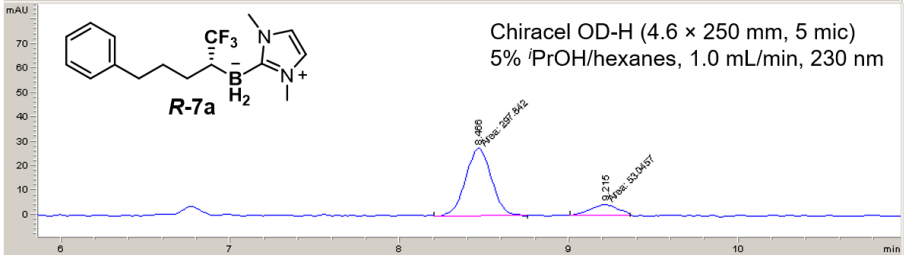

rac-7a			*R*-7a		
Retention Time (min)	Area (mAu)	Area%	Retention Time (min)	Area (mAu)	Area%
7.002	9853	49.7	8.466	298	85
8.748	9967	50.3	9.215	53	15

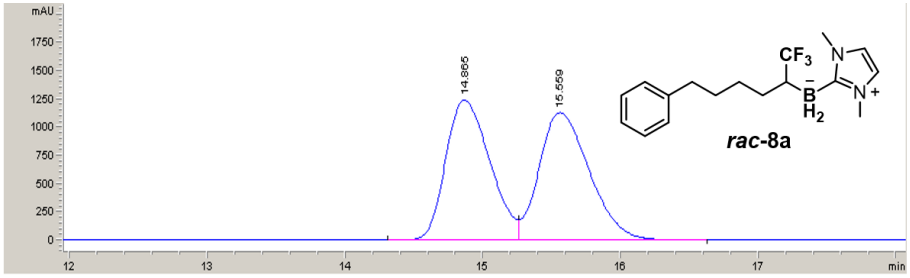

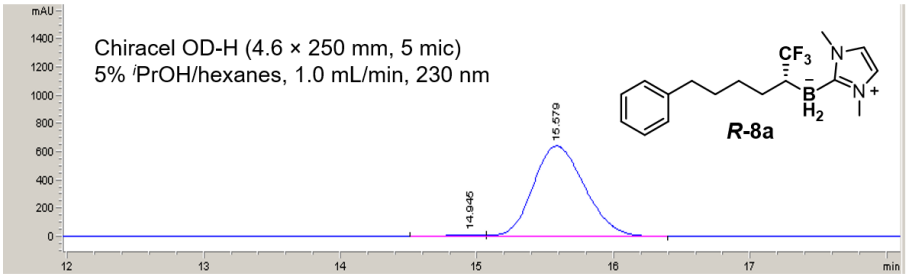

***rac*-8a**			***R*-8a**		
Retention Time (min)	Area (mAu)	Area%	Retention Time (min)	Area (mAu)	Area%
14.865	27660	49.1	14.945	246	1.4
15.559	28711	50.9	15.579	17014	98.6

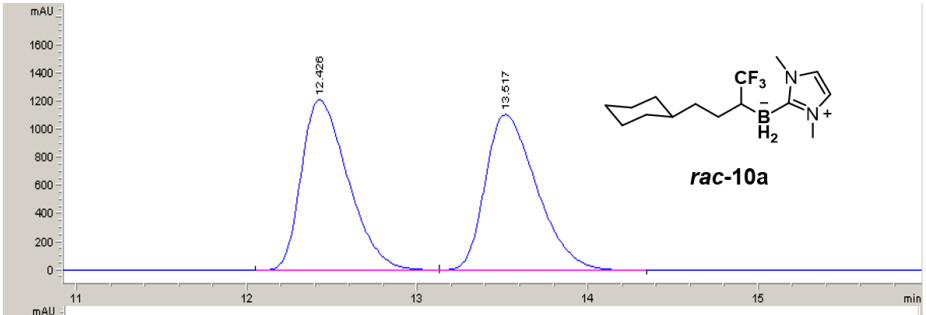

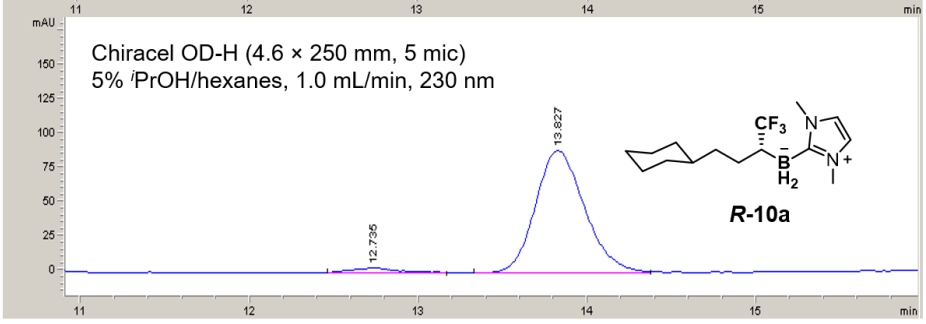

***rac*-10a**			***R*-10a**		
Retention Time (min)	Area (mAu)	Area%	Retention Time (min)	Area (mAu)	Area%
12.426	23251	49.9	12.735	69	3.7
13.517	23380	50.1	13.827	1808	96.3

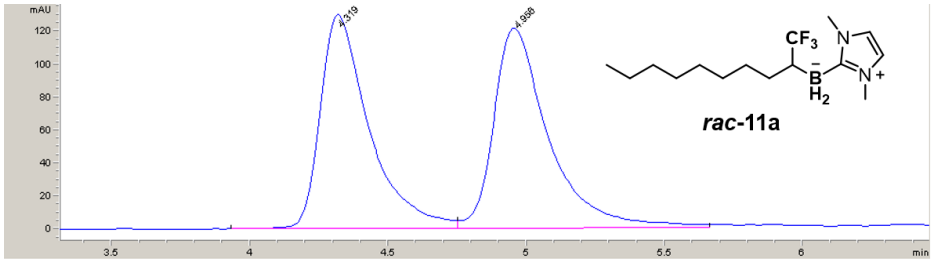

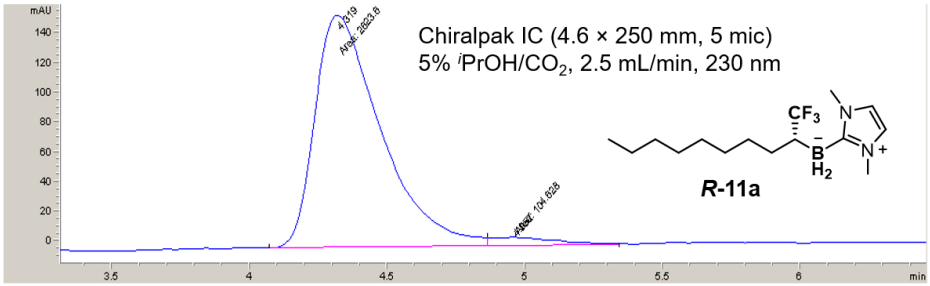

***rac*-11a**			***R*-11a**		
Retention Time (min)	Area (mAu)	Area%	Retention Time (min)	Area (mAu)	Area%
4.319	1611	49.3	4.319	2624	96.2
4.956	1660	50.7	4.957	105	3.8

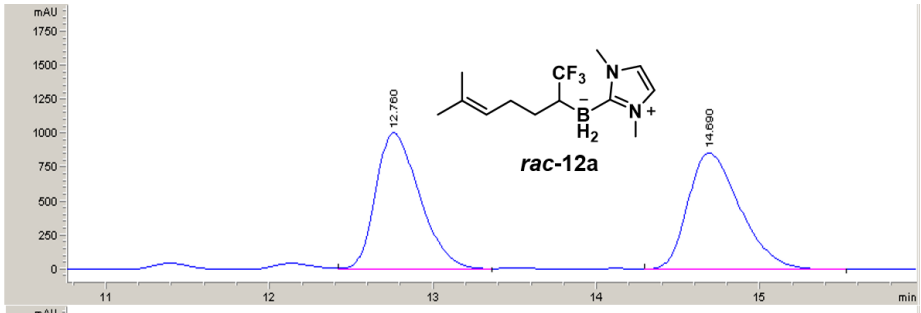

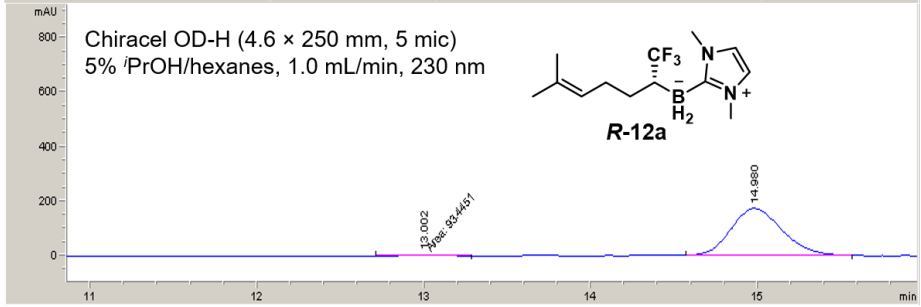

***rac*-12a**			***R*-12a**		
Retention Time (min)	Area (mAu)	Area%	Retention Time (min)	Area (mAu)	Area%
12.760	19013	49.9	13.002	93	2.5
14.690	19106	50.1	14.980	3706	97.5

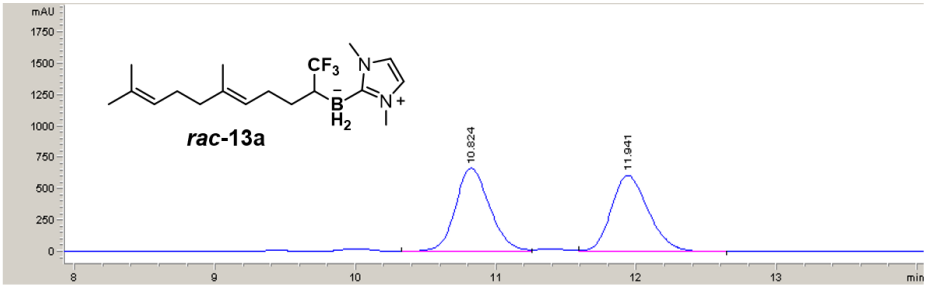

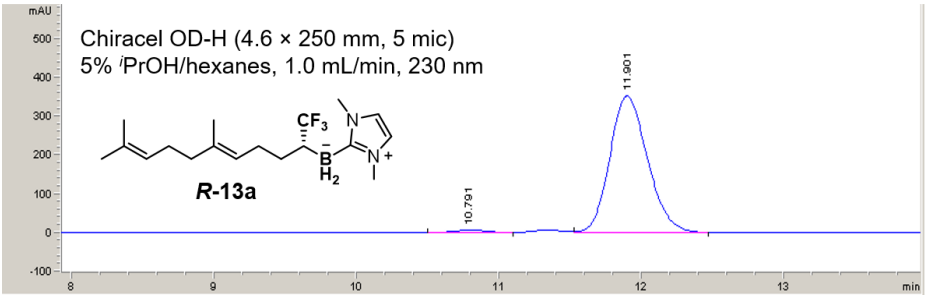

***rac*-13a**			***R*-13a**		
Retention Time (min)	Area (mAu)	Area%	Retention Time (min)	Area (mAu)	Area%
10.824	11402	50.3	10.791	139	2.0
11.941	11268	49.7	11.901	6554	98.0

VII. Preparative Scale Enzymatic Reactions and product derivatization

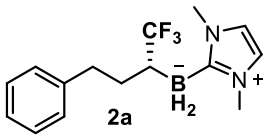

Preparative scale enzymatic synthesis of 2a (0.4 mmol scale reaction). To a 100 mL conical flask were added 20 mL BOR-CF_3 whole-cell solution (OD_{600} = 20), 1 mL glucose solution (1 M), borane substrate **1** (0.7 mL, 400 mM in MeCN) and trifluorodiazo compound **2** (0.5 mL, 400 mM in MeCN). The flask was shaken at 240 rpm in the anaerobic chamber. After 6 hours, another batch of whole-cell solution (20 mL, OD_{600} = 20), glucose (1 mL, 1 M), borane substrate **1** (0.7 mL, 400 mM in MeCN) and diazo **2** (0.5 mL, 400 mM in MeCN) were added to the reaction mixture. The reaction mixture was shaken for a total of 36 hours and then divided between four 50 mL Falcon tubes. 25 mL 3:7 hexanes/EtOAc solution was added to each tube to extract the borylation product via vortexing (30 s for three times) and centrifugation (5,000xg, 5 min). After removal of the organic layers, two additional rounds of extraction were performed. The combined organic extracts were dried over anhydrous Na_2SO_4, concentrated, and purified by flash chromatography with EtOAc/hexanes (0% to 45% EtOAc/hexanes gradient) to afford pure organoborane product **2a** (65 mg, 0.22 mmol, 1620 TTN, 55% yield based on the added trifluorodiazo compound **2**). The stereoselectivity of the product was determined as 97:3 e.r. by normal-phase chiral HPLC. $[\alpha]_D^{23}$ = – 12.9 (*c* 0.18, CH_2Cl_2).

Derivatization of Enzymatic Borylation Product 2a to Free Boronic Acid 2c

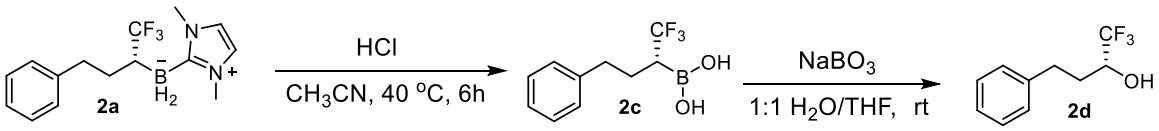

The protocol was modified from ref [12]. To a 4 mL vial with screw cap were added 18 mg enzymatic product **2a** (0.06 mmol) and a stir bar. The vial was evacuated and backfilled with argon for three times. 1.0 mL acetonitrile containing 80 µL of 5M HCl aqueous solution was added to the vial *via* syringe. The resulting solution was stirred for 6 hours at 40 °C. The solvent was then removed under high vacuum followed by addition of 2 mL of diethyl ether. The vial was vortexed for 1 min and the ether solution was passed through a syringe filter to remove the insolubles. The filtrate was dried under vacuum to afford crude **2c**. The yield of **2c** was determined by ^{19}F NMR with fluorobenzene as internal standard (**2c** has a ^{19}F NMR chemical shift at δ -62.3 (d, J = 11.3 Hz)).

The crude **2c** was dissolved in 1:1 THF/H_2O (2 mL) and excess $NaBO_3$•$4H_2O$ (3 eq.) was added to the solution. The reaction was stirred for 4 hours and then extract three times with 5 mL ethylacetate. The combined organic solvent was evaporated and the crude product was purified by flash chromatography (0 - 30% hexanes/EtOAc). 10.0 mg alcohol **2d** was obtained (82% yield). This compound is known (*21*). The specific optical rotation was determined to be $[\alpha]_D^{23}$ = 21.5 (*c* 0.4, $CHCl_3$), suggesting an *R* absolute configuration by comparing with literature values [13]. The e.r. was confirmed by chiral GC with FID detector using a Chirasil-DEX CB column (30.0 m × 0.25 mm) (conditions: 140 °C isothermal at 1.0 mL/min He carrier gas flow). Retention time: 5.20 min for *R* enantiomer, 6.00 min for *S* enantiomer).

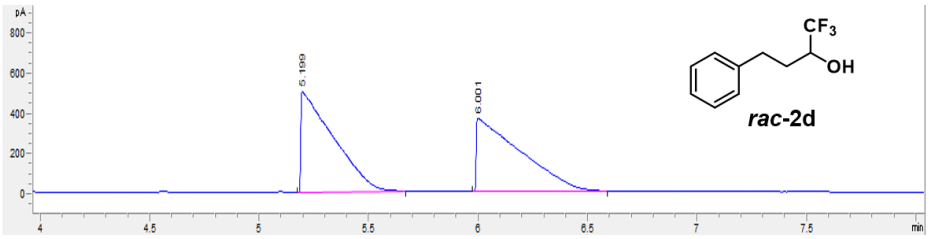

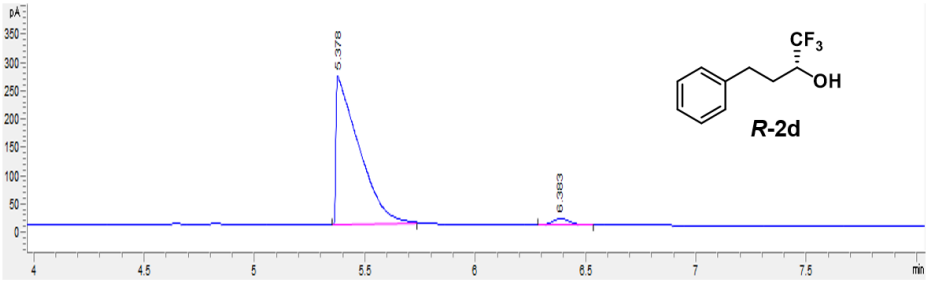

***rac*-2d**			***R*-2d**		
Retention Time (min)	Area (mAu)	Area%	Retention Time (min)	Area (mAu)	Area%
5.20	5107	50.1	5.38	1904	96.8
6.00	5090	49.9	6.38	63	3.2

VIII. Computational Modeling

8.1 Quantum Mechanics (Density Functional Theory) Calculations

DFT calculations were carried out using Gaussian09 [14]. A truncated model containing the porphyrin pyrrole core, Fe center and an imidazole to mimic histidine as Fe-axial ligand was used. Geometry optimizations and frequency calculations were performed using (U)B3LYP [15-17] functional with the SDD basis set for iron and 6-31G(d) on all other atoms. All transition states had one negative force constant corresponding to the desired transformation. All stationary points were verified as minima or first-order saddle points by a vibrational frequency analysis. Enthalpies and entropies were calculated for 1 atm and 298.15 K. A correction to the harmonic oscillator approximation, as discussed by Truhlar and co-workers, was also applied to the entropy calculations by raising all frequencies below 100 cm^{-1} to 100 cm^{-1} [18-19] using Goodvibes v.1.0.1 software [20]. Single point energy calculations were performed using the dispersion-corrected functional (U)B3LYP-D3(BJ) [21-22] with the Def2TZVP basis set on all atoms. The CPCM polarizable conductor model (diethyl ether, $\varepsilon = 4$) [23-24] was used in optimizations and single point calculations to have an estimation of the dielectric permittivity in the enzyme active site. The use of a dielectric constant $\varepsilon=4$ has been proved to be a good and general model to account for electronic polarization and small backbone fluctuations in enzyme active sites [25-26].

The methodology employed in this study, based on the use of (U)B3LYP density functional, is very similar to the one previously used by Shaik group for the study of iron carbene porphyrins [27] and more recently by Luis, Solà, Costas and co-workers to study non-heme iron carbene transfer reactions [28] and has also been tested in our related previous study [29]. (U)B3LYP has also been extensively validated to accurately perform in the computational modeling of iron-oxo chemistry [30-34]. The modeling of the open-shell electronic state was done by a Gaussian09 "stable = opt" calculation [35-37] to generate a singlet open-shell orbital guess from the triplet optimized geometry, followed by a full optimization of the system starting from this guess. All Gibbs energy values discussed in the manuscript and SI correspond to the quasi-harmonic corrected Gibbs energies (ΔG-*qh*) at (U)B3LYP-D3(BJ)/Def2TZVP/PCM(Et_2O) //(U)B3LYP/6-31G(d)+SDD(Fe)/PCM(Et_2O) level, if not otherwise noted. Optimized DFT structures are illustrated with CYLView [38].

8.2 Molecular Dynamics (MD) Simulations

Molecular Dynamics simulations were performed using the GPU code (*pmemd*) [39] of the AMBER 16 package [40]. Parameters for the carbene bound IPC were generated within the *antechamber* and MCPB.py [41] modules in AMBER16 package using the general AMBER force field (*gaff*) [42] with partial charges set to fit the electrostatic potential generated at the B3LYP/6-31G(d) level by the RESP model.[43] The charges were

calculated according to the Merz–Singh–Kollman scheme[44-45] using the Gaussian 09 package [14]. Protonation states of protein residues were predicted using H++ server. Each protein was immersed in a pre-equilibrated truncated cuboid box with a 10 Å buffer of TIP3P [46] water molecules using the *leap* module, resulting in the addition of around 6,400 solvent molecules. The systems were neutralized by addition of explicit counter ions (Na^+ and Cl^-). All subsequent calculations were done using the widely tested Stony Brook modification of the Amber14 force field (*ff14sb*) [47]. A two-stage geometry optimization approach was performed. The first stage minimizes the positions of solvent molecules and ions imposing positional restraints on the solute by a harmonic potential with a force constant of 500 $kcal \cdot mol^{-1} \cdot Å^{-2}$ and the second stage minimizes all the atoms in the simulation cell except those involved in the harmonic distance restraint. The systems were gently heated using six 50 ps steps, incrementing the temperature by 50 K for each step (0–300 K) under constant-volume and periodic-boundary conditions. Water molecules were treated with the SHAKE algorithm such that the angle between the hydrogen atoms was kept fixed. Long-range electrostatic effects were modelled using the particle-mesh-Ewald method [48]. An 8 Å cutoff was applied to Lennard–Jones and electrostatic interactions. Harmonic restraints of 30 $kcal \cdot mol^{-1}$ were applied to the solute and the Andersen equilibration scheme was used to control and equalize the temperature. The time step was kept at 1 fs during the heating stages, allowing potential inhomogeneities to self-adjust. Each system was then equilibrated for 2 ns with a 2 fs time step at a constant volume. Production trajectories were then run for an additional 500 ns under the same simulation conditions. Trajectories were processed and analyzed using the cpptraj [49] module from Ambertools utilities.

Docking calculations were performed using Autodock Vina [50]. Docking predictions were refined by performing constrained molecular simulations: Taking docking structures as a starting points for MD simulations, the distance between the Fe-Porph center and the diazo-C central atom was kept constrained to 3.0-3.4 Å during the MD production run to sample reactant complex conformations that could lead to the carbene forming transition state. Docking calculations were carried out using the most populated cluster structure obtained from MD simulations on the apo state of BOR-CF_3.

8.3 Computational Supporting Figures

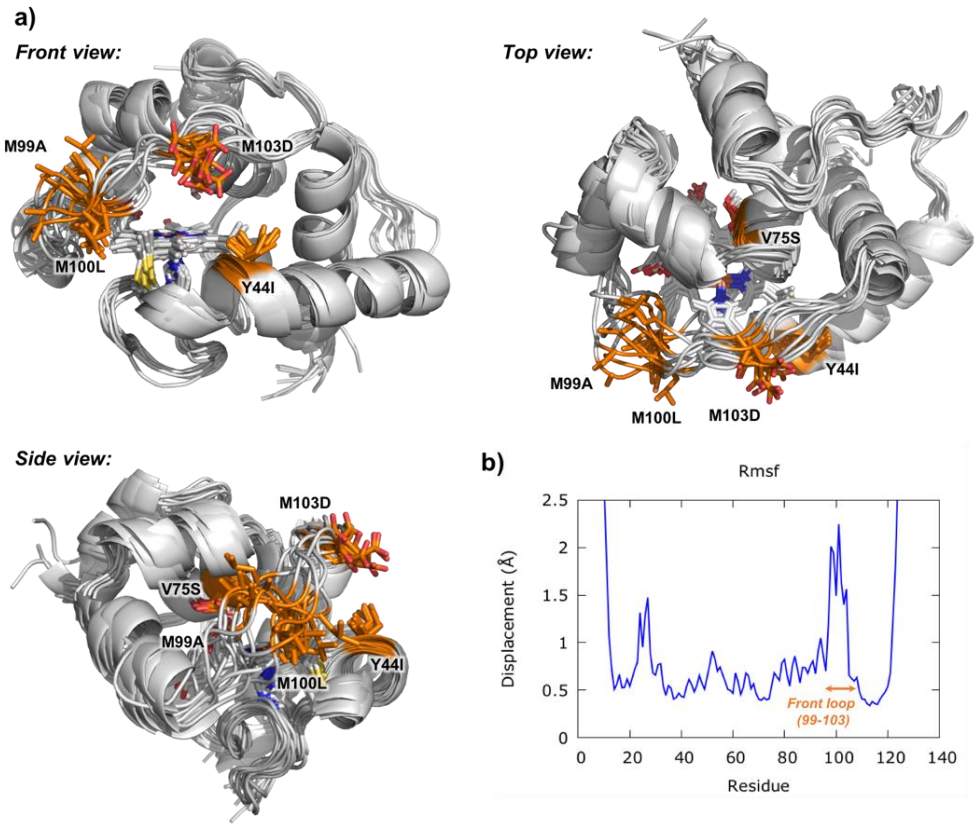

Figure S1. **BOR-CF_3 front loop (residues 99-103) conformational dynamics**. **a**) Overlay of 10 clusters obtained from 500ns MD trajectory on the apo state of BOR-CF_3. **b**) Root-mean square fluctuation (RMSF) measured for each individual Cα during MD trajectory. RMSF measured values describe the large flexibility of the residues on the loop, mainly induced by the newly introduced mutations, becoming especially relevant at M99A and M100L positions.

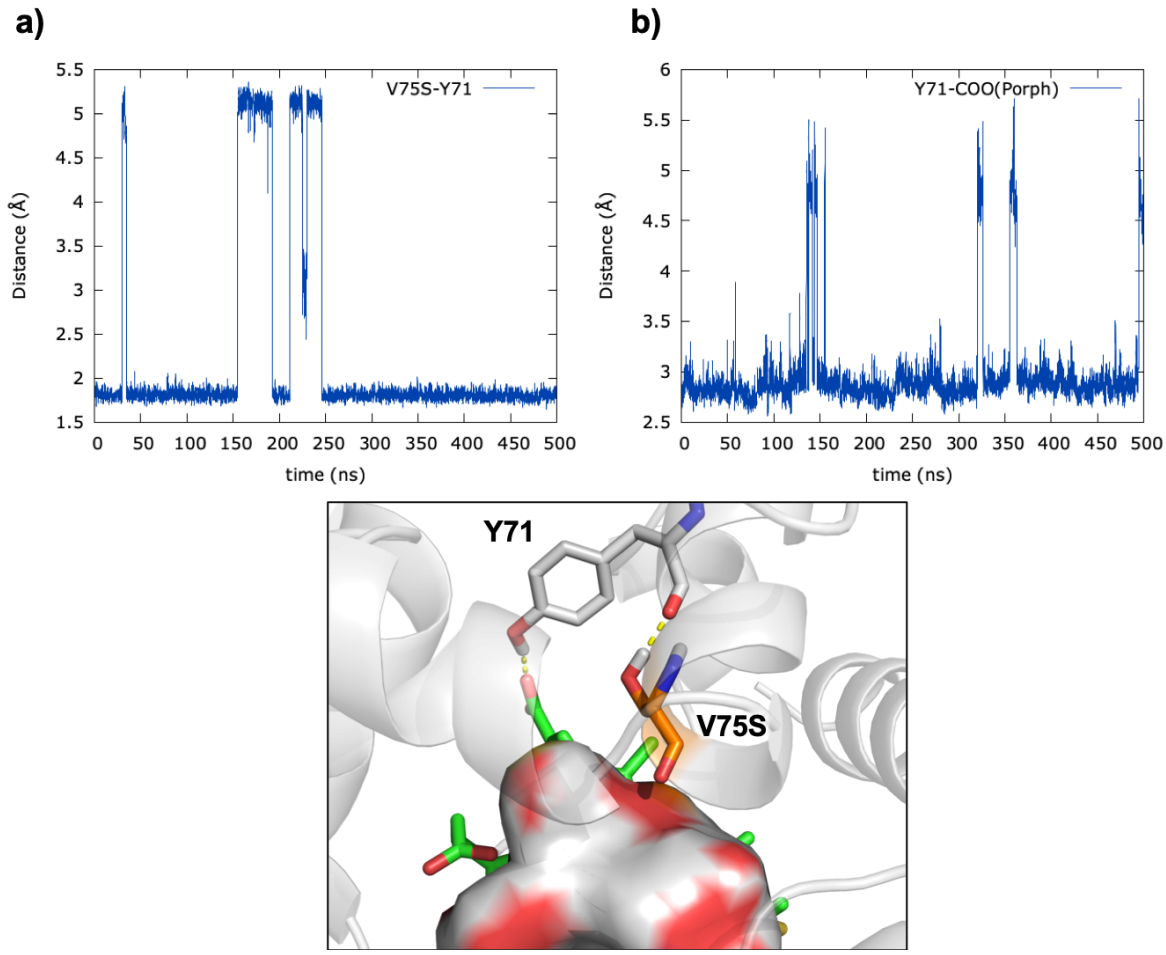

Figure S2. Key interactions of V75S in apo BOR-CF_3. a) H-bond interaction between V75S side chain and Y71 backbone along 500 ns MD trajectory of apo BOR-CF_3. **b**) H-bond interaction between Y71 side chain and heme carboxyl group (centroid between the two O atoms) along 500 ns MD trajectory of apo BOR-CF_3. Both H-bond interactions were kept during the entire trajectory.

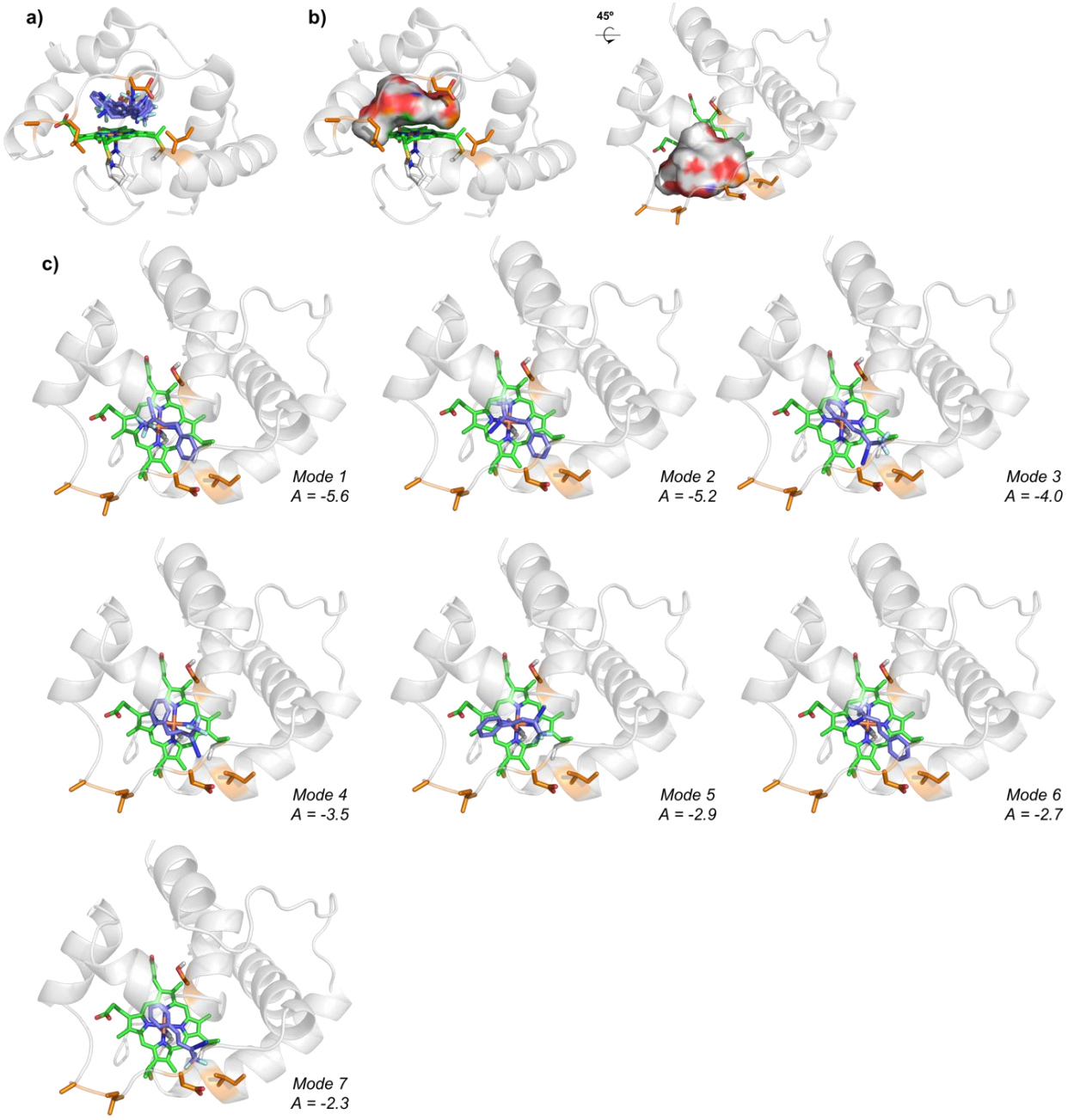

Figure S3. Docking of diazo compound 2 in BOR-CF_3. a) Overlay of the 7 best ranked binding modes predicted by docking simulations of diazo **2** into the heme distal pocket of BOR-CF_3. **b**) Representation of the empty surface area in the most populated cluster obtained from 500 ns MD simulation on apo BOR-CF_3. **c**) Individual top views of the 7 best ranked binding modes predicted by docking simulations of diazo **2** into the heme distal pocket of BOR-CF_3. Mode 1 and 2 were used as starting points for constrained MD simulations (Fe – C(diazo central C) distance was constrained to 3.0-3.4 Å during 500ns MD production run) to better characterize the diazo **2** binding in a catalytically competent pose, as shown in **Figure 4** in the main text.

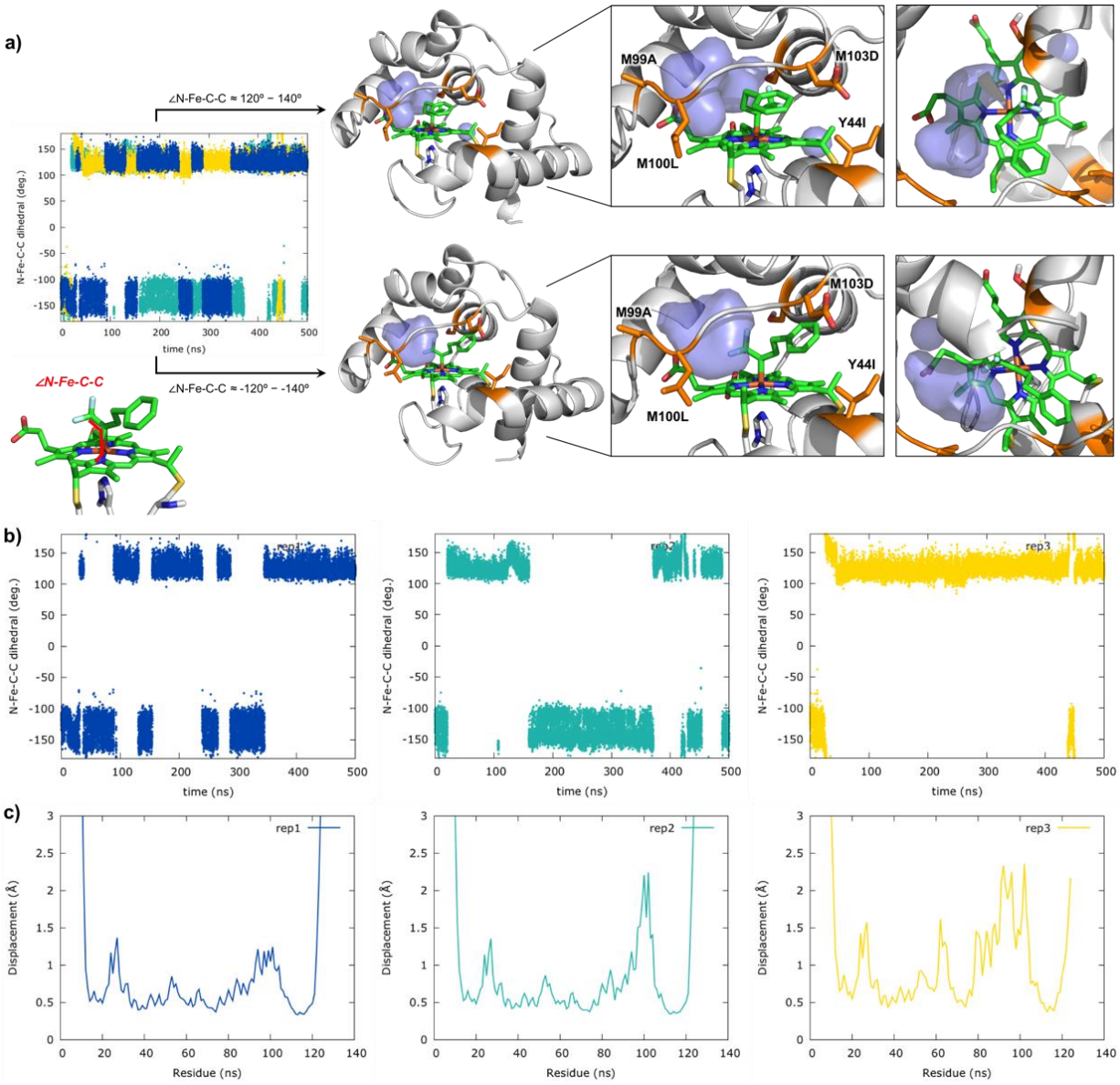

Figure S4. **Conformational analysis of IPC 2b intermediate bound into BOR-CF_3. a**) Conformations explored by IPC **2b** when formed into BOR-CF_3 as function of the defined ∠N(Porph)-Fe-C(carbene)-C(CF_3) dihedral angle, as described in the figure, for three independent 500 ns MD trajectories (replica 1, blue; replica 2, green; replica 3, yellow). Two main conformations are explored, corresponding to dihedral angle values of: Conformer 1 ≈ 110º − 140º; Conformer 2 ≈ -110º − -150º. Both conformations of IPC **2b** generate a new binding pocket for borane **1** (surfaces represented in blue), and they both expose the same face (pro-*R* face) of the carbene intermediate tot the empty volume generated. **b**) Dihedral angle values for ∠N(Porph)-Fe-C(carbene)-C(CF_3) explored during each independent MD replica (replica 1, blue; replica 2, green; replica 3, yellow). **c**) Root-mean square fluctuation (RMSF) measured for each individual Cα during each independent MD replicas (replica 1, blue; replica 2, green; replica 3, yellow). RMSF values indicate a large flexibility of the residues on the loop, even when the carbene intermediate is formed, as observed in the BOR-CF_3 apo state.

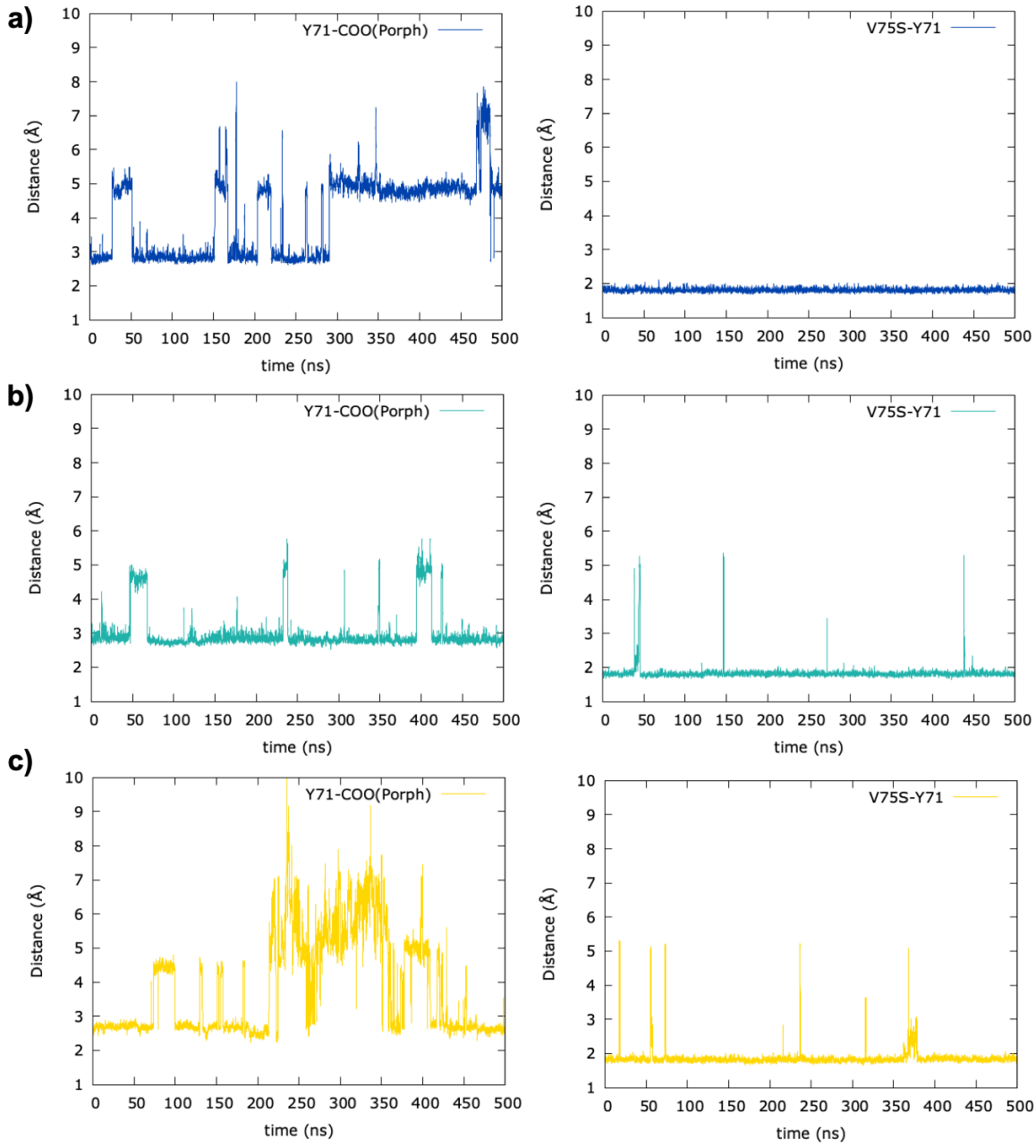

Figure S5. **Key interactions of V75S in IPC 2b intermediate bound into BOR-CF$_3$.** H-bond interaction between V75S side chain and Y71 backbone, and between Y71 side chain and heme carboxyl group (centroid between the two O atoms) along 3 independent 500 ns MD trajectories: **a**) replica 1, blue; **b**) replica 2, green; **c**) replica 3, yellow. Both H-bond interactions are maintained during most of the time along the trajectories.

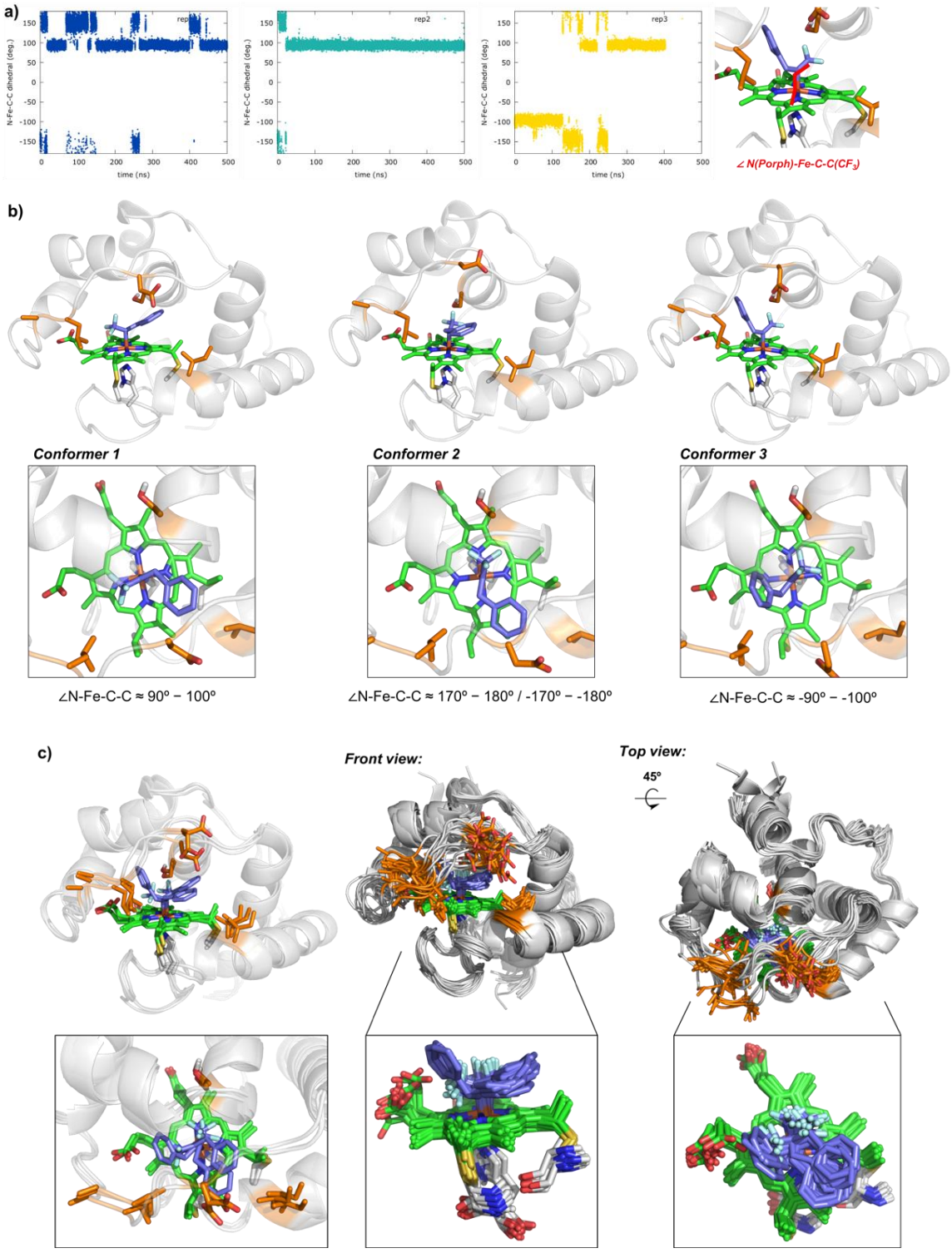

Figure S6. **Conformational analysis of IPC 9b intermediate bound into BOR-CF_3. a)** Conformations explored by IPC **9b** when formed into BOR-CF_3 as function of the defined ∠N(Porph)-Fe-C(carbene)-C(CF_3) dihedral angle, as described in the figure, for three independent 500 ns MD trajectories (replica 1, blue; replica 2, green; replica 3, yellow). 3 main conformations are explored by **9b** IPC, corresponding to dihedral angle values of: Conformer 1 ≈ 90º – 100º; Conformer 2 ≈ 150º – 180º / -150º – -180º; Conformer 3 ≈ -90º – -100º. **b)** Representative

snapshots for the three main conformers explored by **9b** IPC during MD simulations. **c**) Overlay of representative snapshots shown in b) (left), and a set of randomly selected snapshots (right) from replica 3 MD trajectory (1 snapshot every 30 ns). As opposite to **2b** IPC (Figure S4), a conformation with ∠N-Fe-C-C(CF_3) dihedral angle around 90º − 100º (Conformer 1) seems to be preferred by **9b** IPC. In this conformation, CF_3 group is no longer pointing to V75S position. On the contrary, it is occupying the position where borane **1** was proposed to bind in, presumably hampering the interaction between the borane and the carbene C center. Conformer 2, with ∠N-Fe-C-C(CF_3) ≈ 150º − 180º / -150º − -180º, encompasses equivalent conformations characterized for IPC **2b** (Figure S4), although they are poorly visited along the three independent replicas. Finally, in Conformer 3 (∠N-Fe-C-C(CF_3) ≈ -90º − -100º) benzyl R group occupies the proposed binding site for borane **1**, totally blocking its possible binding. This larger conformational flexibility observed for IPC **9b**, in contrast to the fixed conformation kept by phenylethyl R group in IPC **2b** (Figure S4) during MD simulations, is mainly due to the reduced chain length that is not locked in a single conformation when IPC 9b is formed, and allows it to mainly explore catalytically unproductive conformations (conformers 1 and 3). Based on these results, the low activity exhibited by diazo **9** might be attributed to these catalytically unfavorable preferred conformations of IPC **9b**.

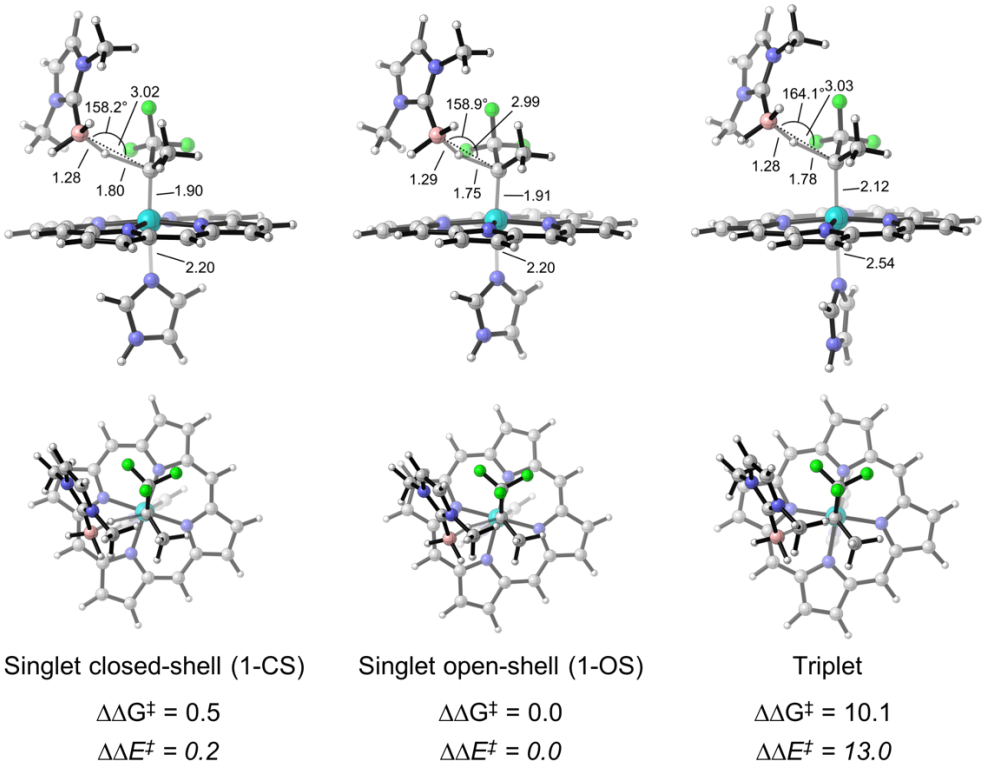

Figure S7. **DFT modeling of the B–H carbene insertion TS (TS-CB)**. DFT optimized transition state (TS) structures for B-H carbene insertion using a truncated model system and considering different electronic states. Key distances, angles and dihedrals are given in angstrom (Å) and degrees (º), respectively. $\Delta\Delta E^{‡}$ and $\Delta\Delta G^{‡}$ values (quasi-harmonic corrected), given in kcal·mol^{-1}, are obtained at (U)B3LYP-D3(BJ)/Def2TZVP/PCM(diethyl ether)//(U)B3LYP/6-31G(d)+SDD(Fe)/PCM(diethyl ether) level. Calculations suggest that singlet open-shell (1-OS) and singlet closed-shell (1-CS) TSs are intrinsically almost isoenergetic, and share very similar structural parameters. Optimized triplet TS is much higher in energy (ca. 10 kcal·mol^{-1}). DFT optimized TS structures correspond all to *early*-TSs, as compared to the previously reported *late*-TS for CuCl-catalyzed B–H carbene insertions (*J. Am. Chem Soc.* **2017**, *139*, 3784-3789).

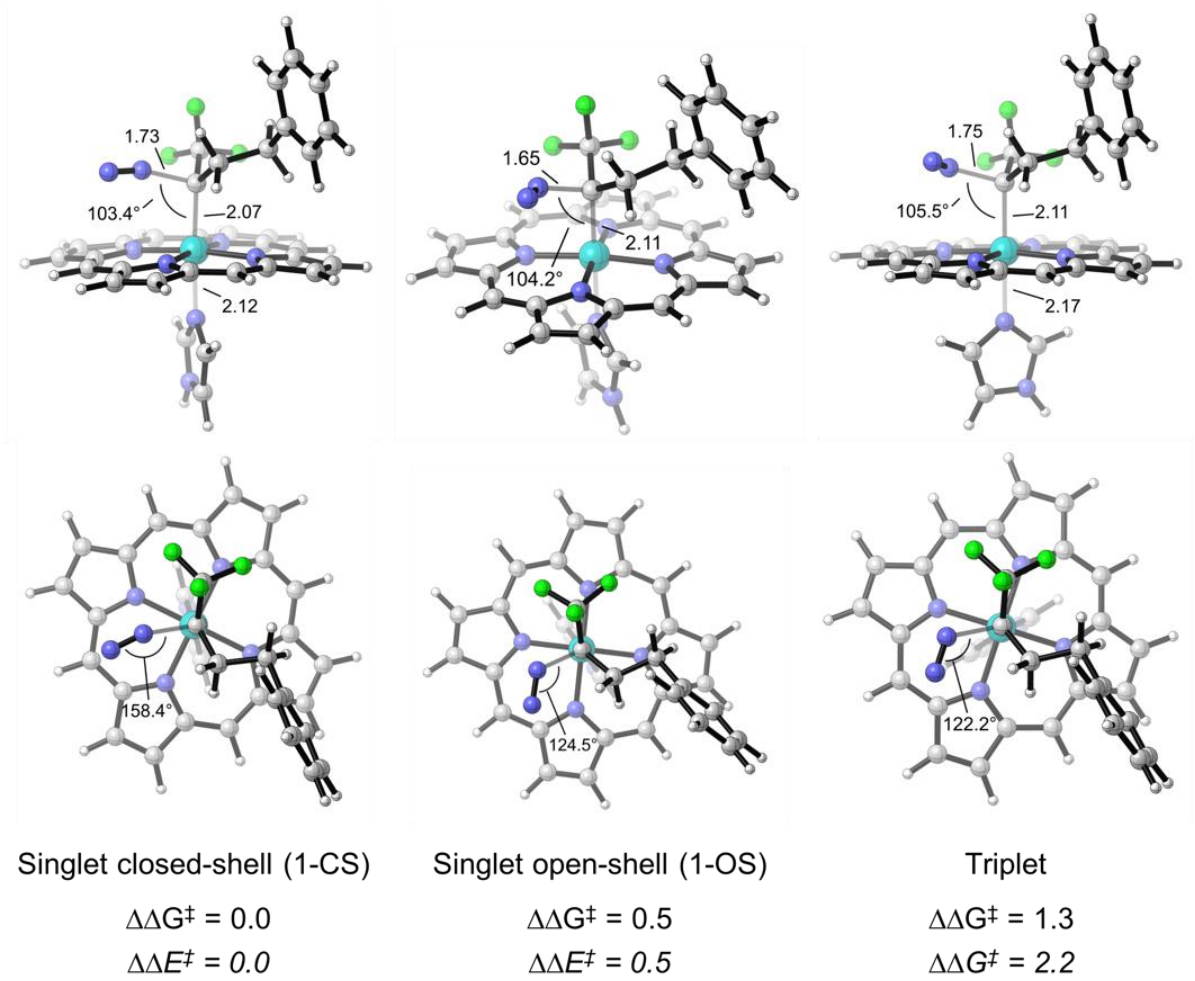

Figure S8. **DFT modeling of the carbene forming TS (TS-carbene)**. DFT optimized transition state (TS) structures for carbene formation from diazo **2b** using a truncated model system and considering different electronic states. Key distances, angles and dihedrals are given in angstrom (Å) and degrees (º), respectively. $\Delta\Delta E^{‡}$ and $\Delta\Delta G^{‡}$ values (quasi-harmonic corrected), given in kcal·mol^{-1}, are obtained at (U)B3LYP-D3(BJ)/Def2TZVP/PCM(diethyl ether)//(U)B3LYP/6-31G(d)+SDD(Fe)/PCM(diethyl ether) level. Calculations indicate that singlet closed-shell (1-CS) and singlet open-shell (1-OS) structures are intrinsically almost isoenergetic, while triplet TS is only 1 kcal·mol^{-1} higher in energy. Structurally, 1-OS and triplet optimized TSs are very similar.

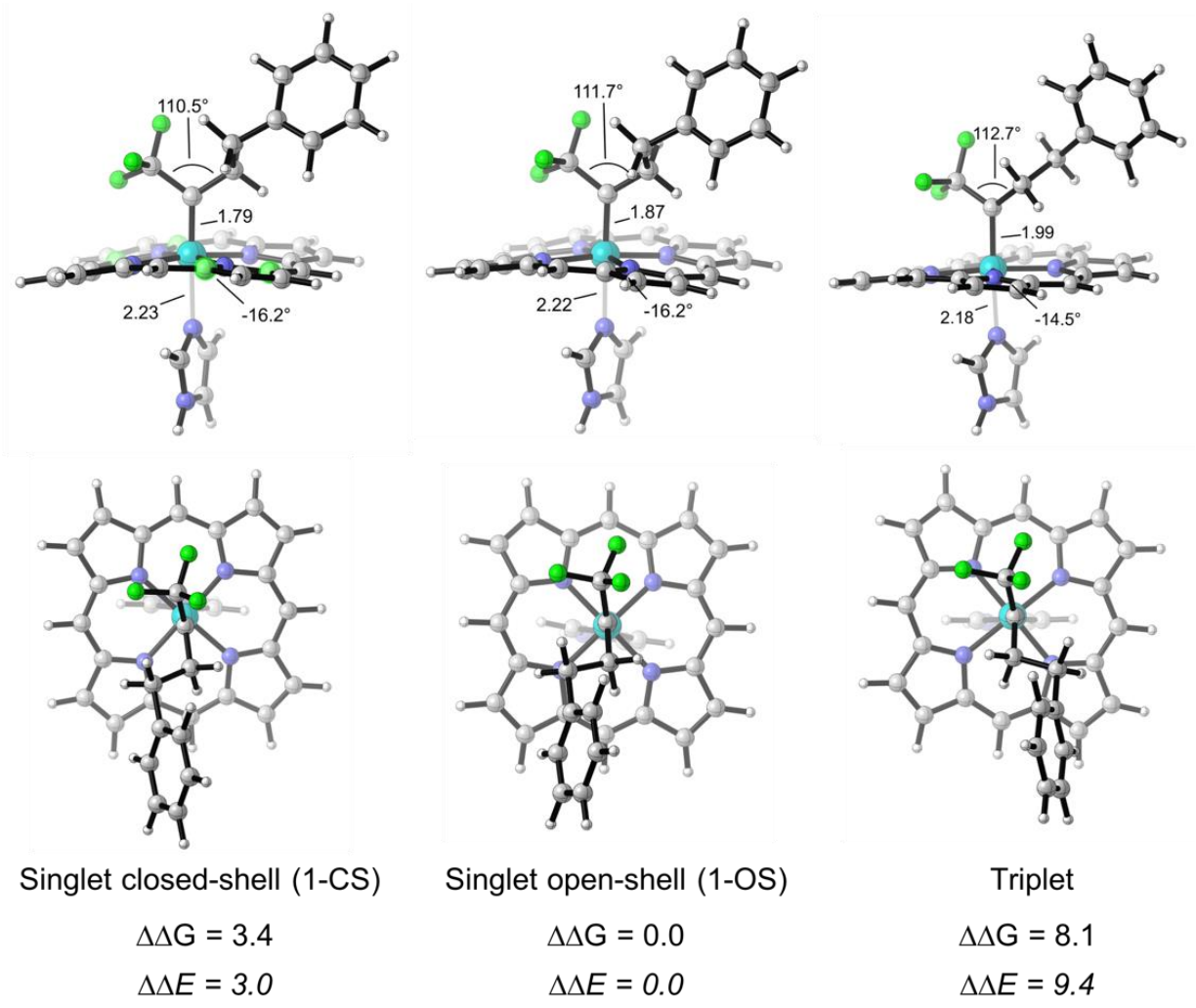

Figure S9. **DFT modeling of the 2b iron porphyrin carbene (IPC) intermediate**. DFT optimized structures for **2b** IPC using a truncated model system and considering different electronic states. Key distances, angles and dihedrals are given in angstrom (Å) and degrees (º), respectively. $\Delta\Delta E^{\ddagger}$ and $\Delta\Delta G^{\ddagger}$ values (quasi-harmonic corrected), given in kcal·mol^{-1}, are obtained at (U)B3LYP-D3(BJ)/Def2TZVP/PCM(diethyl ether)//(U)B3LYP/6-31G(d)+SDD(Fe)/PCM(diethyl ether) level. Calculations indicate that singlet open-shell (1-OS) is >3 kcal·mol^{-1} more stable than the singlet closed-shell (1-CS) and >8 kcal·mol^{-1} than triplet. Structurally, the three optimized structures are very similar, with Fe–C bond lengths increasing from 1-CS < 1-OS < Triplet.

8.4 Energies of all DFT optimized structures

Electronic energies (*E*), zero point energy (*ZPE*), free energy (*G*(T)), quasiharmonic corrected free energy (*qh*-*G*(T)), and electronic energy from high level single point calculation (*E* Single point) of all stationary points (in a.u.).

Structure	***E* (au)**	***ZPE* (au)**	***G*(T) (au)**	***qh*-*G*(T) (au)**	***E* Single Point (au)**
TS-CB (1-CS)	-2085.673518	0.568053	-2085.175561	-2085.167683	-3226.489299
TS-CB (1-OS)	-2085.673640	0.567428	-2085.176110	-2085.168396	-3226.489539
TS-CB (Triplet)	-2085.654096	0.565114	-2085.163395	-2085.153427	-3226.468817
TS-carbene (1-CS)	-2134.016786	0.525530	-2133.559733	-2133.551810	-3274.849364
TS-carbene (1-OS)	-2134.018972	0.525449	-2133.562170	-2133.553877	-3274.848642
TS-carbene (Triplet)	-2134.016453	0.525253	-2133.560957	-2133.552965	-3274.845807
IPC 2b (1-CS)	-2024.541500	0.518244	-2024.090433	-2024.081742	-3165.318420
IPC 2b (1-OS)	-2024.548166	0.517815	-2024.097346	-2024.088967	-3165.323247
IPC 2b (Triplet)	-2024.533122	0.517046	-2024.085063	-2024.075933	-3165.308332

8.5 Cartesian coordinates of DFT optimized structures (in xyz format)

TS-CB (1-CS)

Fe	0.96011	0.06265	-0.02341
N	1.10778	-1.85541	0.64908
N	0.06161	0.59174	1.71039
N	2.11459	-0.43191	-1.62401
N	1.05674	2.01368	-0.56803
C	1.68216	-2.91589	-0.00256
C	-0.33066	1.85252	2.07890
C	0.68145	-2.33913	1.85849
C	-0.21579	-0.22149	2.77971
C	2.53102	-1.68950	-1.98199
C	0.50163	3.07926	0.09327
C	2.61180	0.42118	-2.57576
C	1.70274	2.53769	-1.65888
C	1.59186	-4.11287	0.80735
C	-0.89504	1.83388	3.41179
C	0.97518	-3.75270	1.96680
C	-0.82029	0.54500	3.84887
C	3.29806	-1.63156	-3.20920
C	0.77837	4.31083	-0.61684
C	3.35347	-0.32061	-3.57407
C	1.52761	3.97497	-1.70302
H	1.97014	-5.08581	0.51762
H	-1.27679	2.70311	3.93388
H	0.74054	-4.36920	2.82621
H	-1.12838	0.13703	4.80420
H	3.74110	-2.48857	-3.70200
H	0.44570	5.29311	-0.30385
H	3.84890	0.12088	-4.43039
H	1.93697	4.62424	-2.46756
C	2.31532	-2.85068	-1.24223
C	-0.15527	3.00724	1.31861
C	2.43000	1.80227	-2.59298
C	0.06643	-1.58394	2.85282
H	2.72098	-3.77589	-1.64250
H	-0.52814	3.93778	1.73732
H	2.88837	2.35281	-3.41003
H	-0.21013	-2.09931	3.76883
C	3.17237	1.46766	1.74092
C	3.96665	-0.42771	1.07764
C	4.95141	0.15512	1.83130
N	2.86187	0.39912	1.02759
N	4.42794	1.36293	2.24694
H	5.94526	-0.16551	2.10239
H	3.97435	-1.37905	0.56923
H	2.53032	2.31785	1.91080
H	4.89202	2.05050	2.82331
C	-0.60905	-0.24191	-1.05283
C	-1.52549	-1.44677	-0.84925
H	-1.92201	0.83035	-0.45861
B	-2.96446	1.57586	-0.50767
H	-2.86410	2.34427	0.42192
H	-2.93931	2.12706	-1.58526
C	-5.88671	-0.57745	0.62549
C	-6.17457	-0.48003	-0.69834
H	-6.40353	-1.07920	1.42829
H	-6.99235	-0.87964	-1.27703
C	-4.27221	0.67698	-0.32948
N	-4.72405	0.14122	0.83469
N	-5.17981	0.29595	-1.26770
C	-4.03660	0.24772	2.11952
H	-3.19652	-0.44821	2.15322
H	-3.65602	1.26080	2.24434
H	-4.74662	0.01519	2.91504
C	-5.09058	0.56411	-2.70044
H	-6.09586	0.71899	-3.09792
H	-4.48955	1.45770	-2.85616
H	-4.62069	-0.28184	-3.20995
C	-0.69205	0.20796	-2.49182
F	-0.90406	-2.56147	-1.31869
F	-1.87017	-1.68467	0.43298
F	-2.70860	-1.40152	-1.53889
H	-0.06659	-0.47902	-3.08039
H	-1.70217	0.17936	-2.90606
H	-0.27704	1.20715	-2.61363

TS-CB (1-OS)

Fe	0.95761	0.06387	-0.02251
N	1.11279	-1.85044	0.65734
N	0.06734	0.59757	1.71371
N	2.10262	-0.43429	-1.62755
N	1.04490	2.01201	-0.57689
C	1.68632	-2.91220	0.00703
C	-0.32387	1.85950	2.08014
C	0.69217	-2.33098	1.87018
C	-0.20492	-0.21230	2.78735
C	2.52051	-1.69241	-1.98216
C	0.49262	3.07923	0.08408
C	2.59011	0.41524	-2.58770
C	1.67887	2.53266	-1.67665
C	1.60186	-4.10638	0.82152
C	-0.88196	1.84485	3.41552
C	0.98904	-3.74340	1.98213
C	-0.80508	0.55725	3.85628
C	3.27860	-1.63845	-3.21495
C	0.75870	4.30790	-0.63484
C	3.32694	-0.32926	-3.58719
C	1.49834	3.96882	-1.72661
H	1.98071	-5.07957	0.53344
H	-1.26177	2.71558	3.93650
H	0.75887	-4.35734	2.84456
H	-1.10879	0.15223	4.81424
H	3.72066	-2.49667	-3.70648
H	0.42566	5.29065	-0.32376
H	3.81431	0.10931	-4.44959
H	1.89817	4.61540	-2.49843
C	2.31299	-2.85079	-1.23595
C	-0.15410	3.01166	1.31494
C	2.40222	1.79525	-2.61207
C	0.07967	-1.57384	2.86438
H	2.71877	-3.77664	-1.63453
H	-0.52531	3.94336	1.73254
H	2.85191	2.34295	-3.43581
H	-0.19244	-2.08651	3.78319
C	3.17737	1.47870	1.72817
C	3.97549	-0.41367	1.06046
C	4.96245	0.17365	1.80771
N	2.86700	0.40856	1.01715
N	4.43650	1.37939	2.22622
H	5.95936	-0.14264	2.07260
H	3.98399	-1.36515	0.55232
H	2.53280	2.32626	1.90170
H	4.90137	2.06912	2.79937
C	-0.62819	-0.24910	-1.04529
C	-1.53008	-1.45945	-0.82936
H	-1.89941	0.80745	-0.47699
B	-2.94486	1.56438	-0.51676
H	-2.82754	2.32814	0.41333

H	-2.91787	2.11336	-1.59483
C	-5.87814	-0.56320	0.63213
C	-6.16433	-0.47460	-0.69278
H	-6.39843	-1.05594	1.43823
H	-6.98367	-0.87455	-1.26903
C	-4.25606	0.67475	-0.33126
N	-4.71192	0.15072	0.83695
N	-5.16526	0.29155	-1.26729
C	-4.02573	0.26340	2.12198
H	-3.18655	-0.43331	2.16011
H	-3.64429	1.27673	2.24233
H	-4.73697	0.03567	2.91777
C	-5.07287	0.54781	-2.70194
H	-6.07771	0.69536	-3.10321
H	-4.47499	1.44244	-2.86397
H	-4.59824	-0.30061	-3.20279
C	-0.70244	0.17217	-2.49594
F	-0.90823	-2.57797	-1.29039
F	-1.86972	-1.68841	0.45709
F	-2.71789	-1.42739	-1.51419
H	-0.08451	-0.52891	-3.07491
H	-1.71358	0.14589	-2.90883
H	-0.28220	1.16687	-2.63594

TS-CB (Triplet)

Fe	-0.98043	0.01898	0.07349
N	-0.92932	-1.51476	-1.24251
N	-0.22314	1.26519	-1.34127
N	-1.98983	-1.15963	1.36978
N	-1.34867	1.63576	1.25454
C	-1.37750	-2.79931	-1.04674
C	-0.00615	2.61560	-1.23058
C	-0.42628	-1.47857	-2.52029
C	0.19118	0.91787	-2.60012
C	-2.28706	-2.49348	1.22692
C	-0.96872	2.93611	1.02372
C	-2.52886	-0.77902	2.57492
C	-1.96909	1.63197	2.47920
C	-1.14051	-3.59679	-2.22569
C	0.57912	3.13349	-2.44849
C	-0.55067	-2.77598	-3.14114
C	0.69837	2.07881	-3.30157
C	-3.00112	-2.97596	2.38782
C	-1.35623	3.77416	2.13427
C	-3.15267	-1.91179	3.22334
C	-1.97986	2.96443	3.03742
H	-1.40489	-4.64206	-2.32786
H	0.84288	4.17075	-2.61425
H	-0.23087	-3.01091	-4.14906
H	1.07871	2.07064	-4.31591
H	-3.34751	-3.99353	2.51977
H	-1.17235	4.83953	2.19822
H	-3.64835	-1.87470	4.18570
H	-2.41193	3.23033	3.99447
C	-1.99712	-3.26578	0.10799
C	-0.33659	3.39589	-0.12791
C	-2.51685	0.51022	3.09800
C	0.10498	-0.35766	-3.15115
H	-2.30080	-4.30839	0.12687
H	-0.10082	4.45493	-0.17726
H	-2.98442	0.65635	4.06757
H	0.46185	-0.48508	-4.16937
C	-3.99242	1.58075	-0.68707
C	-3.92295	-0.18111	-1.92365
C	-5.09530	0.45689	-2.24092
N	-3.24342	0.52730	-0.95416
N	-5.12478	1.58154	-1.44146
H	-5.88727	0.22651	-2.93694
H	-3.52153	-1.09933	-2.32671
H	-3.75853	2.35361	0.03007
H	-5.85443	2.28021	-1.41915
C	0.87061	-0.36656	1.04070
C	1.71209	-1.51662	0.53697
H	2.17114	0.82451	0.81654
B	3.21860	1.55219	0.96659
H	3.01913	2.55237	0.30666
H	3.32604	1.77493	2.15385
C	5.92598	-0.21481	-1.03194
C	6.32854	-0.52328	0.22781
H	6.34514	-0.46987	-1.99241
H	7.16834	-1.09972	0.58232
C	4.46893	0.74696	0.40094
N	4.79142	0.56728	-0.90804
N	5.43064	0.07808	1.09359
C	3.99478	1.05417	-2.03065
H	3.13999	0.39482	-2.19421
H	3.62800	2.05539	-1.80628
H	4.62410	1.07874	-2.92233
C	5.46905	-0.08523	2.54376
H	6.50024	-0.27234	2.84928
H	5.10152	0.82308	3.01872
H	4.83896	-0.92746	2.84214
C	0.84465	-0.37043	2.55214
F	1.07014	-2.71184	0.67063
F	2.05963	-1.40935	-0.77116
F	2.89930	-1.67941	1.20497
H	0.20441	-1.18673	2.91374
H	1.83935	-0.52573	2.98231
H	0.43628	0.56492	2.93845

TS-carbene (1-CS)

Fe	-0.88070	0.17471	0.06929
N	-1.49500	-1.35564	1.25637
N	-2.35211	-0.29713	-1.25507
N	0.43472	0.77518	1.49570
N	-0.40710	1.81700	-1.03182
C	-1.01865	-1.65695	2.50653
C	-2.72572	0.43234	-2.35630
C	-2.48384	-2.26909	0.99635
C	-3.23470	-1.34733	-1.17886
C	0.62550	0.19225	2.72299
C	-1.03848	2.24883	-2.17194
C	1.24704	1.87955	1.46578
C	0.54251	2.76746	-0.74167
C	-1.71025	-2.81138	3.04291
C	-3.85048	-0.19532	-3.01695
C	-2.61929	-3.19287	2.10414
C	-4.16339	-1.30303	-2.28834
C	1.60085	0.94175	3.48667
C	-0.44240	3.48253	-2.63976
C	1.98714	1.99033	2.70600
C	0.54321	3.80130	-1.75554
H	-1.51780	-3.25173	4.01372
H	-4.32859	0.17908	-3.91396
H	-3.32899	-4.01026	2.14493
H	-4.95409	-2.02283	-2.46205
H	1.92759	0.69148	4.48857
H	-0.75560	4.02414	-3.52399
H	2.68997	2.78108	2.93938
H	1.20222	4.66096	-1.76173
C	-0.03188	-0.94693	3.18594
C	-2.11588	1.61030	-2.78688
C	1.32710	2.79027	0.41105

C	-3.28681	-2.27901	-0.14361
H	0.23388	-1.29893	4.17907
H	-2.51806	2.07510	-3.68281
H	2.02528	3.61562	0.51962
H	-4.04176	-3.05739	-0.21330
C	-3.53446	1.00300	1.42172
C	-2.18485	2.69158	1.46882
C	-3.34227	3.11017	2.06939
N	-2.31470	1.37522	1.06854
N	-4.19043	2.02233	2.03002
H	-3.63256	4.05184	2.50845
H	-1.27300	3.24072	1.29807
H	-3.96793	0.02960	1.25631
H	-5.13387	1.98490	2.38898
C	0.59599	-0.96335	-0.83473
C	0.54877	-2.50136	-0.81020
C	2.07165	-0.48832	-0.89961
F	0.74958	-2.94246	0.44537
F	-0.61557	-3.00706	-1.25597
F	1.51614	-3.08728	-1.58072
H	2.53456	-0.81688	-1.83643
H	2.08027	0.60140	-0.89297
N	0.23490	-0.82050	-2.52517
N	0.02229	-0.32760	-3.49711
C	2.99082	-1.01185	0.23907
H	2.62303	-0.66620	1.20674
H	2.97681	-2.10424	0.25535
C	4.41765	-0.54757	0.01612
C	4.92138	0.59574	0.65077
C	5.26307	-1.25537	-0.85199
C	6.23248	1.02222	0.42366
H	4.28101	1.14843	1.33330
C	6.57295	-0.83239	-1.08316
H	4.89046	-2.15031	-1.34665
C	7.06258	0.31069	-0.44521
H	6.60617	1.90908	0.92944
H	7.21273	-1.39783	-1.75594
H	8.08319	0.64039	-0.62072

TS-carbene (1-OS)

Fe	-0.89403	0.16922	0.04807
N	-1.57170	-1.35045	1.20441
N	-2.33064	-0.27169	-1.29447
N	0.38992	0.74289	1.50276
N	-0.37320	1.81471	-1.00364
C	-1.12265	-1.67136	2.46094
C	-2.63463	0.45150	-2.42175
C	-2.56796	-2.24996	0.91790
C	-3.22205	-1.32043	-1.26621
C	0.54824	0.13523	2.72480
C	-0.95231	2.24531	-2.17170
C	1.22660	1.83258	1.50739
C	0.58659	2.75090	-0.69033
C	-1.84292	-2.81414	2.97225
C	-3.72514	-0.17092	-3.13506
C	-2.73993	-3.17426	2.01282
C	-4.08553	-1.27298	-2.42129
C	1.51904	0.85329	3.51458
C	-0.32321	3.46566	-2.62122
C	1.94052	1.90770	2.75857
C	0.63537	3.77619	-1.70576
H	-1.67465	-3.26428	3.94258
H	-4.14754	0.20297	-4.05923
H	-3.46261	-3.98027	2.03105
H	-4.86872	-1.98973	-2.63376
H	1.82323	0.57781	4.51653
H	-0.59440	4.00099	-3.52244
H	2.65575	2.67919	3.01521
H	1.31199	4.62136	-1.69531
C	-0.13702	-0.99234	3.16688
C	-2.00585	1.62154	-2.83097
C	1.34478	2.76052	0.47469
C	-3.33578	-2.25161	-0.24220
H	0.10573	-1.36063	4.15912
H	-2.36195	2.08274	-3.74695
H	2.05705	3.56934	0.60496
H	-4.09366	-3.02215	-0.34401
C	-2.19104	2.64683	1.45077
C	-3.66663	1.06294	1.37214
C	-4.27456	2.12578	1.98338
N	-2.36664	1.39861	1.04421
N	-3.32056	3.12273	2.02449
H	-5.26777	2.26203	2.38143
H	-4.06892	0.08858	1.14642
H	-1.28447	3.22193	1.34939
H	-3.43820	4.04788	2.41397
C	0.58199	-0.98051	-0.92662
C	0.51236	-2.49279	-0.76331
C	2.05469	-0.50644	-0.87493
F	0.73080	-2.89179	0.51467
F	-0.65763	-3.03717	-1.15316
F	1.47124	-3.12833	-1.50990
H	2.53307	-0.81145	-1.81384
H	2.06858	0.58393	-0.87490
N	0.17416	-0.89389	-2.52019
N	0.63046	-0.13840	-3.27488
C	2.96740	-1.02194	0.26636
H	2.60222	-0.68129	1.23757
H	2.95430	-2.11474	0.28428
C	4.39831	-0.56250	0.05634
C	4.92379	0.54215	0.74028
C	5.23050	-1.23559	-0.85218
C	6.23798	0.96520	0.52318
H	4.29715	1.06897	1.45543
C	6.54318	-0.81683	-1.07441
H	4.84331	-2.10059	-1.38707
C	7.05275	0.28807	-0.38643
H	6.62600	1.82228	1.06845
H	7.17000	-1.35584	-1.78045
H	8.07567	0.61442	-0.55520

TS-carbene (Triplet)

Fe	-0.90124	0.13843	0.09291
N	-1.56113	-1.60537	0.86816
N	-2.31160	0.06010	-1.35302
N	0.35647	0.31444	1.66410
N	-0.39423	1.98265	-0.56139
C	-1.08596	-2.27063	1.97433
C	-2.56706	0.98881	-2.33435
C	-2.59867	-2.36467	0.38703
C	-3.23597	-0.93916	-1.52875
C	0.57203	-0.59000	2.67752
C	-0.89592	2.66179	-1.64625
C	1.13346	1.40798	1.95768
C	0.50747	2.83221	0.03260
C	-1.83049	-3.48783	2.18373
C	-3.66098	0.54910	-3.16677
C	-2.77373	-3.54295	1.20225
C	-4.07809	-0.64596	-2.66545
C	1.52163	-0.06032	3.62480
C	-0.27116	3.95773	-1.75756
C	1.86425	1.18344	3.18234
C	0.59758	4.06500	-0.71440

H	-1.64906	-4.19058	2.98719
H	-4.05059	1.10060	-4.01305
H	-3.52539	-4.30324	1.03078
H	-4.88231	-1.28117	-3.01496
H	1.86183	-0.57868	4.51236
H	-0.48855	4.68098	-2.53327
H	2.54181	1.89690	3.63470
H	1.24324	4.89491	-0.45613
C	-0.07623	-1.81363	2.81243
C	-1.90541	2.20108	-2.48473
C	1.21472	2.57409	1.20169
C	-3.38128	-2.06082	-0.72131
H	0.19498	-2.43551	3.65994
H	-2.21111	2.84382	-3.30416
H	1.88394	3.35091	1.55860
H	-4.16842	-2.76199	-0.98126
C	-2.68542	0.80377	2.58161
C	-3.21919	2.16810	0.98578
C	-4.01831	2.48825	2.04982
N	-2.39156	1.11576	1.32867
N	-3.66376	1.61024	3.05456
H	-4.78341	3.23691	2.18283
H	-3.18133	2.61557	0.00567
H	-2.22373	0.02051	3.16173
H	-4.06297	1.57006	3.98217
C	0.60266	-0.72937	-1.11335
C	0.54270	-2.23273	-1.31254
C	2.06106	-0.25839	-0.94686
F	0.77894	-2.92812	-0.16832
F	-0.63414	-2.67691	-1.80090
F	1.49176	-2.66697	-2.20040
H	2.54006	-0.31624	-1.93179
H	2.06049	0.79991	-0.68028
N	0.19902	-0.28576	-2.75300
N	0.71977	0.58796	-3.30018
C	2.99196	-1.02139	0.03173
H	2.62461	-0.93820	1.05686
H	2.99982	-2.08464	-0.22141
C	4.41101	-0.49318	-0.05821
C	4.89480	0.46843	0.83966
C	5.27262	-0.94844	-1.06855
C	6.19753	0.96244	0.73255
H	4.24425	0.82615	1.63386
C	6.57445	-0.45774	-1.18135
H	4.91714	-1.69941	-1.77136
C	7.04258	0.50179	-0.27939
H	6.55331	1.70487	1.44291
H	7.22492	-0.82787	-1.96992
H	8.05693	0.88321	-0.36279
C	-1.02550	3.77218	-1.31061
C	2.17451	-3.02714	2.54807
C	3.18316	0.08150	-3.56820
C	3.12452	-3.11292	1.57557
C	3.86414	-0.84955	-2.84505
H	-1.63841	-0.08105	4.63356
H	-0.33831	3.96975	-3.39697
H	-2.42472	2.27060	3.53715
H	-1.66322	4.62778	-1.12577
H	2.07552	-3.62056	3.44863
H	3.39063	0.44474	-4.56714
H	3.96202	-3.79650	1.51006
H	4.74135	-1.41656	-3.13133
C	0.27319	-1.43969	2.97993
C	1.25195	1.60613	-3.05274
C	3.53230	-1.87518	-0.57562
C	-1.27355	2.67677	0.93966
H	0.06912	-1.96438	3.90886
H	1.35471	2.04223	-4.04217
H	4.40604	-2.49680	-0.74876
H	-1.93373	3.48510	1.24033
C	2.83642	1.31571	2.13829
C	3.01461	2.48242	0.32931
C	3.89540	3.03021	1.22467
N	2.36035	1.41455	0.90954
N	3.76793	2.27453	2.37263
H	4.58007	3.86117	1.15582
H	2.80657	2.77932	-0.68698
H	2.53914	0.58161	2.87121
H	4.27670	2.40635	3.23556
C	-0.50983	-0.89490	-0.69107
C	-0.34880	-2.33778	-1.15984
F	0.86369	-2.66601	-1.63198
F	-0.61263	-3.18287	-0.12303
F	-1.22471	-2.66850	-2.15401
C	-1.94968	-0.46340	-0.79551
H	-2.04999	0.57575	-0.49288
H	-2.24072	-0.52279	-1.85572
C	-2.97496	-1.31295	0.02232
H	-2.95515	-2.35177	-0.31653
H	-2.67135	-1.30615	1.07436
C	-4.37701	-0.75983	-0.11502
C	-4.86522	0.19973	0.78363
C	-5.21180	-1.17898	-1.16141
C	-6.15110	0.72610	0.64150
H	-4.23116	0.53108	1.60318
C	-6.49772	-0.65510	-1.30784
H	-4.85082	-1.92671	-1.86470
C	-6.97215	0.30064	-0.40564
H	-6.51325	1.46550	1.35151
H	-7.13054	-0.99677	-2.12302
H	-7.97402	0.70720	-0.51571

IPC 2b (1-CS)

Fe	0.80231	0.11630	-0.01421
N	-0.30232	0.53083	1.63146
N	0.11408	1.80607	-0.88844
N	1.69325	-1.40163	0.97734
N	2.11605	-0.11157	-1.52688
C	-0.43902	-0.26536	2.74137
C	0.35958	2.21685	-2.17398
C	-1.09350	1.62989	1.84246
C	-0.72926	2.73963	-0.34071
C	1.29668	-1.93857	2.17659
C	2.10405	0.55305	-2.72605
C	2.81253	-2.09561	0.59573
C	3.18293	-0.97115	-1.57412
C	-1.35859	0.34370	3.67743
C	-0.36310	3.43955	-2.45297
C	-1.75339	1.52655	3.12628

IPC 2b (1-OS)

Fe	0.83409	0.13669	-0.00777
N	-0.28816	0.62064	1.60035
N	0.13713	1.77058	-0.96893
N	1.69718	-1.35210	1.04135
N	2.12859	-0.18875	-1.51400
C	-0.43733	-0.12800	2.74131
C	0.37964	2.11117	-2.27555
C	-1.07865	1.73023	1.75862
C	-0.70800	2.73168	-0.47148
C	1.28530	-1.83743	2.25745
C	2.11219	0.41214	-2.74667
C	2.80325	-2.08353	0.68916
C	3.18174	-1.06780	-1.52845

C	-1.36082	0.52314	3.64291
C	-0.34387	3.31602	-2.61800
C	-1.74689	1.68373	3.03978
C	-1.00500	3.70978	-1.49410
C	2.14182	-2.92595	2.67290
C	3.17553	-0.11745	-3.57217
C	3.09347	-3.06653	1.70814
C	3.85107	-1.02062	-2.80884
H	-1.65112	0.13877	4.61284
H	-0.32213	3.79356	-3.58970
H	-2.41997	2.44576	3.41282
H	-1.64438	4.57266	-1.35528
H	2.02765	-3.48391	3.59399
H	3.37636	0.18949	-4.59108
H	3.91686	-3.76892	1.67071
H	4.71583	-1.61576	-3.07472
C	0.26375	-1.29618	3.03420
C	1.26733	1.45341	-3.12384
C	3.52447	-1.92844	-0.49095
C	-1.25355	2.73494	0.80910
H	0.04754	-1.78178	3.98127
H	1.36671	1.83516	-4.13560
H	4.38572	-2.57310	-0.63936
H	-1.91390	3.55705	1.06861
C	2.88609	1.39679	2.07434
C	3.02659	2.51692	0.23075
C	3.91882	3.09213	1.09677
N	2.38920	1.46135	0.85111
N	3.81495	2.36653	2.26614
H	4.59754	3.92443	0.99433
H	2.79965	2.78532	-0.78935
H	2.60524	0.68064	2.83102
H	4.33739	2.52451	3.11653
C	-0.53989	-0.94763	-0.67398
C	-0.37609	-2.39788	-1.05024
F	0.83620	-2.74524	-1.52598
F	-0.61083	-3.21133	0.02646
F	-1.26541	-2.79931	-2.01097
C	-1.97653	-0.49885	-0.79209
H	-2.05777	0.56037	-0.55636
H	-2.29804	-0.61735	-1.83840
C	-2.99484	-1.27358	0.10205
H	-2.97588	-2.33695	-0.15284
H	-2.68024	-1.18439	1.14741
C	-4.40020	-0.73728	-0.06311
C	-4.88695	0.28304	0.76711
C	-5.24092	-1.23055	-1.07217
C	-6.17470	0.79603	0.59529
H	-4.24932	0.67281	1.55772
C	-6.52871	-0.72057	-1.24872
H	-4.88203	-2.02570	-1.72253
C	-7.00079	0.29608	-0.41435
H	-6.53454	1.58339	1.25313
H	-7.16504	-1.12039	-2.03428
H	-8.00414	0.69206	-0.54753

IPC 2b (Triplet)

Fe	0.86951	0.14920	0.03076
N	0.29257	0.38046	1.95434
N	-0.34377	1.65745	-0.53917
N	2.19913	-1.22414	0.63236
N	1.54674	0.02576	-1.85892
C	0.63500	-0.40221	3.02878
C	-0.59877	2.08434	-1.81912
C	-0.55832	1.34358	2.43675
C	-1.09029	2.45636	0.28970
C	2.31633	-1.78975	1.87992
C	1.02851	0.63743	-2.97473
C	3.18406	-1.79017	-0.13913
C	2.60968	-0.72299	-2.29199
C	-0.03029	0.06945	4.22123
C	-1.53686	3.18100	-1.79933
C	-0.75833	1.16186	3.85683
C	-1.82973	3.42266	-0.48912
C	3.39487	-2.74803	1.89143
C	1.77476	0.24643	-4.14878
C	3.94349	-2.73604	0.64419
C	2.76713	-0.58309	-3.72213
H	0.07086	-0.37806	5.20205
H	-1.90163	3.69732	-2.67833
H	-1.38474	1.79166	4.47619
H	-2.48658	4.17679	-0.07365
H	3.68935	-3.33428	2.75282
H	1.56550	0.58803	-5.15471
H	4.77731	-3.31632	0.26920
H	3.53608	-1.07123	-4.30784
C	1.56257	-1.43928	2.99473
C	0.00517	1.57893	-2.96758
C	3.40263	-1.53673	-1.48923
C	-1.17495	2.33198	1.67471
H	1.75494	-1.97342	3.92008
H	-0.29887	1.99930	-3.92137
H	4.22149	-2.06476	-1.96852
H	-1.81854	3.03310	2.19746
C	3.09965	1.80489	1.49976
C	2.81268	2.65588	-0.47025
C	3.78718	3.40443	0.13357
N	2.39218	1.66177	0.39086
N	3.95626	2.84759	1.38592
H	4.35959	4.25602	-0.19924
H	2.38672	2.75935	-1.45594
H	3.02057	1.18727	2.38084
H	4.60367	3.15971	2.09648
C	-0.59803	-1.15870	-0.25732
C	-0.33571	-2.58568	-0.56324
F	0.67694	-2.81565	-1.43621
F	-0.03131	-3.32872	0.55700
F	-1.42390	-3.22860	-1.10511
C	-2.02594	-0.90794	0.17164
H	-2.41182	-1.77227	0.73518
H	-2.08073	-0.05258	0.84633
C	-3.00795	-0.64503	-1.01222
H	-2.95082	-1.48587	-1.70966
H	-2.67563	0.24837	-1.55069
C	-4.43491	-0.46686	-0.54131
C	-4.95849	0.80700	-0.27544
C	-5.26159	-1.58072	-0.32678
C	-6.26623	0.96504	0.18995
H	-4.33356	1.68184	-0.44220
C	-6.56898	-1.42873	0.13877
H	-4.87394	-2.57664	-0.53173
C	-7.07697	-0.15309	0.39945
H	-6.65346	1.96237	0.38465
H	-7.19286	-2.30566	0.29348
H	-8.09572	-0.03204	0.75855

IX. Supplemental References

(1) Gibson, D. G.; Young, L.; Chuang, R.-Y.; Venter, J. C.; Hutchison Iii, C. A.; Smith, H. O. Enzymatic assembly of DNA molecules up to several hundred kilobases. *Nat. Meth.* **2009**, *6*, 343.

(2) Arslan, E.; Schulz, H.; Zufferey, R.; Künzler, P.; Thöny-Meyer, L. Overproduction of the *Bradyrhizobium japonicum* c-type cytochrome subunits of the cbb3 oxidase in *Escherichia coli*. *Biochem. Biophys. Res. Commun.* **1998**, *251*, 744-747.

(3) Barr, I.; Guo, F. Pyridine hemochromagen assay for determining the concentration of heme in purified protein solutions. *Bio. Protoc.* **2015**, *5*, e1594.

(4) Kille, S.; Acevedo-Rocha, C. G.; Parra, L. P.; Zhang, Z.-G.; Opperman, D. J.; Reetz, M. T.; Acevedo, J. P. Reducing codon redundancy and screening effort of combinatorial protein libraries created by saturation mutagenesis. *ACS Syn. Biol.* **2013**, *2*, 83-92.

(5) Kan, S. B. J.; Huang, X.; Gumulya, Y.; Chen, K.; Arnold, F. H. Genetically programmed chiral organoborane synthesis. *Nature* **2017**, *552*, 132-136.

(6) Prier, C. K.; Zhang, R. K.; Buller, A. R.; Brinkmann-Chen, S.; Arnold, F. H. Enantioselective, intermolecular benzylic C–H amination catalysed by an engineered iron-haem enzyme. *Nat. Chem.* **2017**, *9*, 629-634.

(7) Knezz, S. N.; Waltz, T. A.; Haenni, B. C.; Burrmann, N. J.; McMahon, R. J. Spectroscopy and photochemistry of triplet 1,3-dimethylpropynylidene (MeC_3Me). *J. Am. Chem. Soc.* **2016**, *138*, 12596-12604.

(8) Jiang, C. J.; Cheng, C. L.; Yuan, S. F. Economical and Practical Strategies for Synthesis of α-Trifluoromethylated Amines. *Asian J. Chem.* **2015**, *27*, 2406-2408.

(9) Dolence, J. M.; Dale Poulter, C. Synthesis of analogs of farnesyl diphosphate. *Tetrahedron* **1996**, *52*, 119-130.

(10) Emer, E.; Twilton, J.; Tredwell, M.; Calderwood, S.; Collier, T. L.; Liégault, B.; Taillefer, M.; Gouverneur, V. Diversity-oriented approach to CF_3CHF-, CF_3CFBr-, CF_3CF_2-, $(CF_3)_2CH$-, and $CF_3(SCF_3)CH$-substituted arenes from 1-(diazo-2,2,2-trifluoroethyl)arenes. *Org. Lett.* **2014**, *16*, 6004-6007.

(11) Li, X.; Curran, D. P. Insertion of reactive rhodium carbenes into boron–hydrogen bonds of stable *N*-heterocyclic carbene boranes. *J. Am. Chem. Soc.* **2013**, *135*, 12076-12081.

(12) Yang, J.-M.; Li, Z.-Q.; Li, M.-L.; He, Q.; Zhu, S.-F.; Zhou, Q.-L. Catalytic B–H bond insertion reactions using alkynes as carbene precursors. *J. Am. Chem. Soc.* **2017**, *139*, 3784-3789.

(13) Šterk, D.; Stephan, M.; Mohar, B. Highly enantioselective transfer hydrogenation of fluoroalkyl ketones. *Org. Lett.* **2006**, *8*, 5935-5938.

(14) M. J. Frisch, G. W. T., H. B. Schlegel, G. E. Scuseria, M. A. Robb, J. R. Cheeseman, G. Scalmani, V. Barone, G. A. Petersson, H. Nakatsuji, X. Li, M. Caricato, A. Marenich, J. Bloino, B. G. Janesko, R. Gomperts, B. Mennucci, H. P. Hratchian, J. V. Ortiz, A. F. Izmaylov, J. L. Sonnenberg, D. Williams-Young, F. Ding, F. Lipparini, F. Egidi, J. Goings, B. Peng, A. Petrone, T. Henderson, D. Ranasinghe, V. G. Zakrzewski, J. Gao, N. Rega, G. Zheng, W. Liang, M. Hada, M. Ehara, K. Toyota, R. Fukuda, J. Hasegawa, M. Ishida, T. Nakajima, Y. Honda, O. Kitao, H. Nakai, T. Vreven, K. Throssell, J. A. Montgomery, Jr., J. E. Peralta, F. Ogliaro, M.

Bearpark, J. J. Heyd, E. Brothers, K. N. Kudin, V. N. Staroverov, T. Keith, R. Kobayashi, J. Normand, K. Raghavachari, A. Rendell, J. C. Burant, S. S. Iyengar, J. Tomasi, M. Cossi, J. M. Millam, M. Klene, C. Adamo, R. Cammi, J. W. Ochterski, R. L. Martin, K. Morokuma, O. Farkas, J. B. Foresman, and D. J. Fox. Gaussian 09, Revision A. 02. Gaussian. *Inc.: Wallingford, CT* **2009**.

(15) Becke, A. D. Density-functional exchange-energy approximation with correct asymptotic behavior. *Phys. Rev. A* **1988**, *38*, 3098-3100.

(16) Becke, A. D. Density‐functional thermochemistry. III. The role of exact exchange. *J. Chem. Phys.* **1993**, *98*, 5648-5652.

(17) Lee, C.; Yang, W.; Parr, R. G. Development of the Colle-Salvetti correlation-energy formula into a functional of the electron density. *Physical Review B* **1988**, *37*, 785-789.

(18) Ribeiro, R. F.; Marenich, A. V.; Cramer, C. J.; Truhlar, D. G. Use of solution-phase vibrational frequencies in continuum models for the free energy of solvation. *J. Phys. Chem. B* **2011**, *115*, 14556-14562.

(19) Zhao, Y.; Truhlar, D. G. Computational characterization and modeling of buckyball tweezers: density functional study of concave-convex pi...pi interactions. *Phys. Chem. Chem. Phys.* **2008**, *10*, 2813-2818.

(20) Funes-Ardoiz, I.; Paton, R.; GoodVibesv1.0.0 DOI:10.5281/zenodo.56091.

(21) Grimme, S.; Ehrlich, S.; Goerigk, L. Effect of the damping function in dispersion corrected density functional theory. *J. Comput. Chem.* **2011**, *32*, 1456-1465.

(22) Grimme, S.; Antony, J.; Ehrlich, S.; Krieg, H. A consistent and accurate ab initio parametrization of density functional dispersion correction (DFT-D) for the 94 elements H-Pu. *J. Chem. Phys.* **2010**, *132*, 154104.

(23) Barone, V.; Cossi, M. Quantum calculation of molecular energies and energy gradients in solution by a conductor solvent model. *J. Phys. Chem. A* **1998**, *102*, 1995-2001.

(24) Cossi, M.; Rega, N.; Scalmani, G.; Barone, V. Energies, structures, and electronic properties of molecules in solution with the C-PCM solvation model. *J. Comput. Chem.* **2003**, *24*, 669-681.

(25) Schutz, C. N.; Warshel, A. What are the dielectric "constants" of proteins and how to validate electrostatic models? *Proteins: Struct., Funct., Bioinf.* **2001**, *44*, 400-417.

(26) Li, L.; Li, C.; Zhang, Z.; Alexov, E. On the dielectric "constant" of proteins: Smooth dielectric function for macromolecular modeling and its implementation in DelPhi. *J. Chem. Theory Comput.* **2013**, *9*, 2126-2136.

(27) Sharon, D. A.; Mallick, D.; Wang, B.; Shaik, S. Computation sheds insight into iron porphyrin carbenes' electronic structure, formation, and N–H insertion reactivity. *J. Am. Chem. Soc.* **2016**, *138*, 9597-9610.

(28) Postils, V.; Rodriguez, M.; Sabenya, G.; Conde, A.; Diaz-Requejo, M. M.; Pérez, P. J.; Costas, M.; Solà, M.; Luis, J. M. The mechanism of the selective Fe-catalyzed arene carbon-hydrogen bond functionalization. *ACS Catal.* **2018**, *8*, 4313-4322.

(29) Lewis, R. D.; Garcia-Borràs, M.; Chalkley, M. J.; Buller, A. R.; Houk, K. N.; Kan, S. B. J.; Arnold, F. H. Catalytic iron-carbene intermediate revealed in a cytochrome *c* carbene transferase. *Proc. Natl. Acad. Sci. U. S. A.* **2018**, *115*, 7308.

(30) Narayan, A. R. H.; Jiménez-Osés, G.; Liu, P.; Negretti, S.; Zhao, W.; Gilbert, M. M.; Ramabhadran, R. O.; Yang, Y.-F.; Furan, L. R.; Li, Z.; Podust, L. M.; Montgomery, J.; Houk, K. N.; Sherman, D. H. Enzymatic hydroxylation of an unactivated methylene C–H bond guided by molecular dynamics simulations. *Nat. Chem.* **2015**, *7*, 653.

(31) Gilbert, M. M.; DeMars, M. D.; Yang, S.; Grandner, J. M.; Wang, S.; Wang, H.; Narayan, A. R. H.; Sherman, D. H.; Houk, K. N.; Montgomery, J. Synthesis of diverse 11- and 12-membered macrolactones from a common linear substrate using a single biocatalyst. *ACS Cent. Sci.* **2017**, *3*, 1304-1310.

(32) Shaik, S.; Cohen, S.; Wang, Y.; Chen, H.; Kumar, D.; Thiel, W. P450 enzymes: Their structure, reactivity, and selectivity—modeled by QM/MM calculations. *Chem. Rev.* **2010**, *110*, 949-1017.

(33) Chen, H.; Lai, W.; Shaik, S. Exchange-enhanced H-abstraction reactivity of high-valent nonheme iron(IV)-oxo from coupled cluster and density functional theories. *J. Phys. Chem. Lett.* **2010**, *1*, 1533-1540.

(34) Altun, A.; Breidung, J.; Neese, F.; Thiel, W. Correlated ab initio and density functional studies on H_2 activation by FeO^+. *J. Chem. Theory Comput.* **2014**, *10*, 3807-3820.

(35) Seeger, R.; Pople, J. A. Self‐consistent molecular orbital methods. XVIII. Constraints and stability in Hartree–Fock theory. *J. Chem. Phys.* **1977**, *66*, 3045-3050.

(36) Bauernschmitt, R.; Ahlrichs, R. Stability analysis for solutions of the closed shell Kohn–Sham equation. *J. Chem. Phys.* **1996**, *104*, 9047-9052.

(37) Schlegel, H. B.; McDouall, J. J. W. In *Computational advances in organic chemistry: molecular structure and reactivity*; Ögretir, C., Csizmadia, I. G., Eds.; Springer Netherlands: Dordrecht, 1991, p 167-185.

(38) Legault, C. CYLview, 1.0 b, Université de Sherbrooke, Sherbrooke, Québec, Canada, 2009. *URL http://www. cylview. org (accessed February 1, 2016)*.

(39) Salomon-Ferrer, R.; Götz, A. W.; Poole, D.; Le Grand, S.; Walker, R. C. Routine microsecond molecular dynamics simulations with AMBER on GPUs. 2. Explicit solvent particle mesh Ewald. *J. Chem. Theory Comput.* **2013**, *9*, 3878-3888.

(40) D.A. Case, D. S. C., T.E. Cheatham, III, T.A. Darden, R.E. Duke, T.J. Giese, H. Gohlke, A.W. Goetz, D. Greene, N. Homeyer, S. Izadi, A. Kovalenko, T.S. Lee, S. LeGrand, P. Li, C. Lin, J. Liu, T. Luchko, R. Luo, D. Mermelstein, K.M. Merz, G. Monard, H. Nguyen, I. Omelyan, A. Onufriev, F. Pan, R. Qi, D.R. Roe, A. Roitberg, C. Sagui, C.L. Simmerling, W.M. Botello-Smith, J. Swails, R.C. Walker, J. Wang, R.M. Wolf, X. Wu, L. Xiao, D.M. York and P.A. Kollman University of California, San Francisco, 2017.

(41) Li, P.; Merz, K. M. MCPB.py: A python based metal center parameter builder. *J. Chem. Inf. Model.* **2016**, *56*, 599-604.

(42) Wang, J.; Wolf, R. M.; Caldwell, J. W.; Kollman, P. A.; Case, D. A. Development and testing of a general amber force field. *J. Comput. Chem.* **2004**, *25*, 1157-1174.

(43) Bayly, C. I.; Cieplak, P.; Cornell, W.; Kollman, P. A. A well-behaved electrostatic potential based method using charge restraints for deriving atomic charges: the RESP model. *J. Phys. Chem.* **1993**, *97*, 10269-10280.

(44) Besler, B. H.; Merz, K. M.; Kollman, P. A. Atomic charges derived from semiempirical methods. *J. Comput. Chem.* **1990**, *11*, 431-439.

(45) Singh, U. C.; Kollman, P. A. An approach to computing electrostatic charges for molecules. *J. Comput. Chem.* **1984**, *5*, 129-145.

(46) Jorgensen, W. L.; Chandrasekhar, J.; Madura, J. D.; Impey, R. W.; Klein, M. L. Comparison of simple potential functions for simulating liquid water. *J. Chem. Phys.* **1983**, *79*, 926-935.

(47) Maier, J. A.; Martinez, C.; Kasavajhala, K.; Wickstrom, L.; Hauser, K. E.; Simmerling, C. ff14SB: Improving the accuracy of protein side chain and backbone parameters from ff99SB. *J. Chem. Theory Comput.* **2015**, *11*, 3696-3713.

(48) Darden, T.; York, D.; Pedersen, L. Particle mesh Ewald: An N·log(N) method for Ewald sums in large systems. *J. Chem. Phys.* **1993**, *98*, 10089-10092.

(49) Roe, D. R.; Cheatham, T. E. PTRAJ and CPPTRAJ: Software for processing and analysis of molecular dynamics trajectory data. *J. Chem. Theory Comput.* **2013**, *9*, 3084-3095.

(50) Trott, O.; Olson, A. J. AutoDock Vina: Improving the speed and accuracy of docking with a new scoring function, efficient optimization, and multithreading. *J. Comput. Chem.* **2009**, *31*, 455-461.

X. NMR Spectra

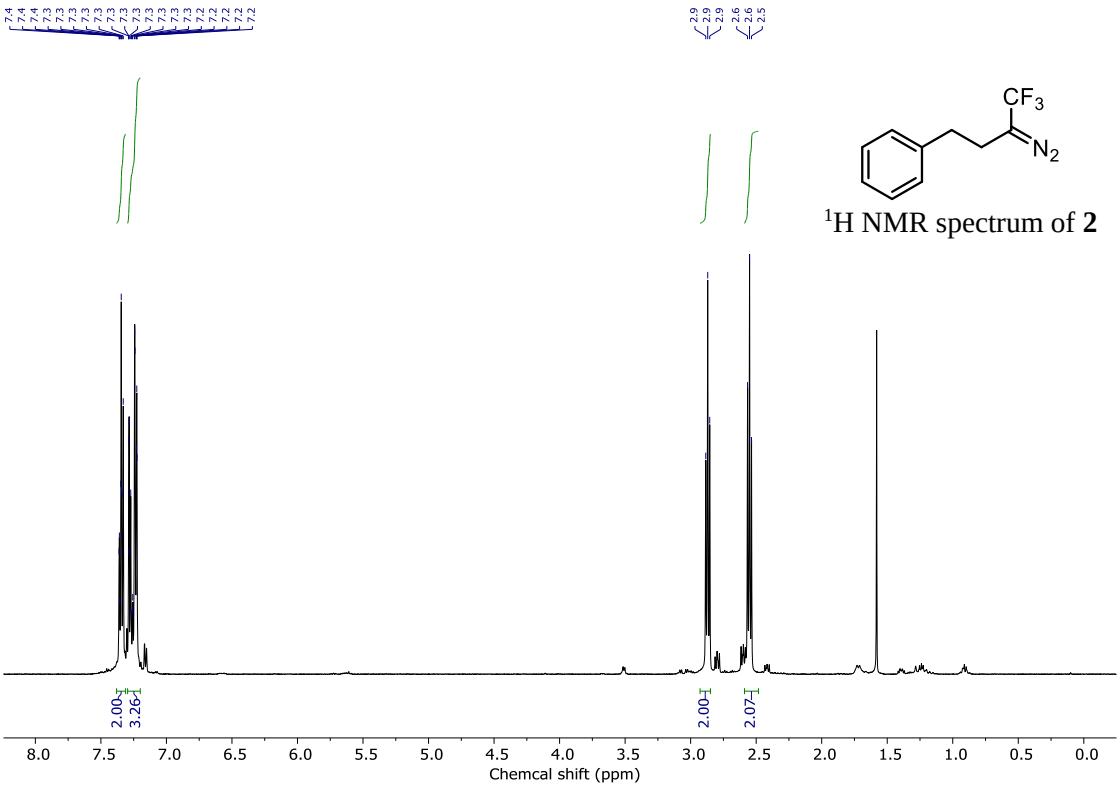

^{1}H NMR spectrum of **2**

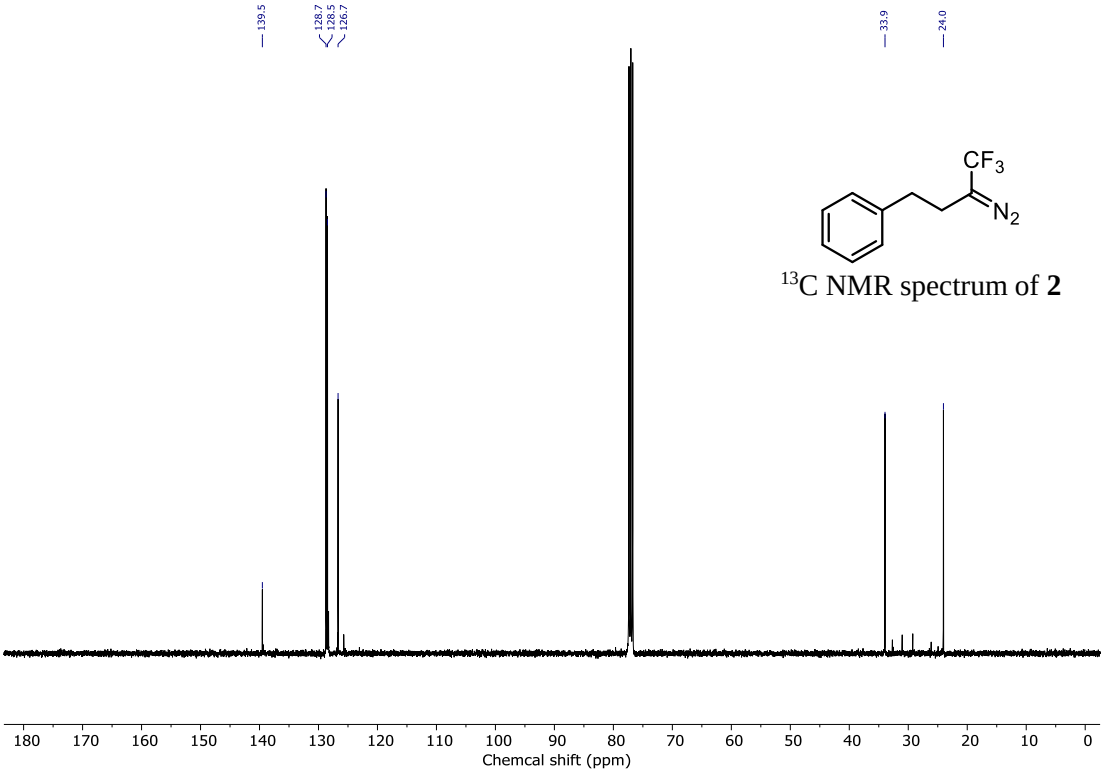

^{13}C NMR spectrum of **2**

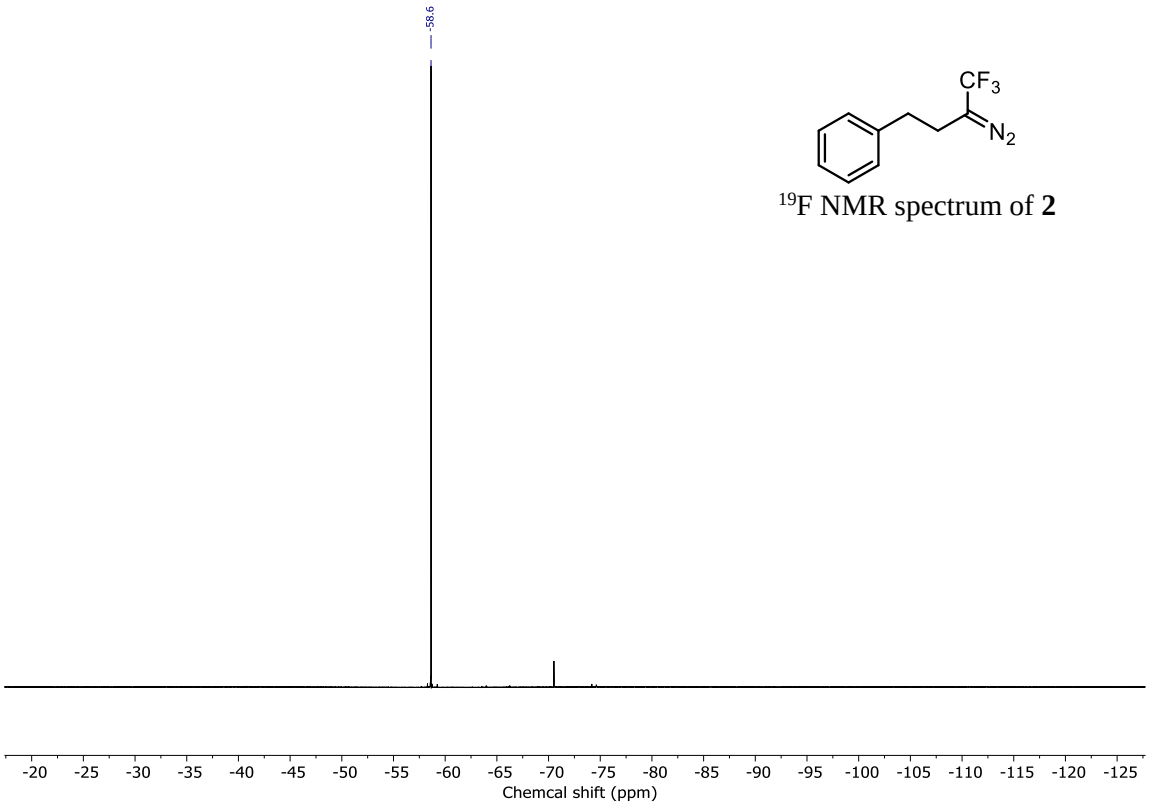

^{19}F NMR spectrum of **2**

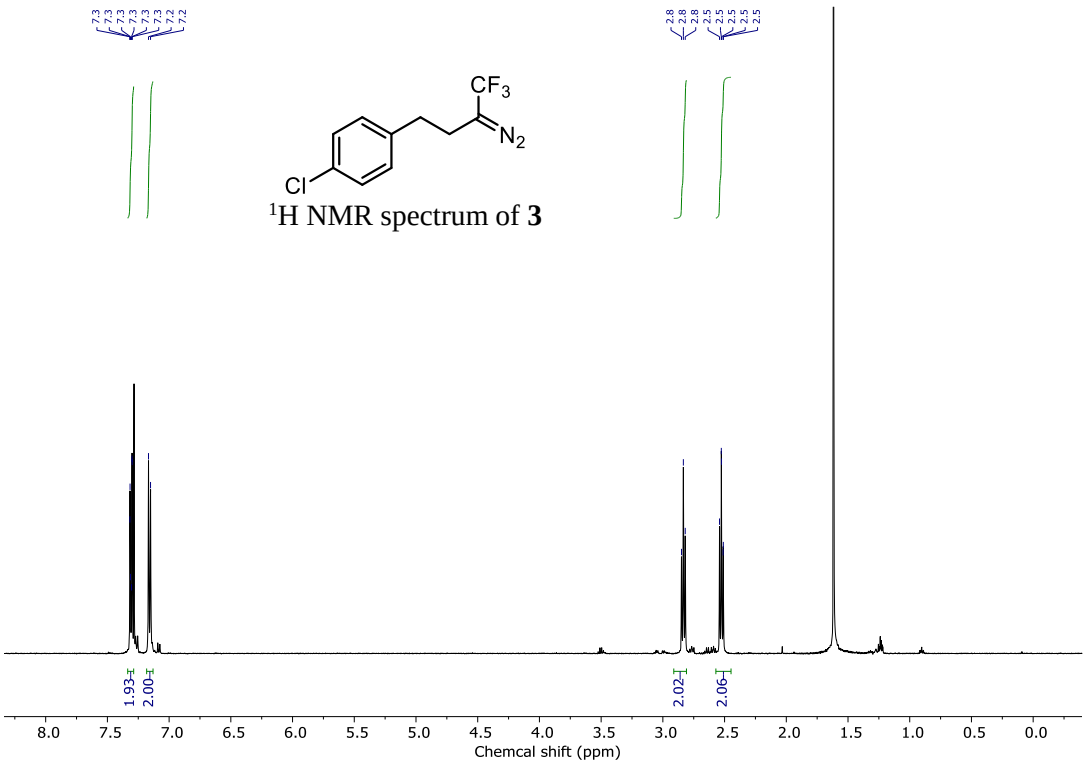

^{1}H NMR spectrum of **3**

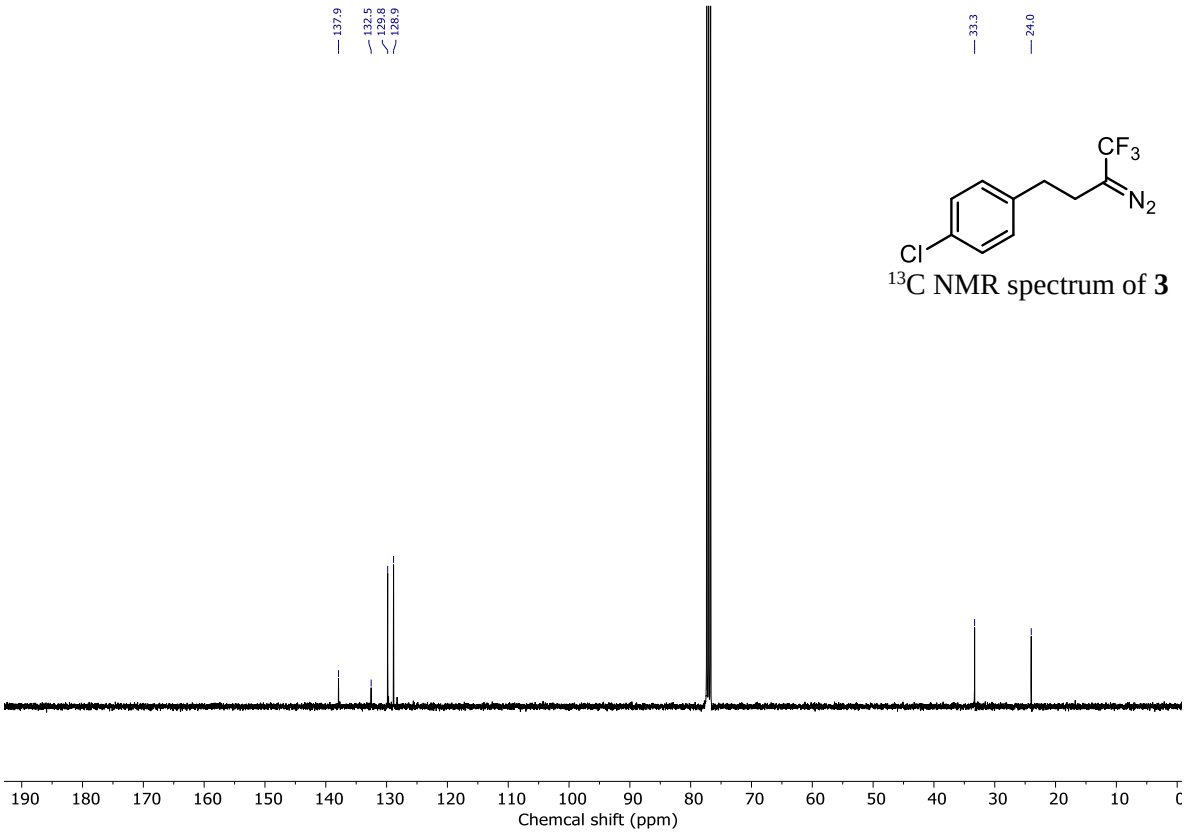

^{13}C NMR spectrum of **3**

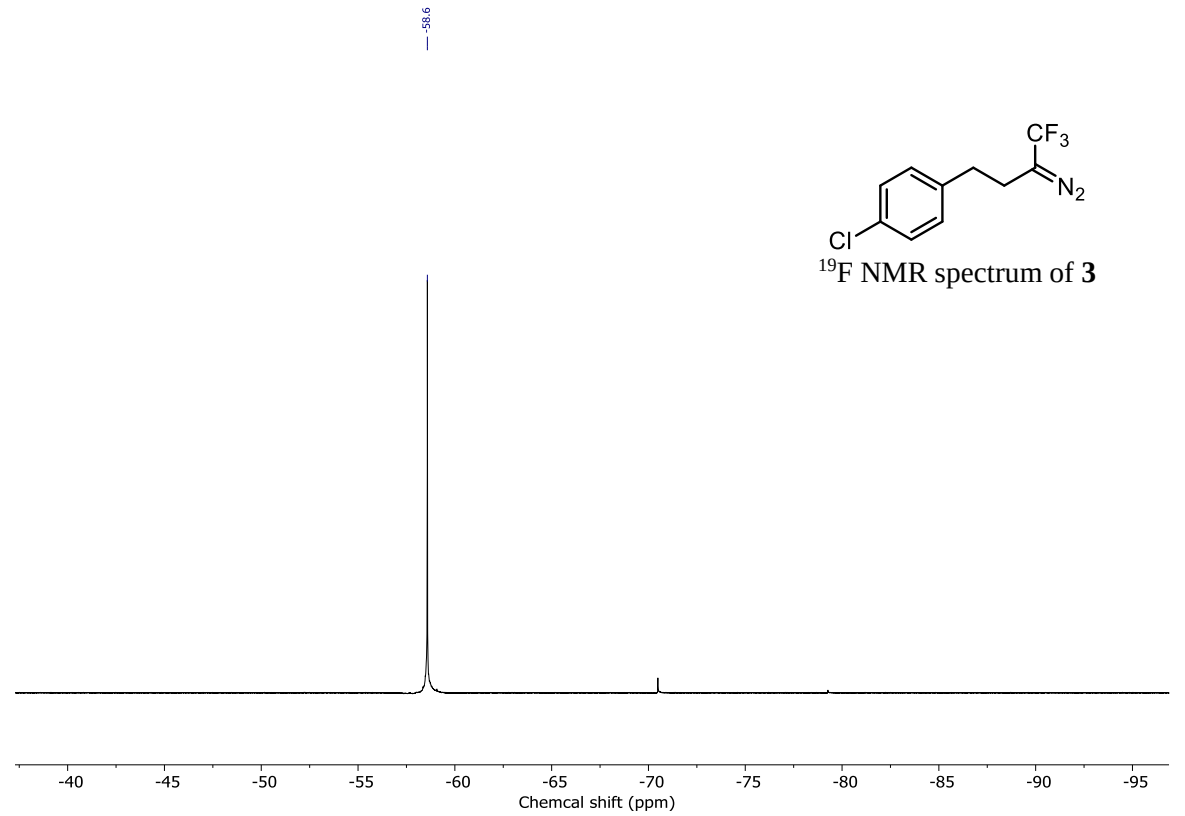

^{19}F NMR spectrum of **3**

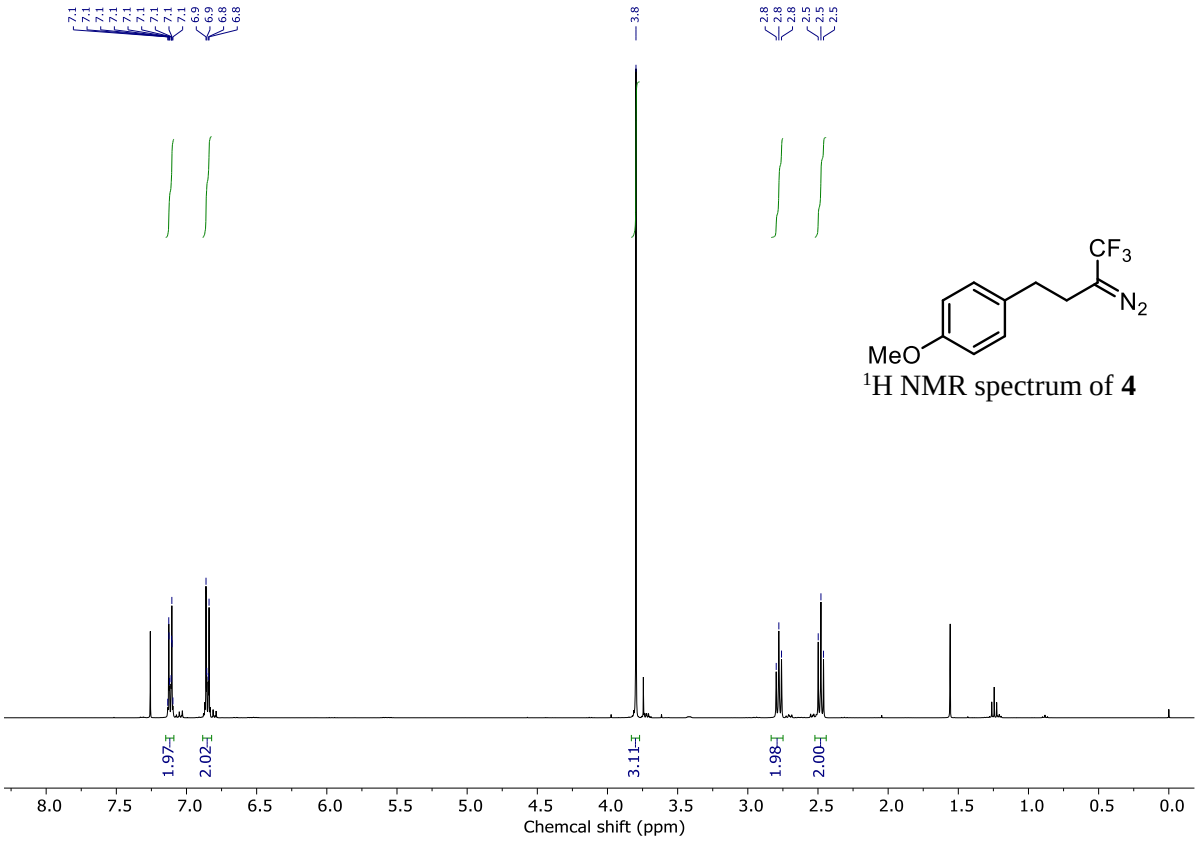

^{1}H NMR spectrum of **4**

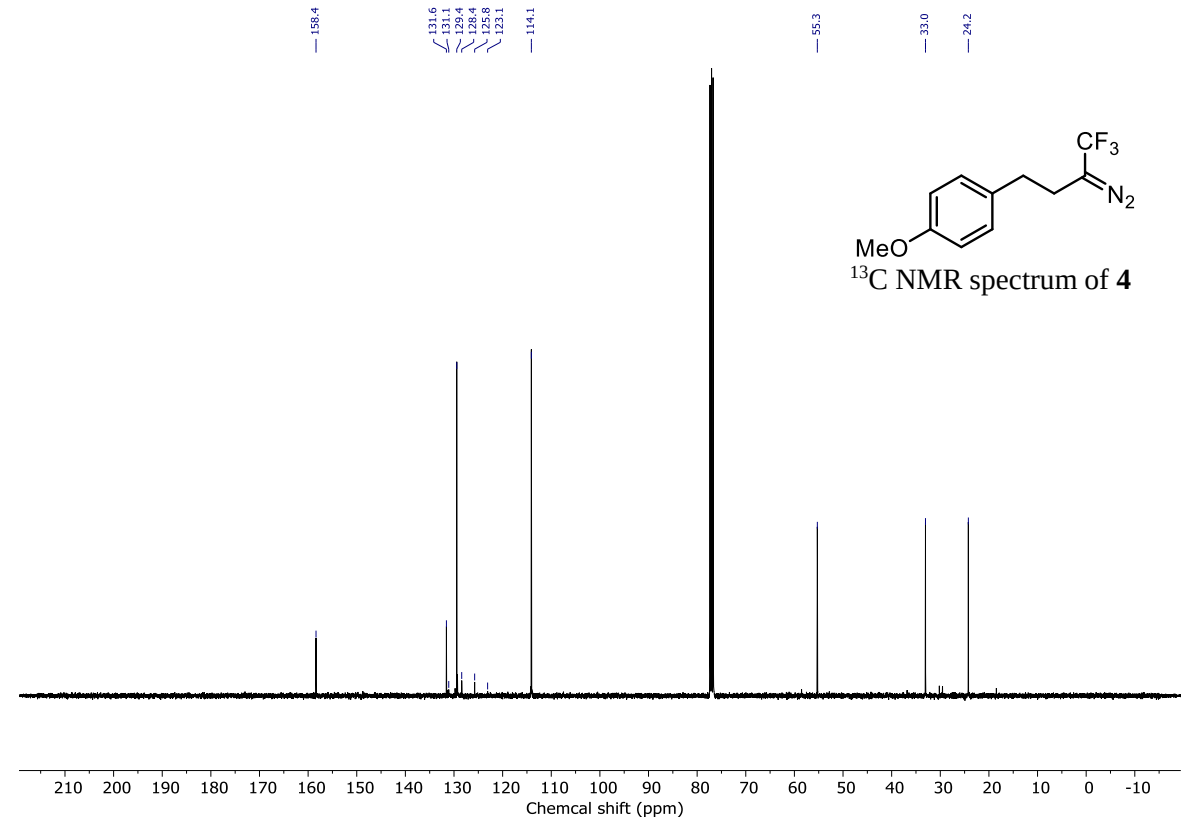

^{13}C NMR spectrum of **4**

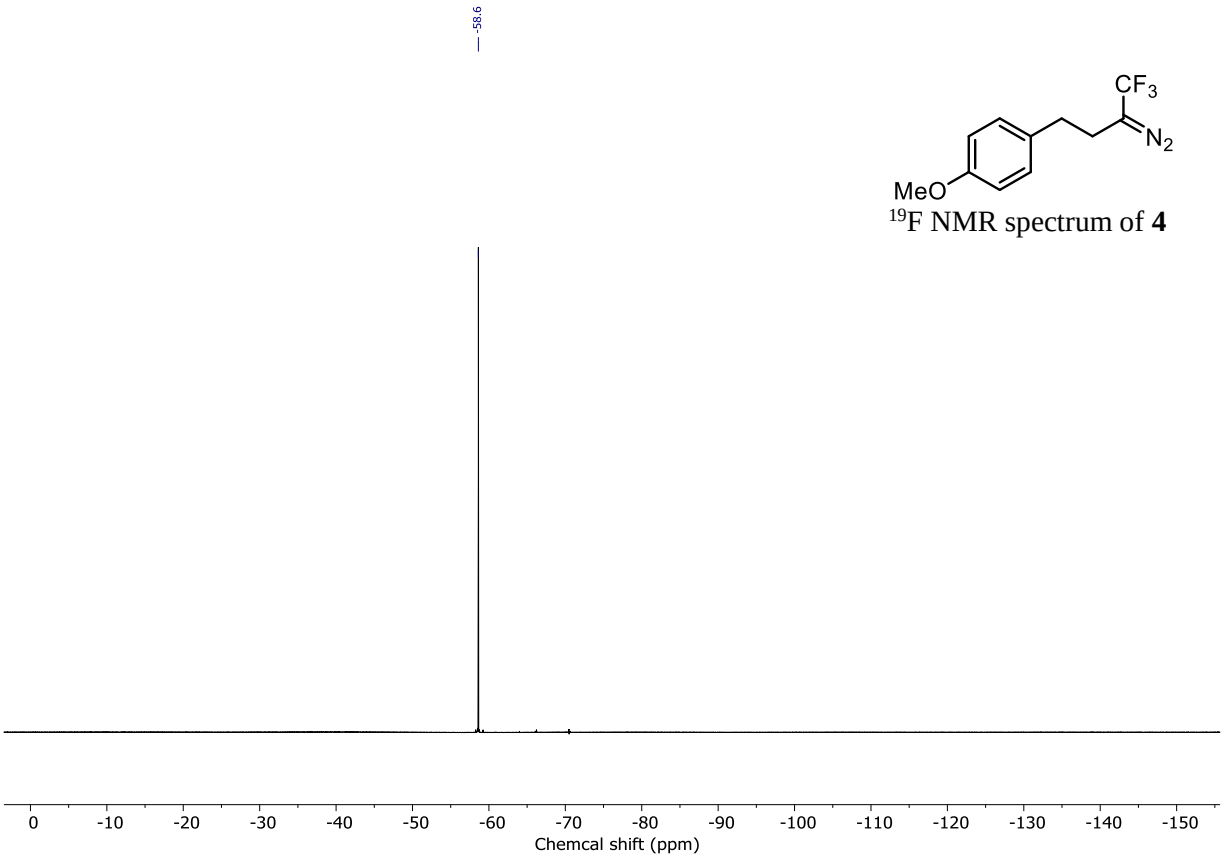

^{19}F NMR spectrum of **4**

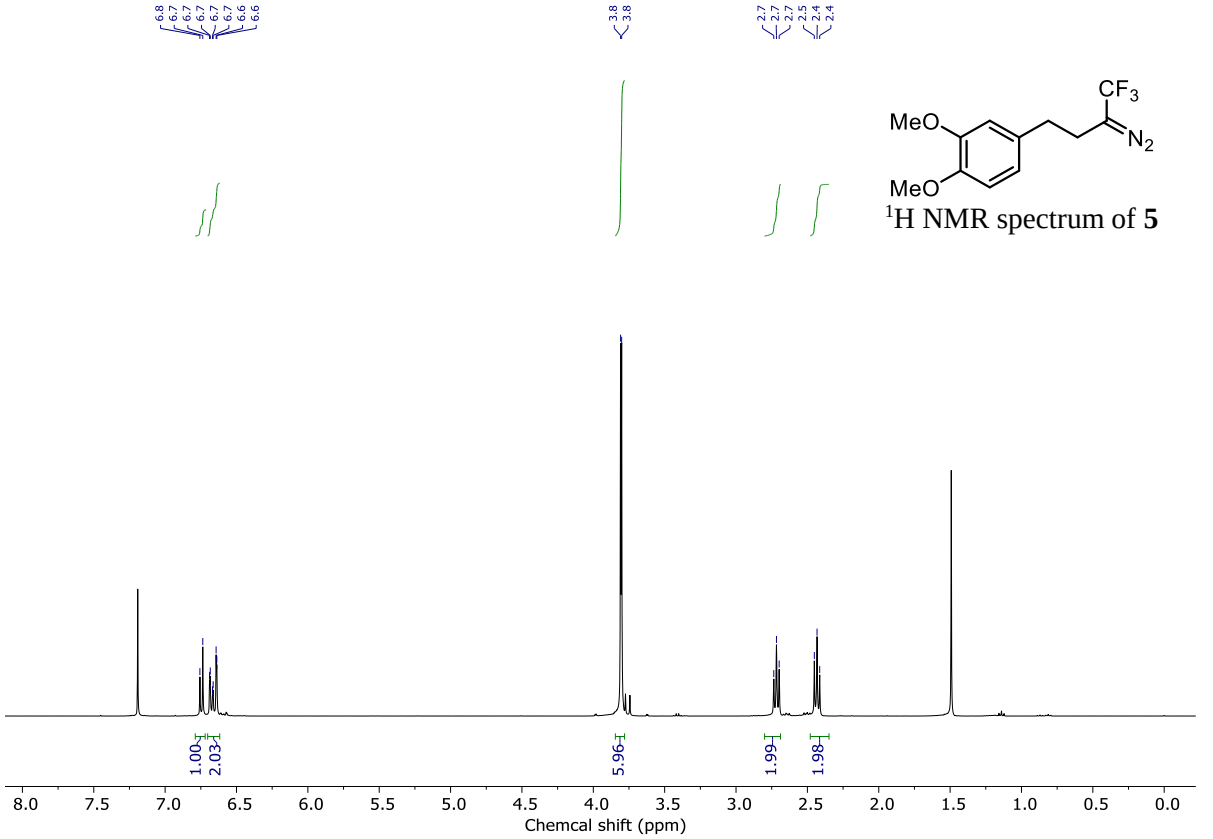

^{1}H NMR spectrum of **5**

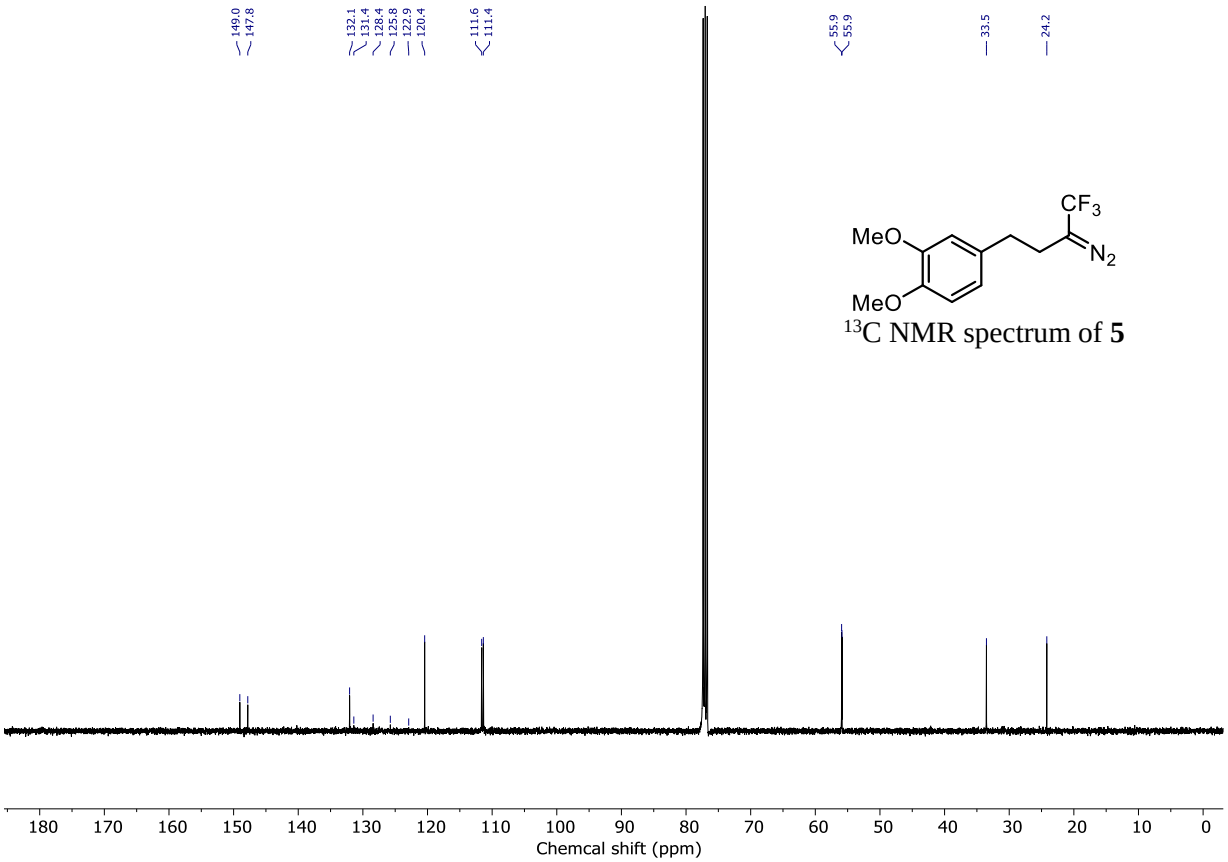

^{13}C NMR spectrum of **5**

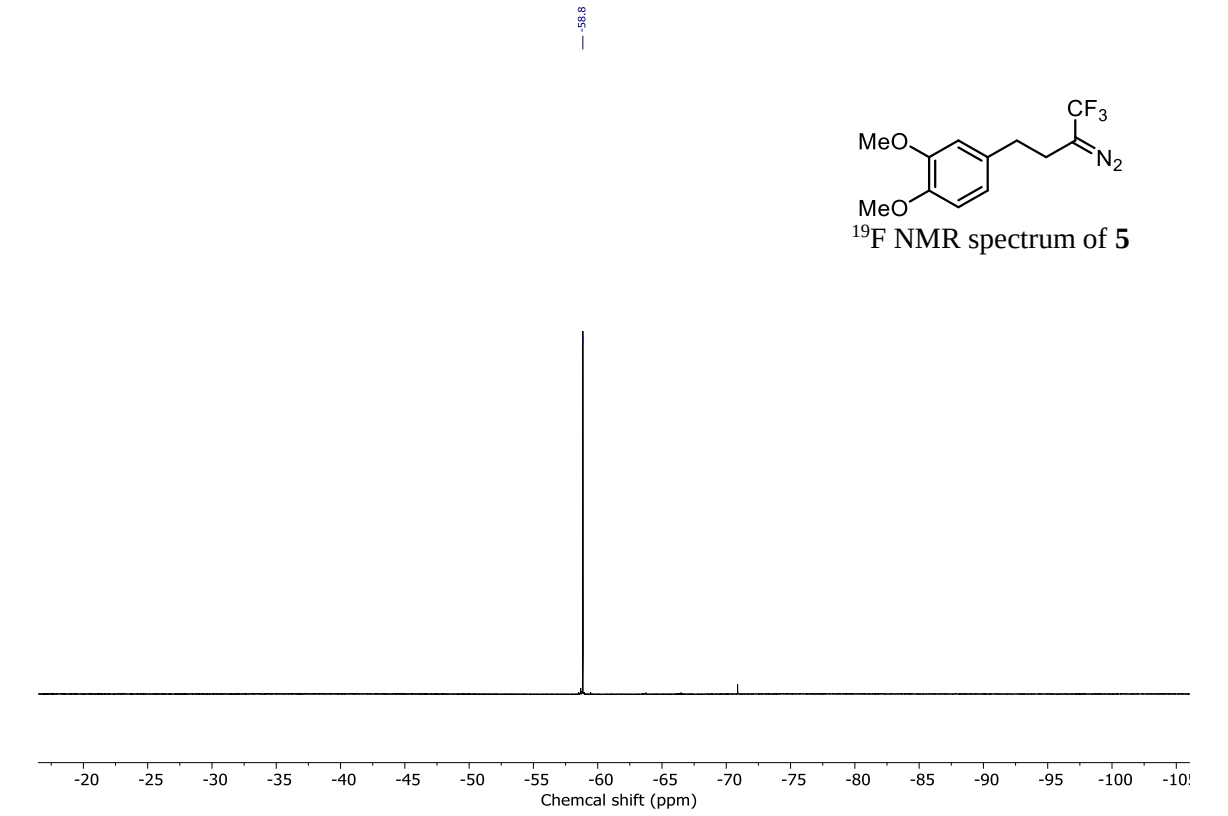

^{19}F NMR spectrum of **5**

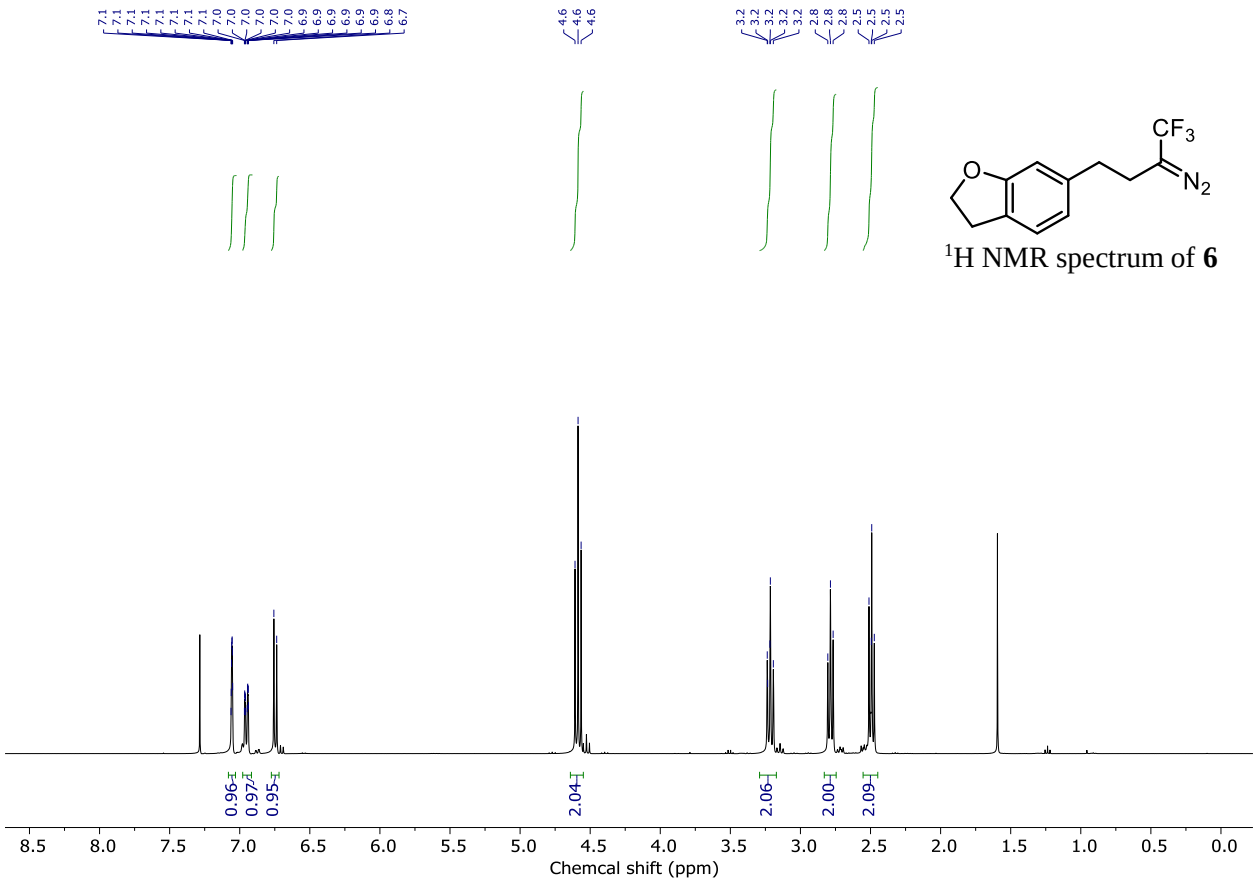

^{1}H NMR spectrum of **6**

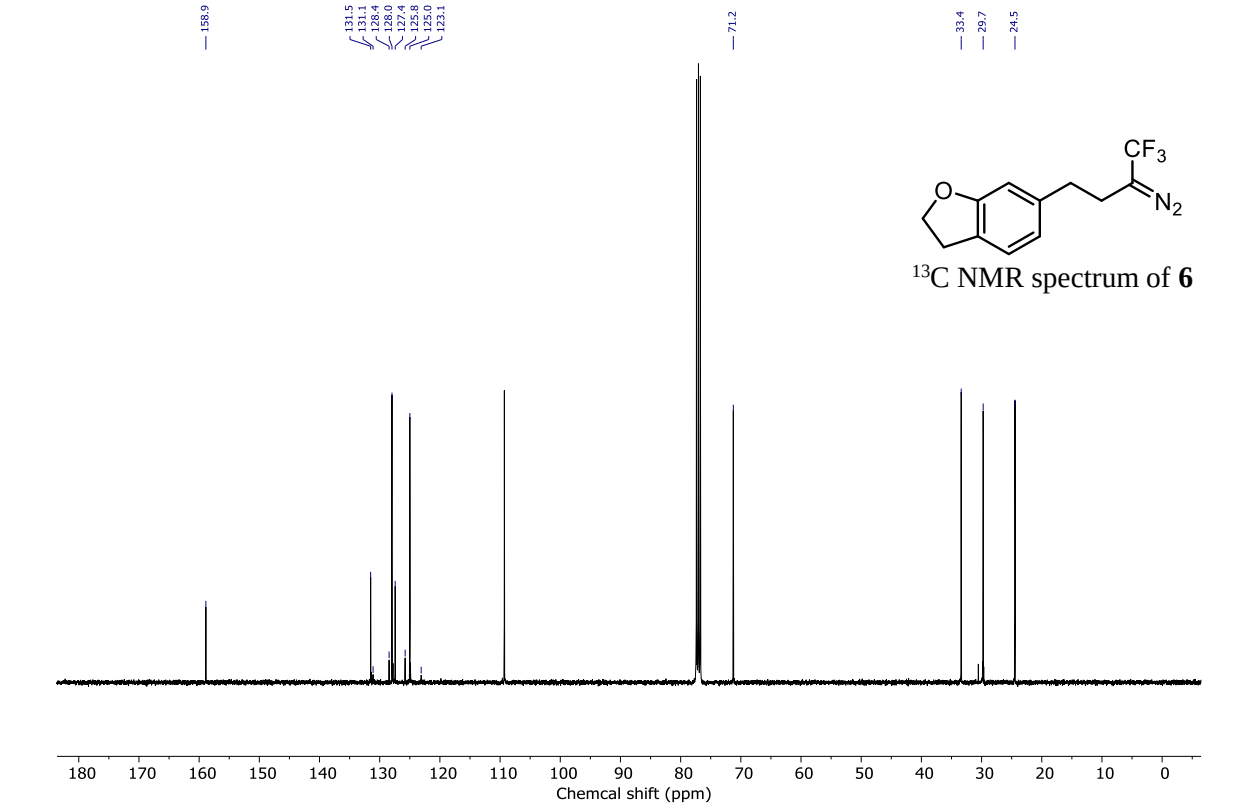

^{13}C NMR spectrum of **6**

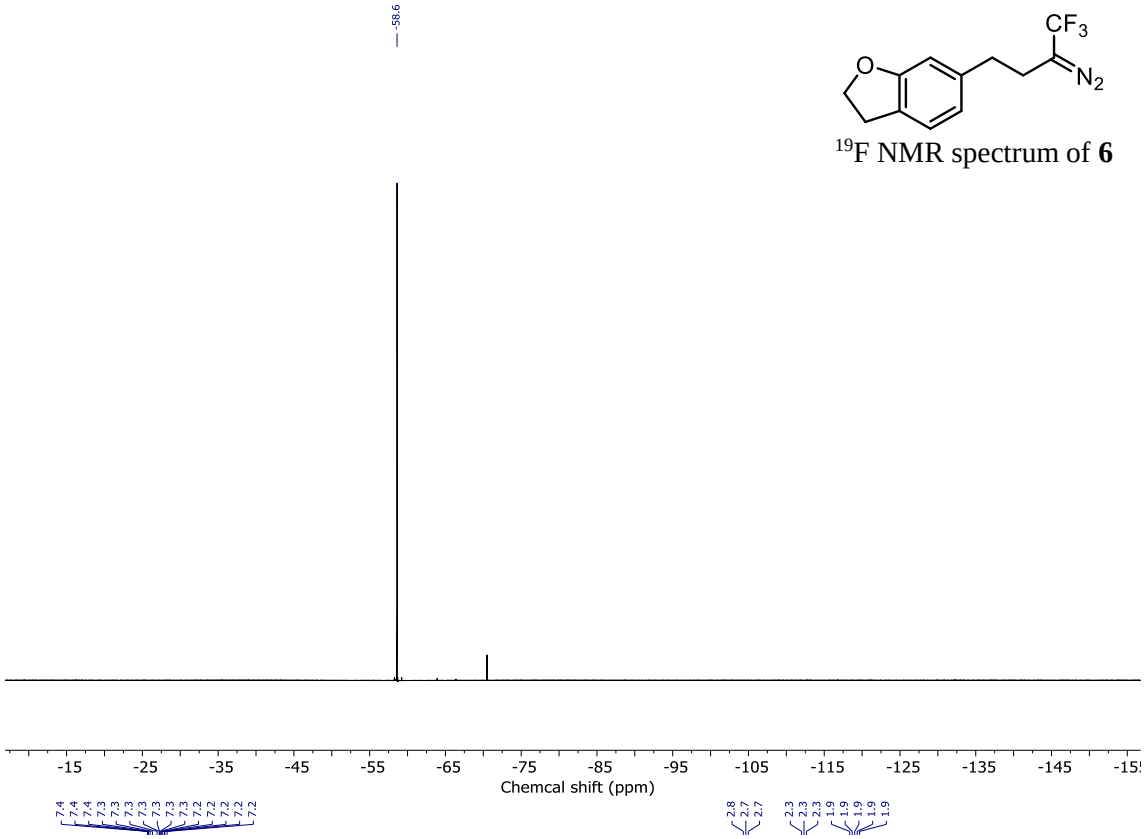

^{19}F NMR spectrum of **6**

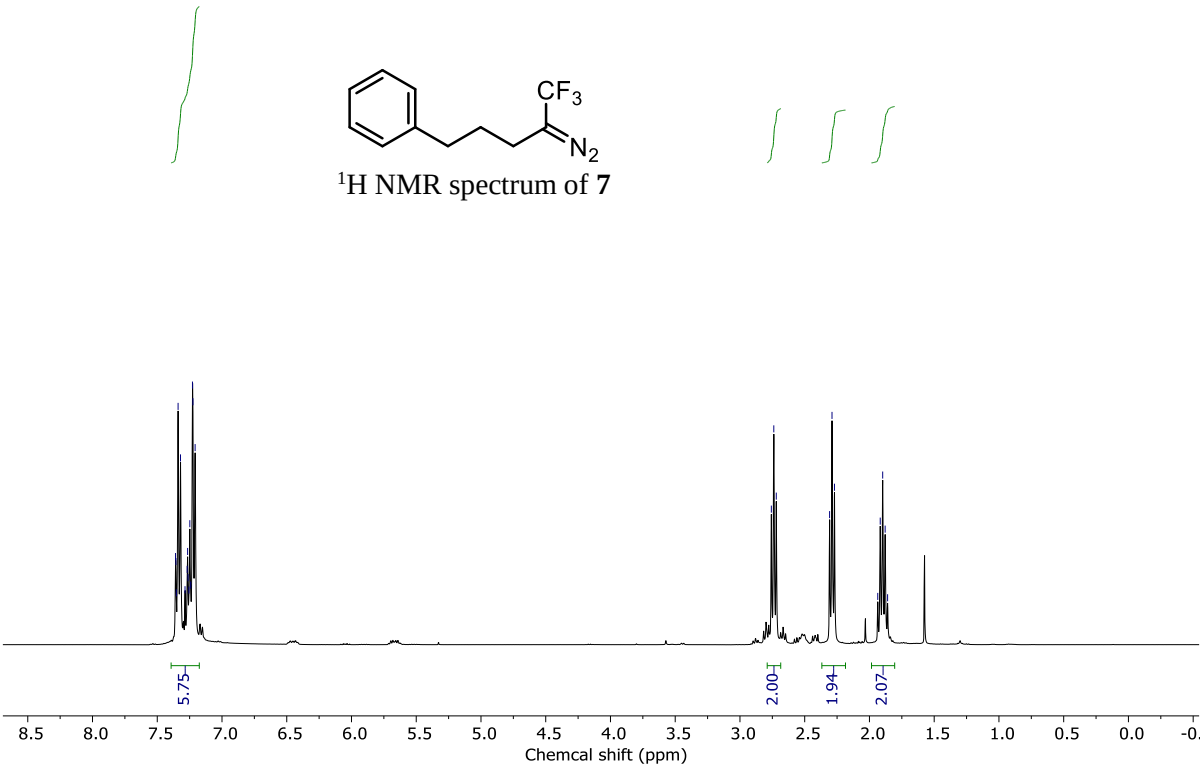

^{1}H NMR spectrum of **7**

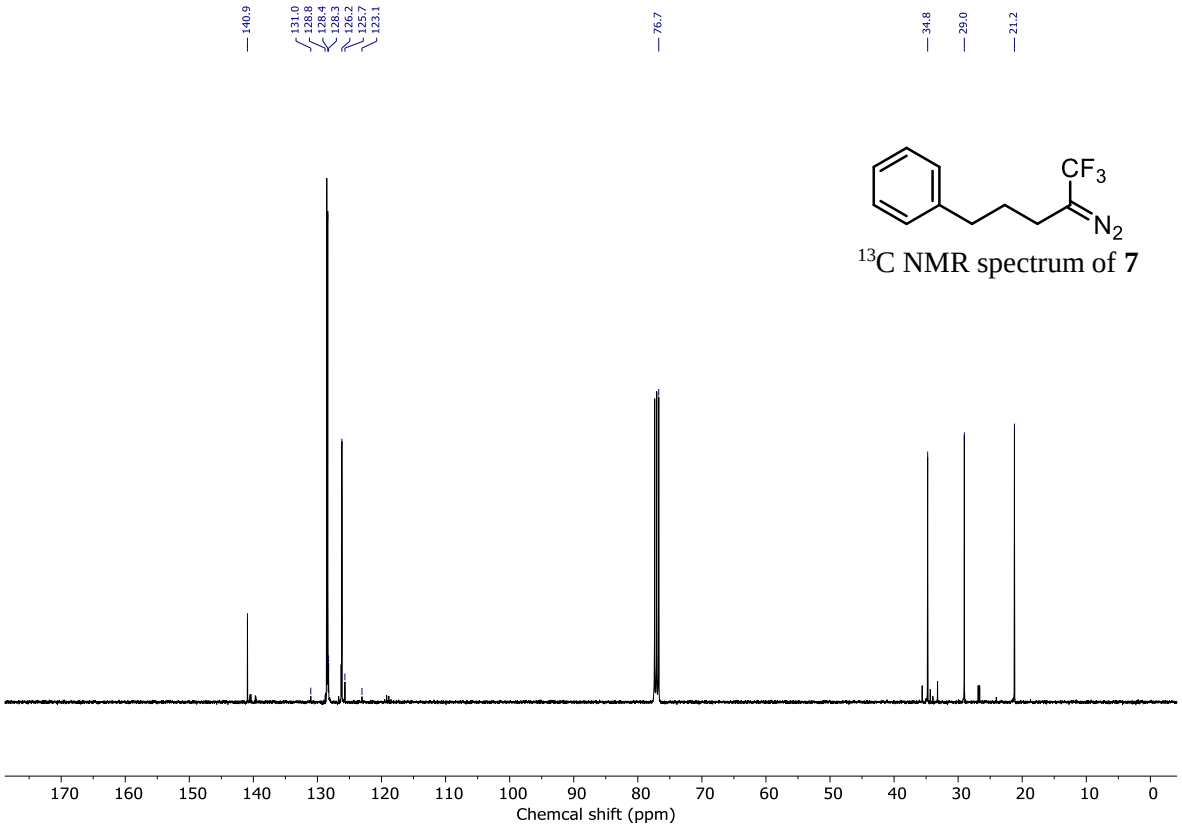

^{13}C NMR spectrum of **7**

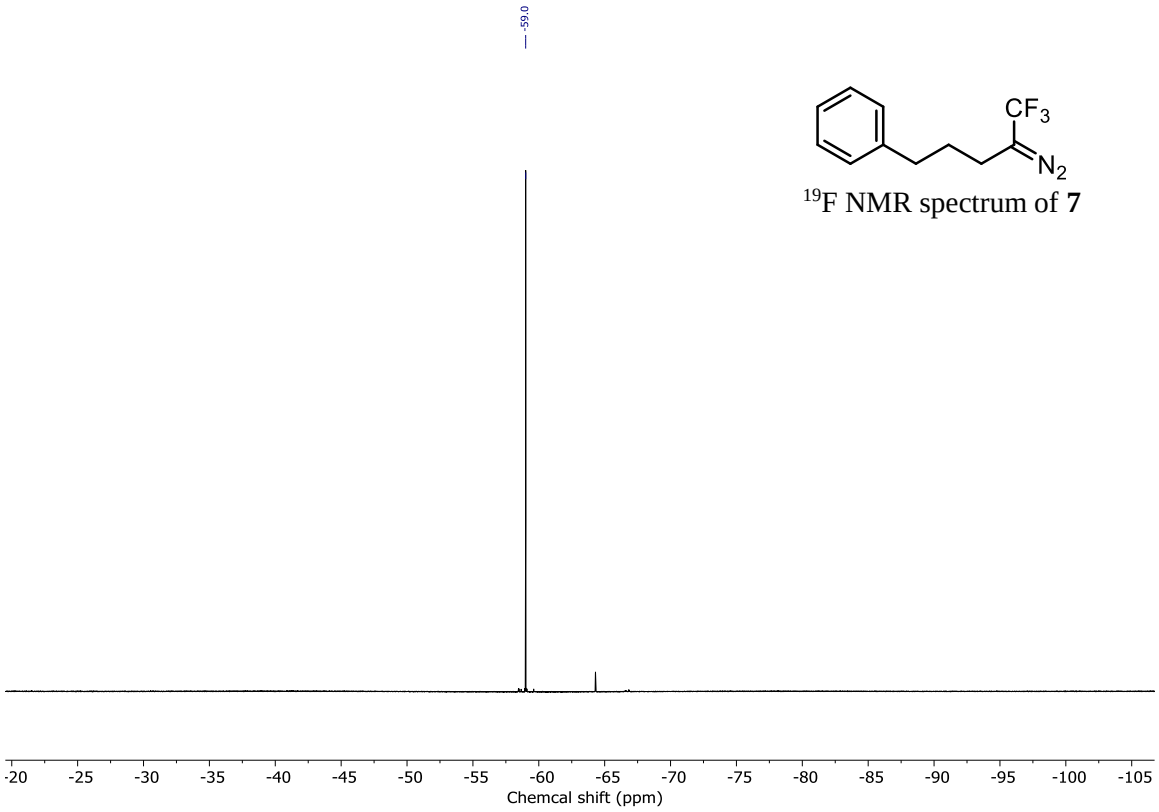

^{19}F NMR spectrum of **7**

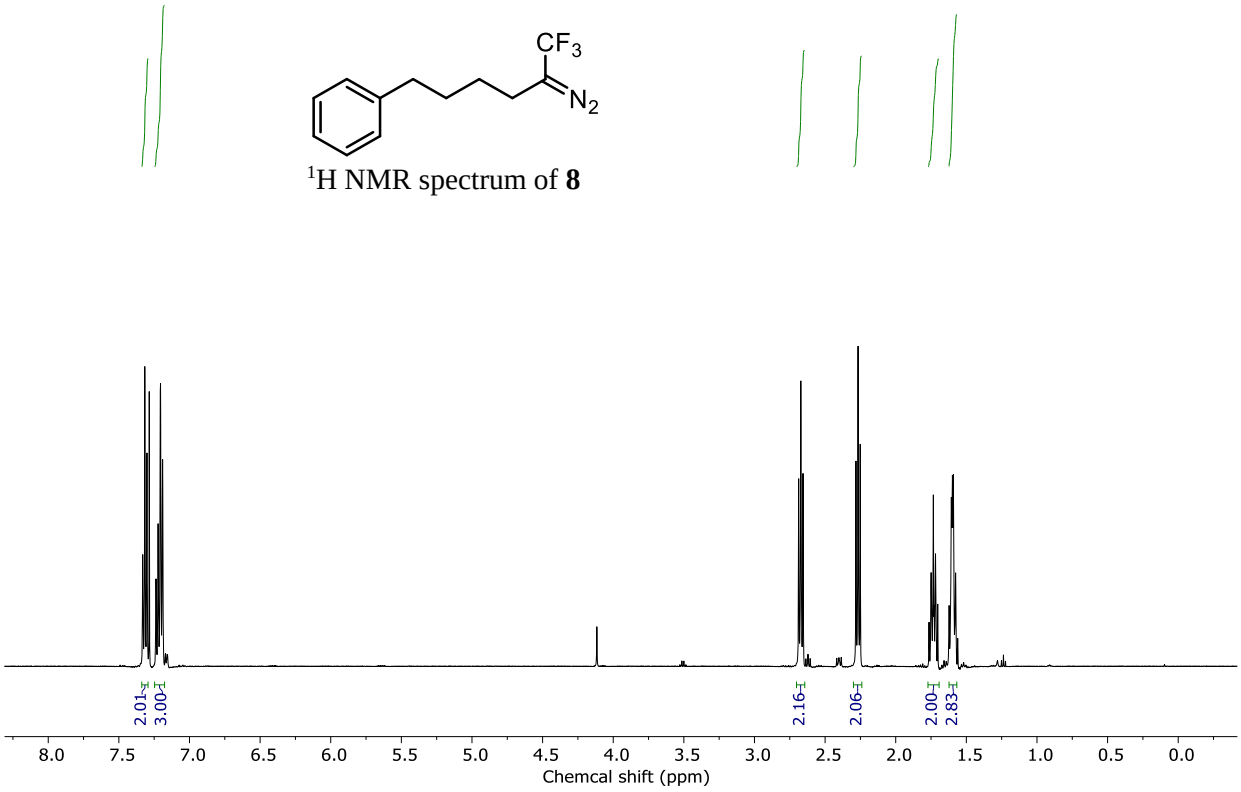

^{1}H NMR spectrum of **8**

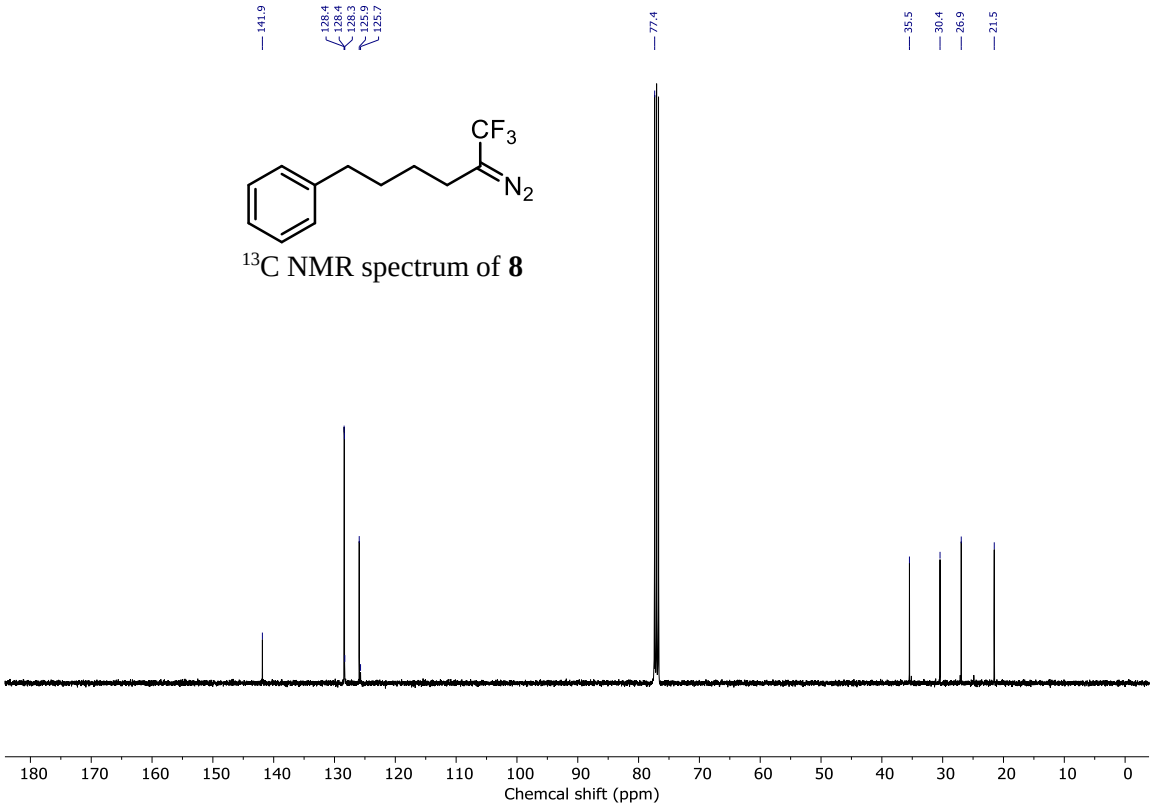

^{13}C NMR spectrum of **8**

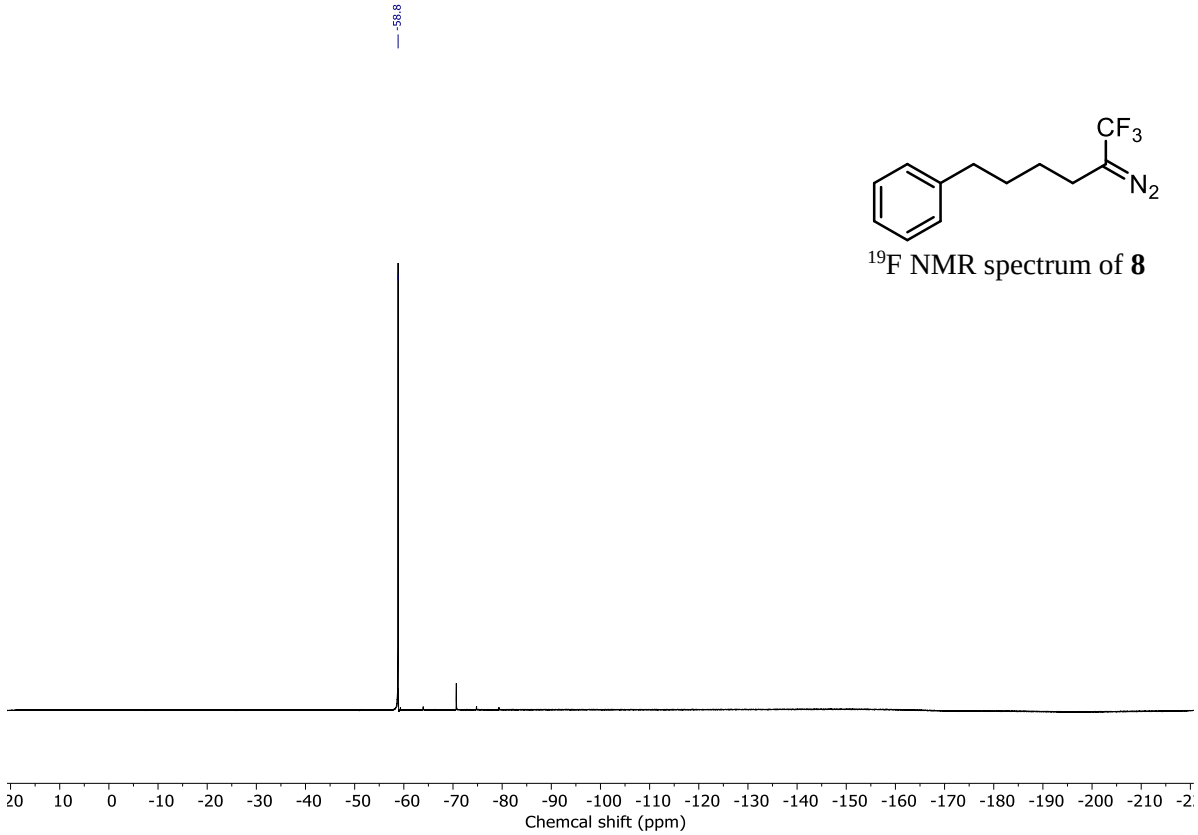

^{19}F NMR spectrum of **8**

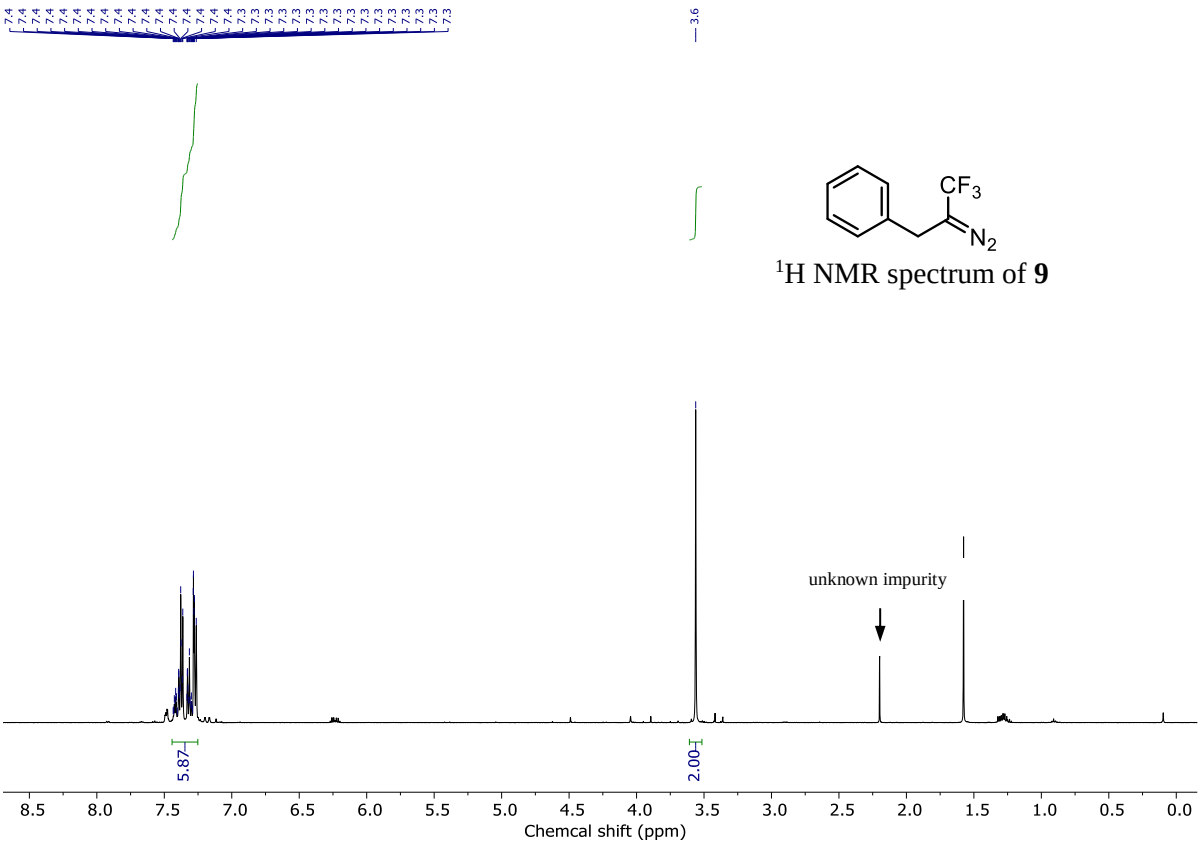

^{1}H NMR spectrum of **9**

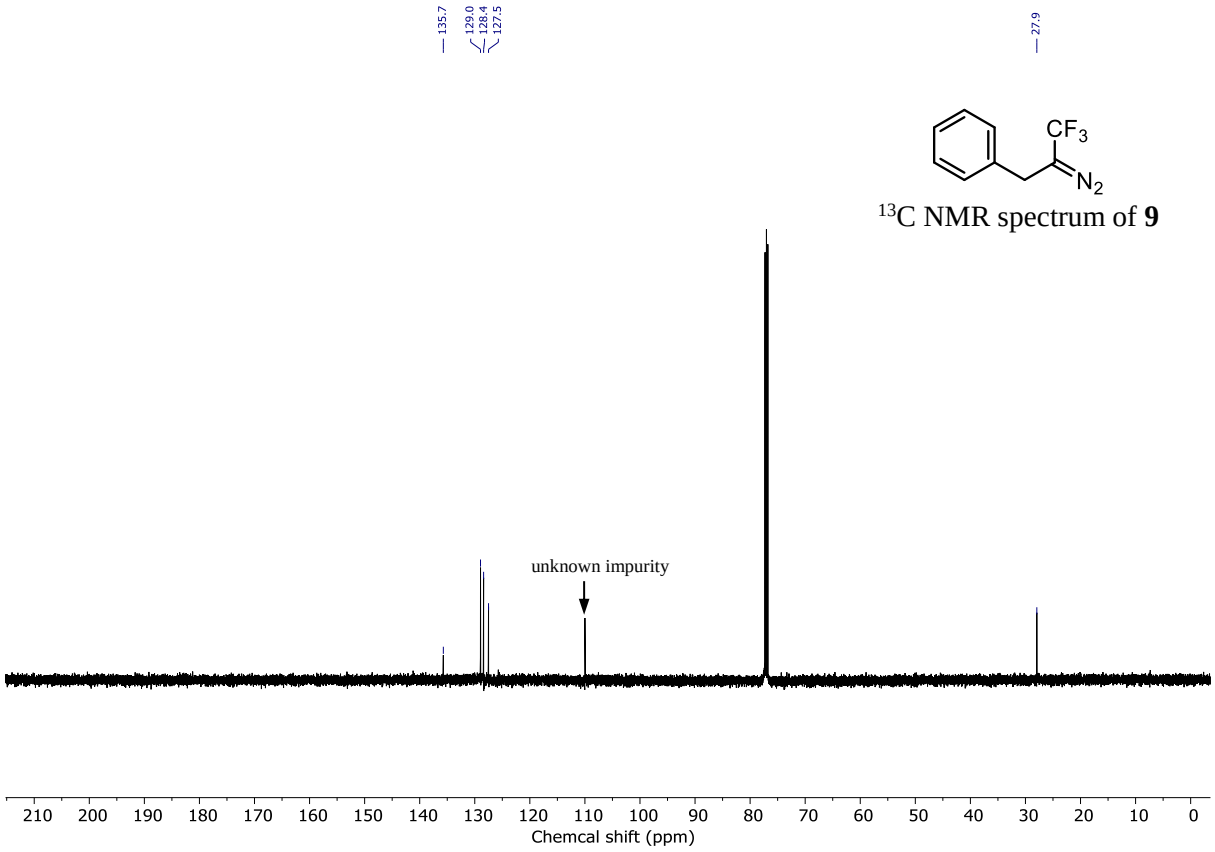

^{13}C NMR spectrum of **9**

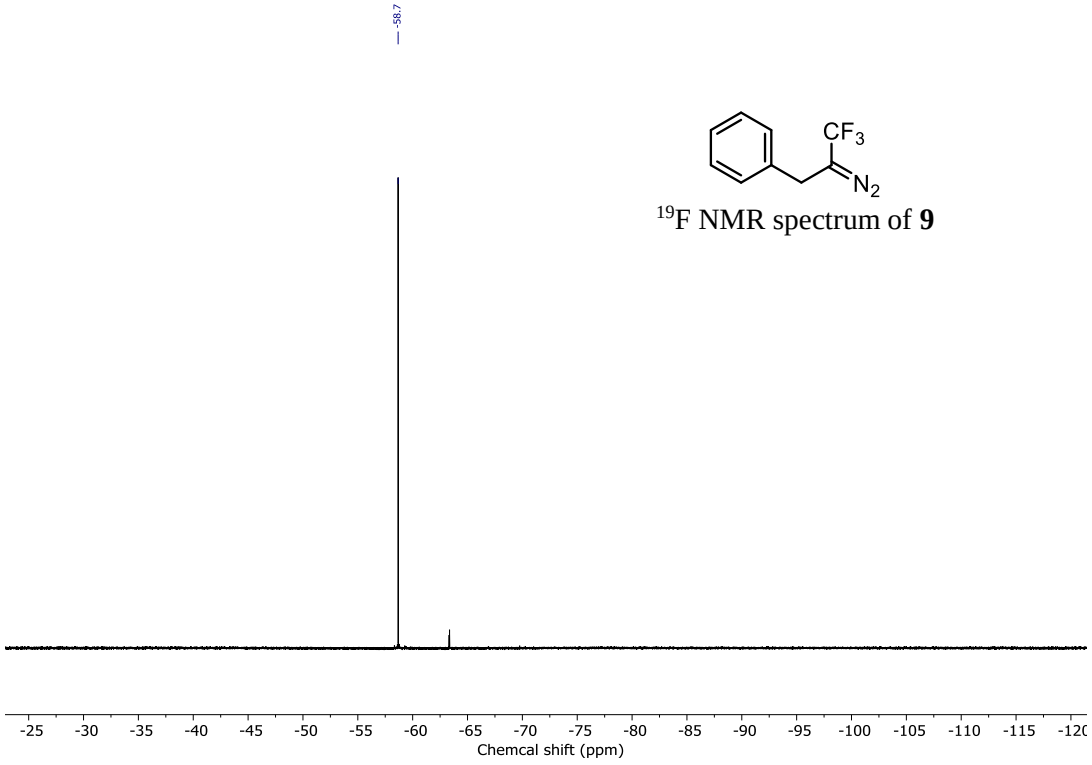

^{19}F NMR spectrum of **9**

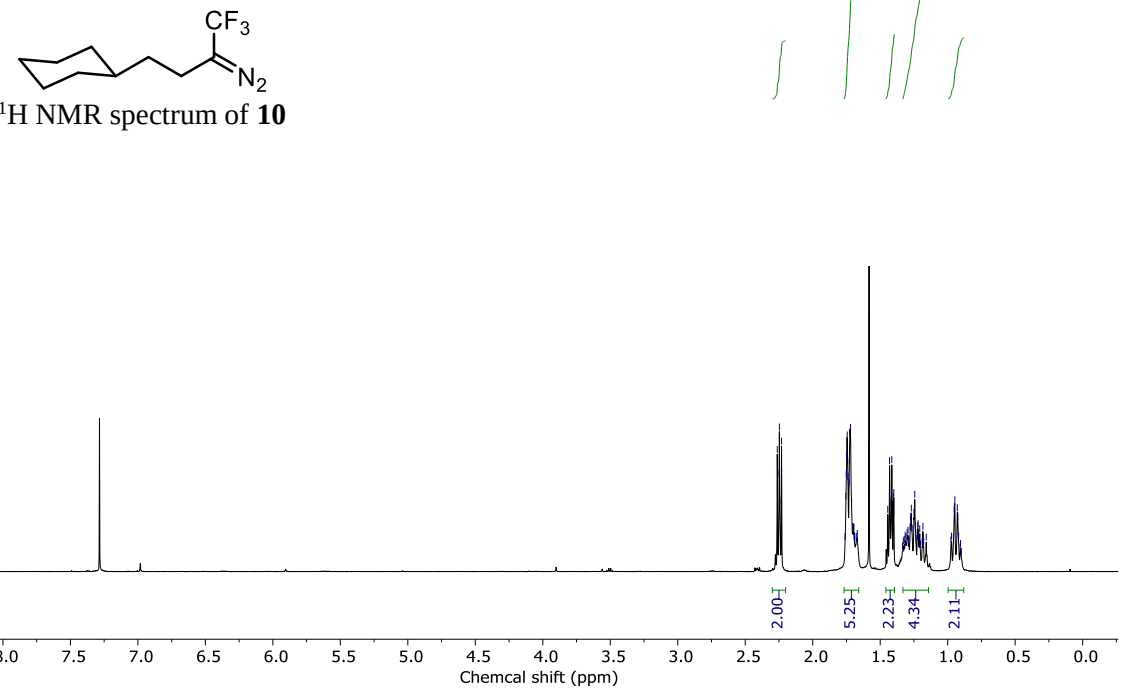

^{1}H NMR spectrum of **10**

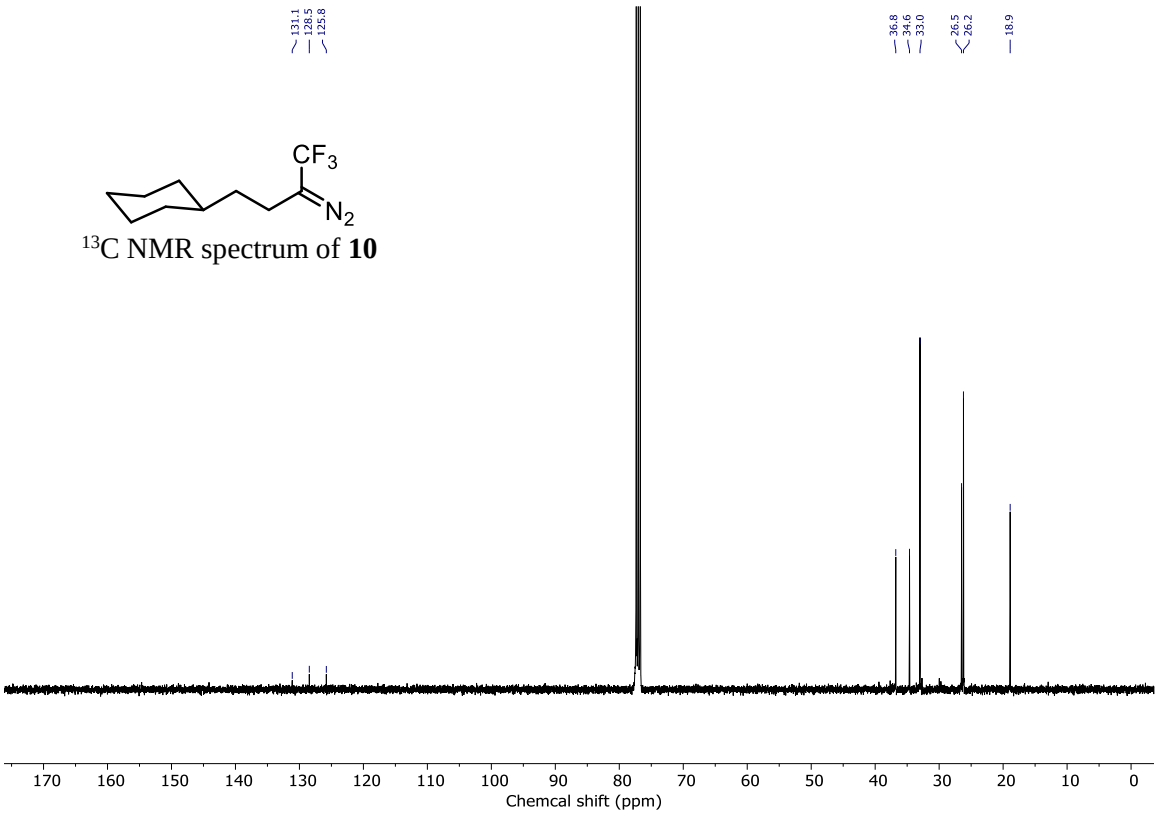

^{13}C NMR spectrum of **10**

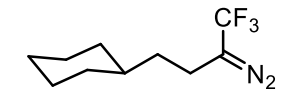

^{19}F NMR spectrum of **10**

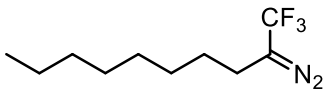

^{1}H NMR spectrum of **11**

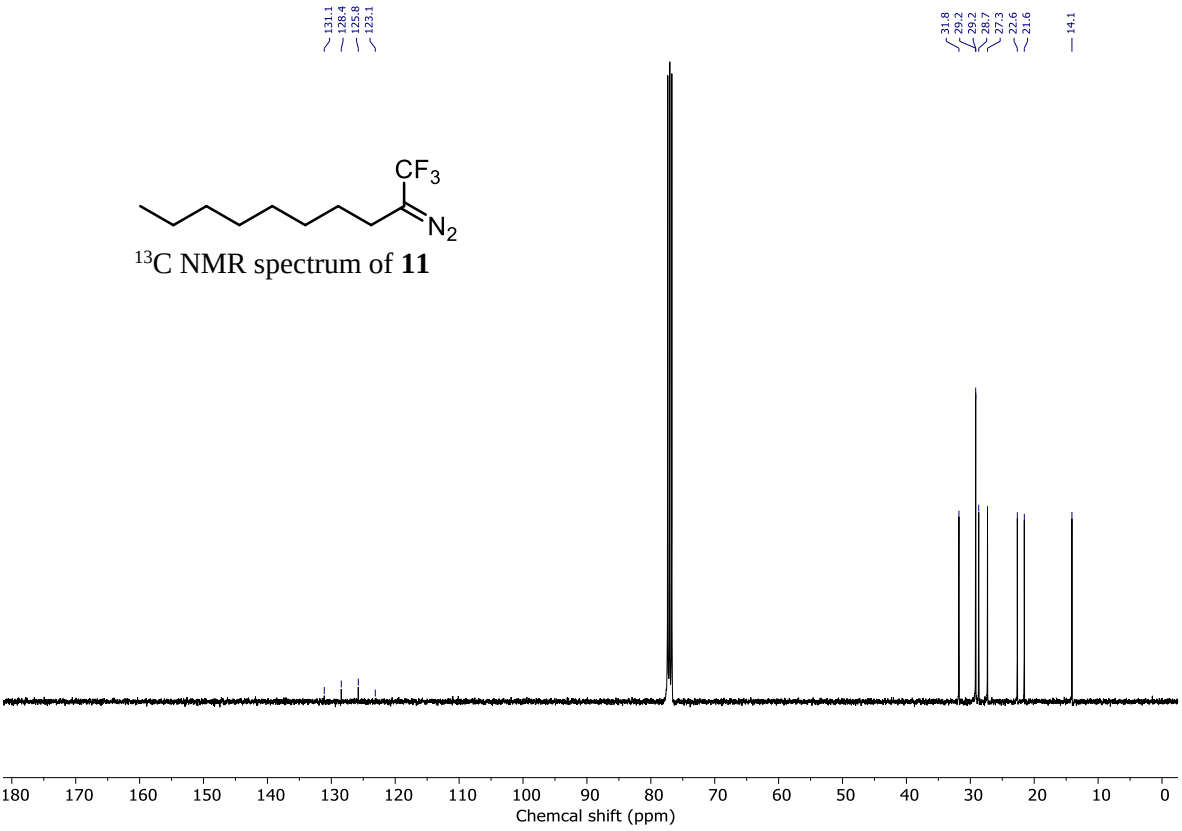

^{13}C NMR spectrum of **11**

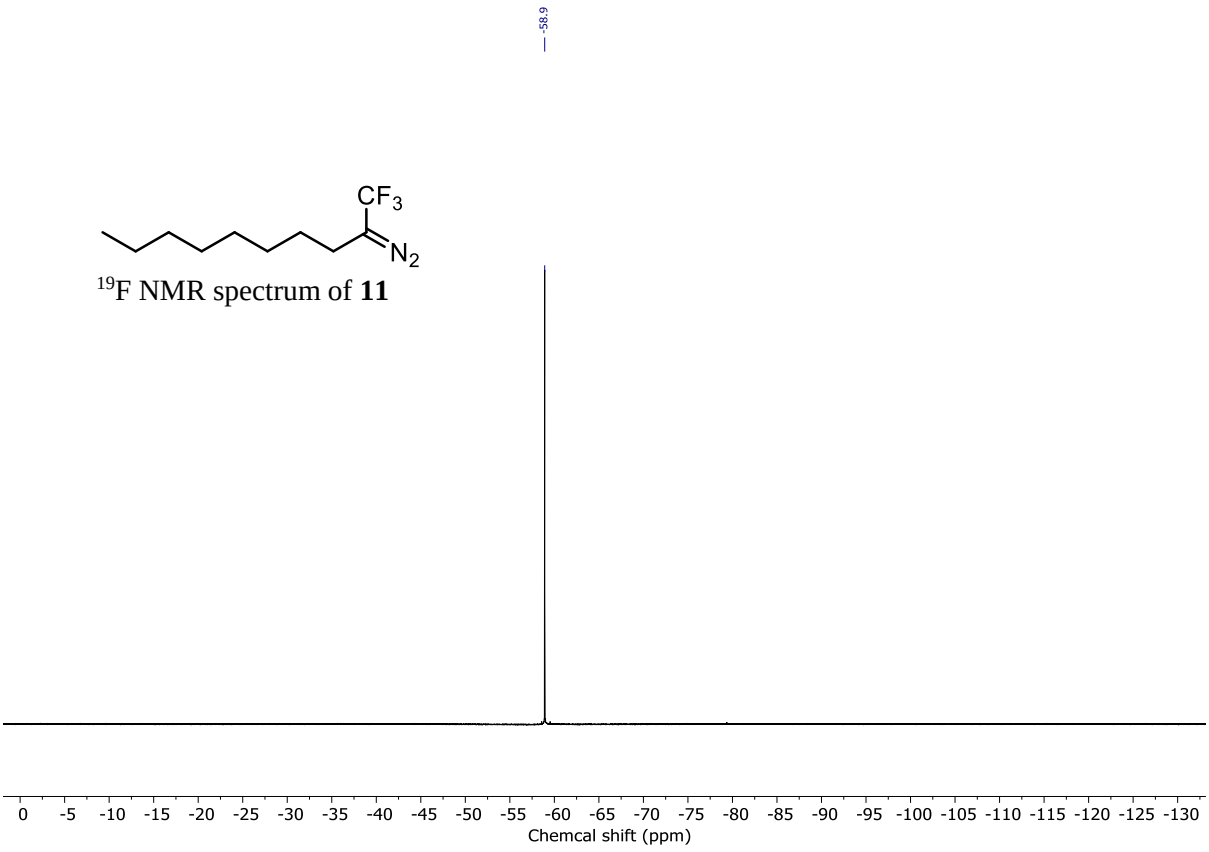

^{19}F NMR spectrum of **11**

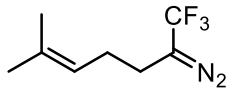

^{1}H NMR spectrum of **12**

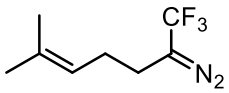

^{13}C NMR spectrum of **12**

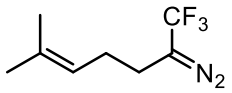

^{19}F NMR spectrum of **12**

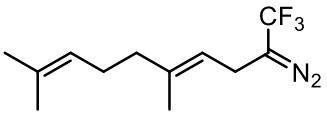

^{1}H NMR spectrum of **13**

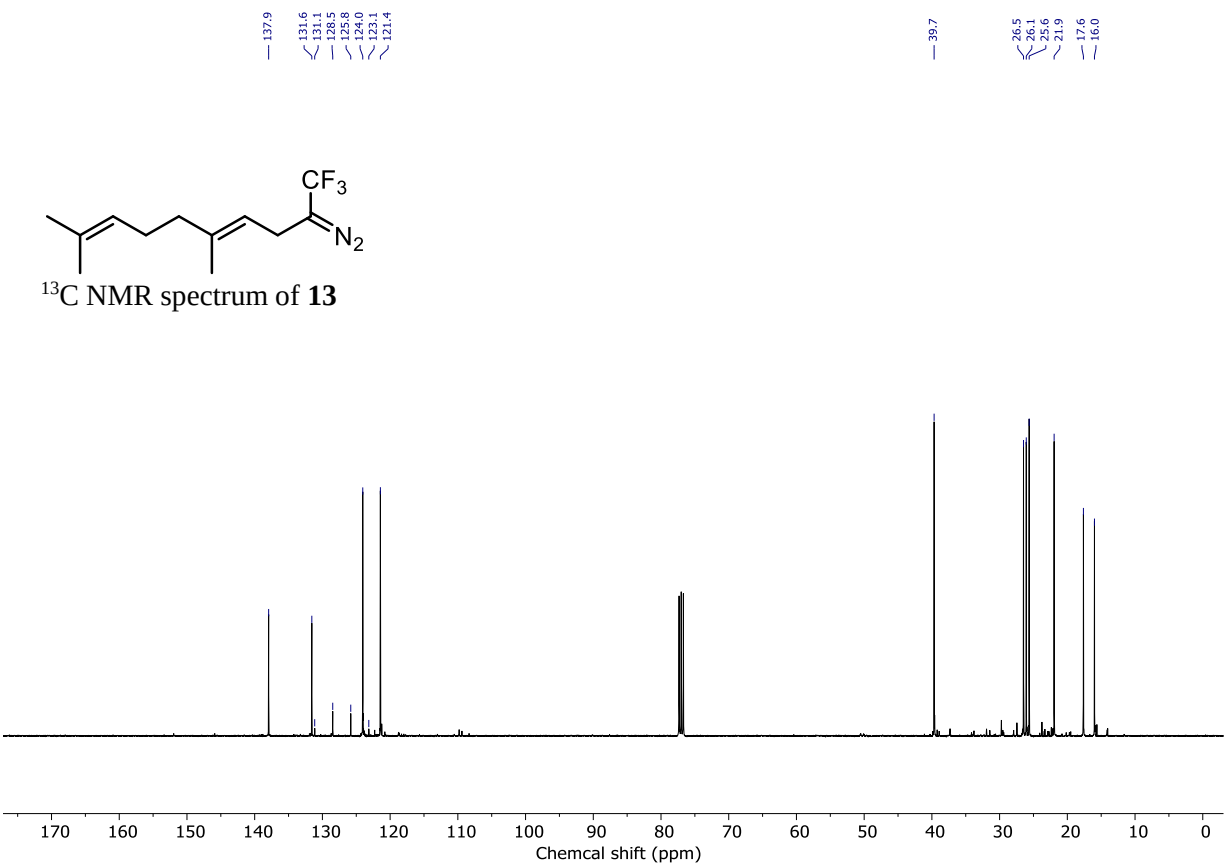

^{13}C NMR spectrum of **13**

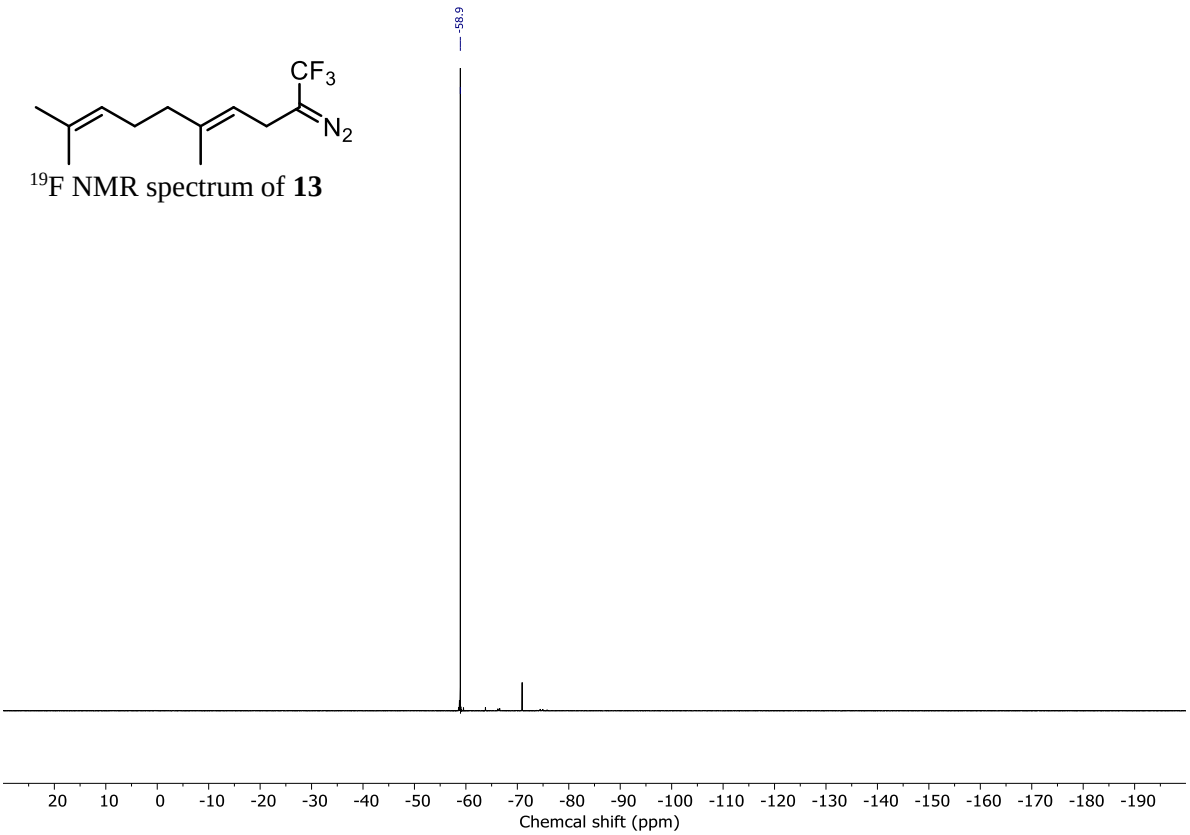

^{19}F NMR spectrum of **13**

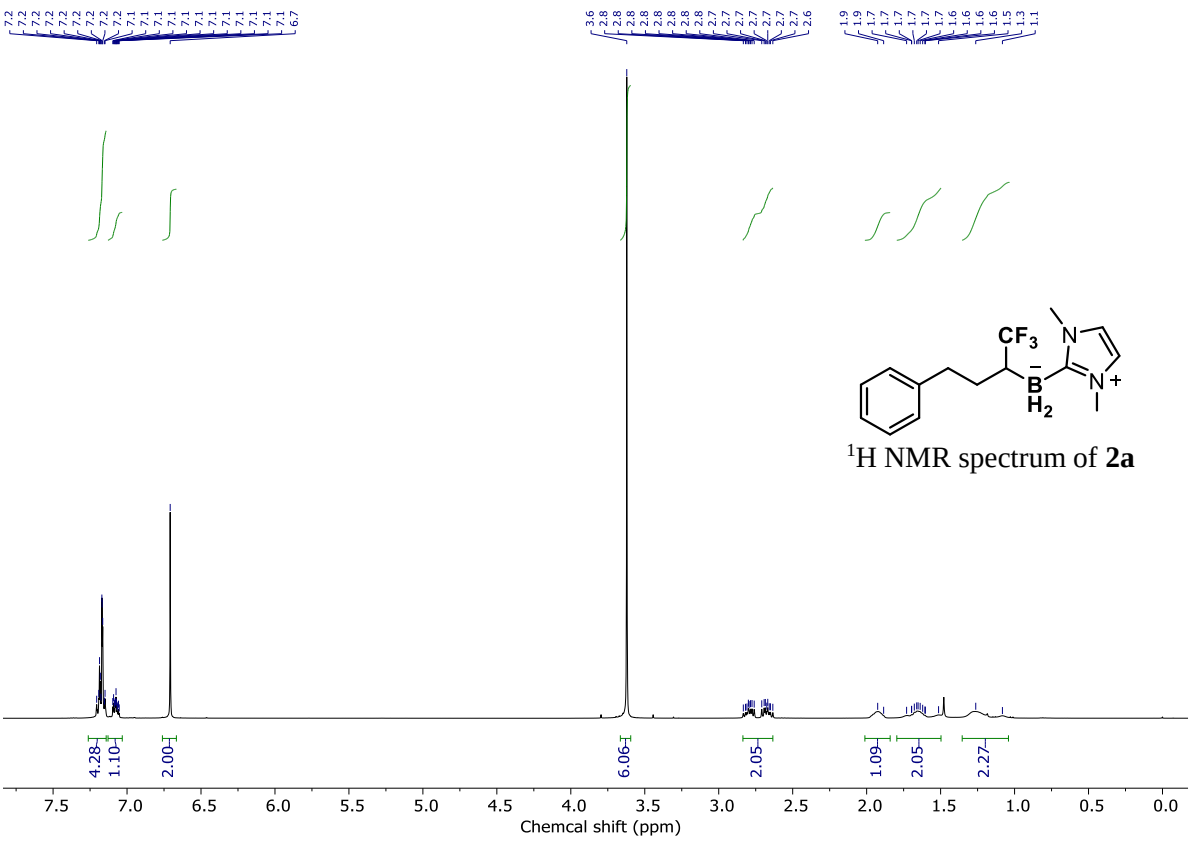

^{1}H NMR spectrum of **2a**

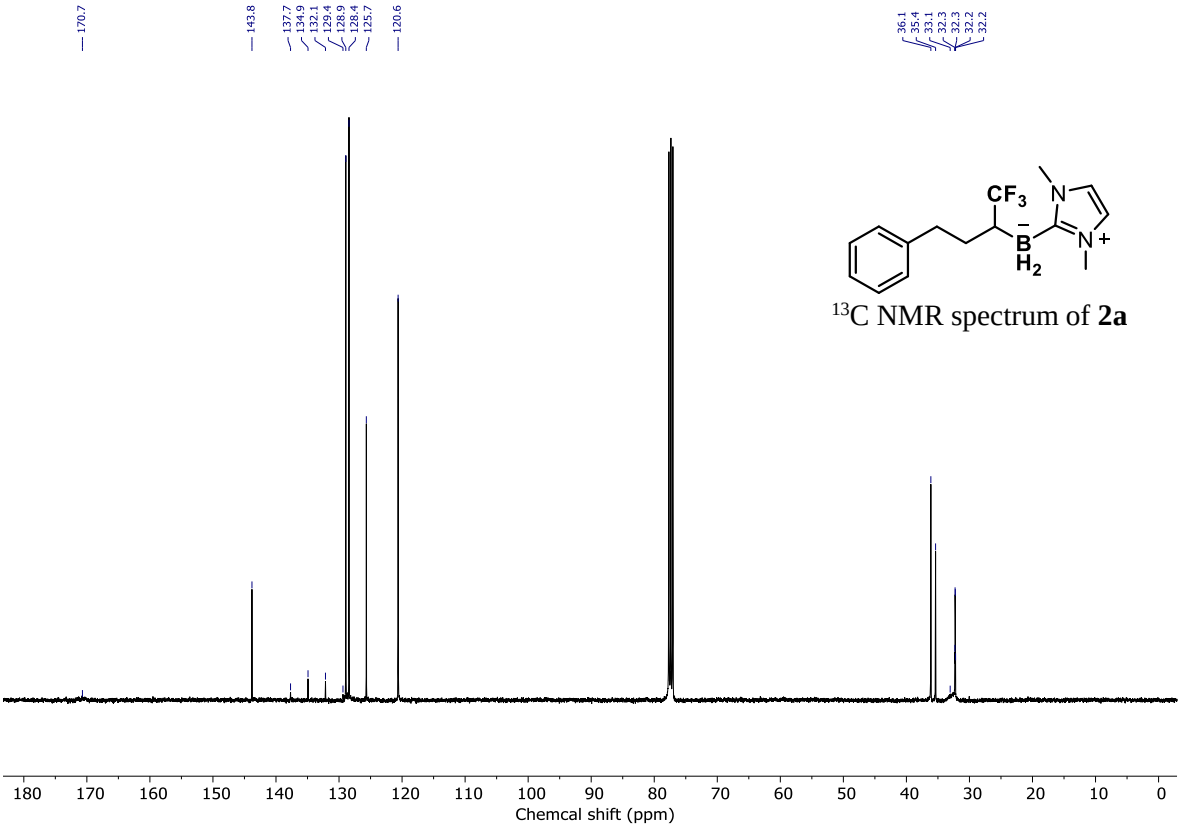

^{13}C NMR spectrum of **2a**

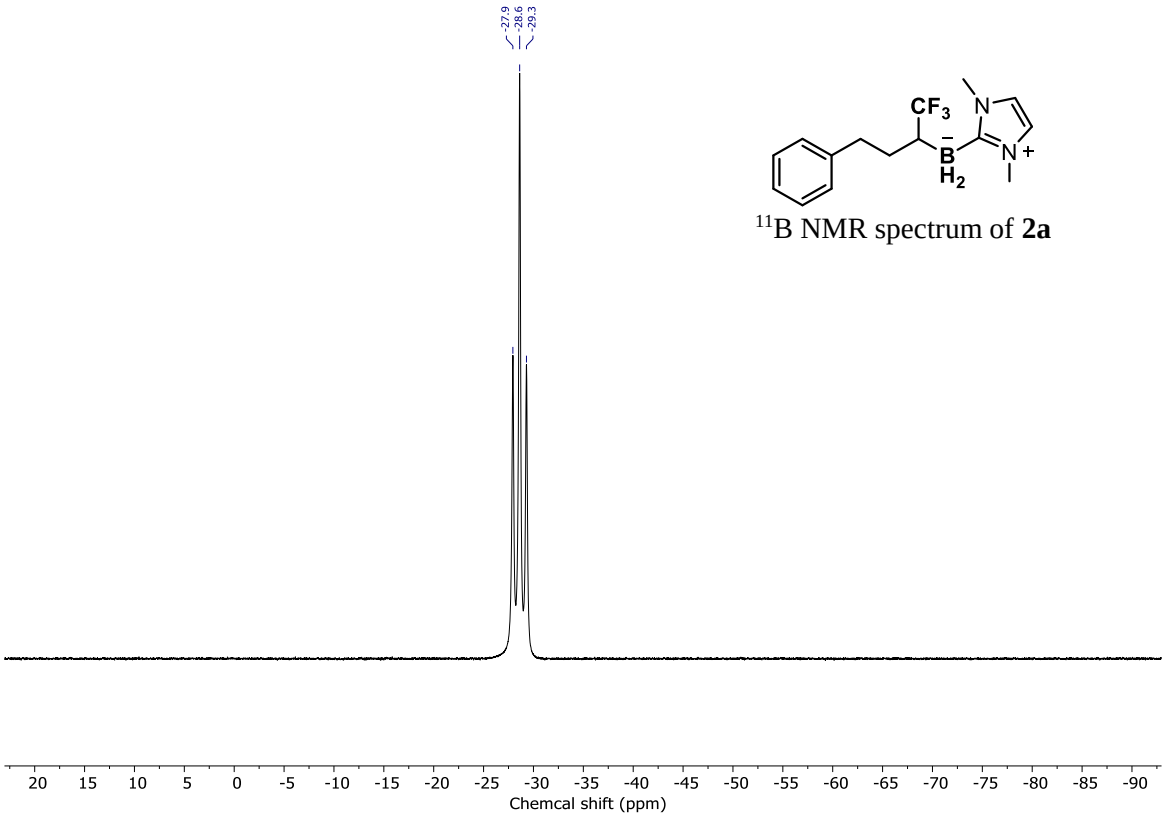

^{11}B NMR spectrum of **2a**

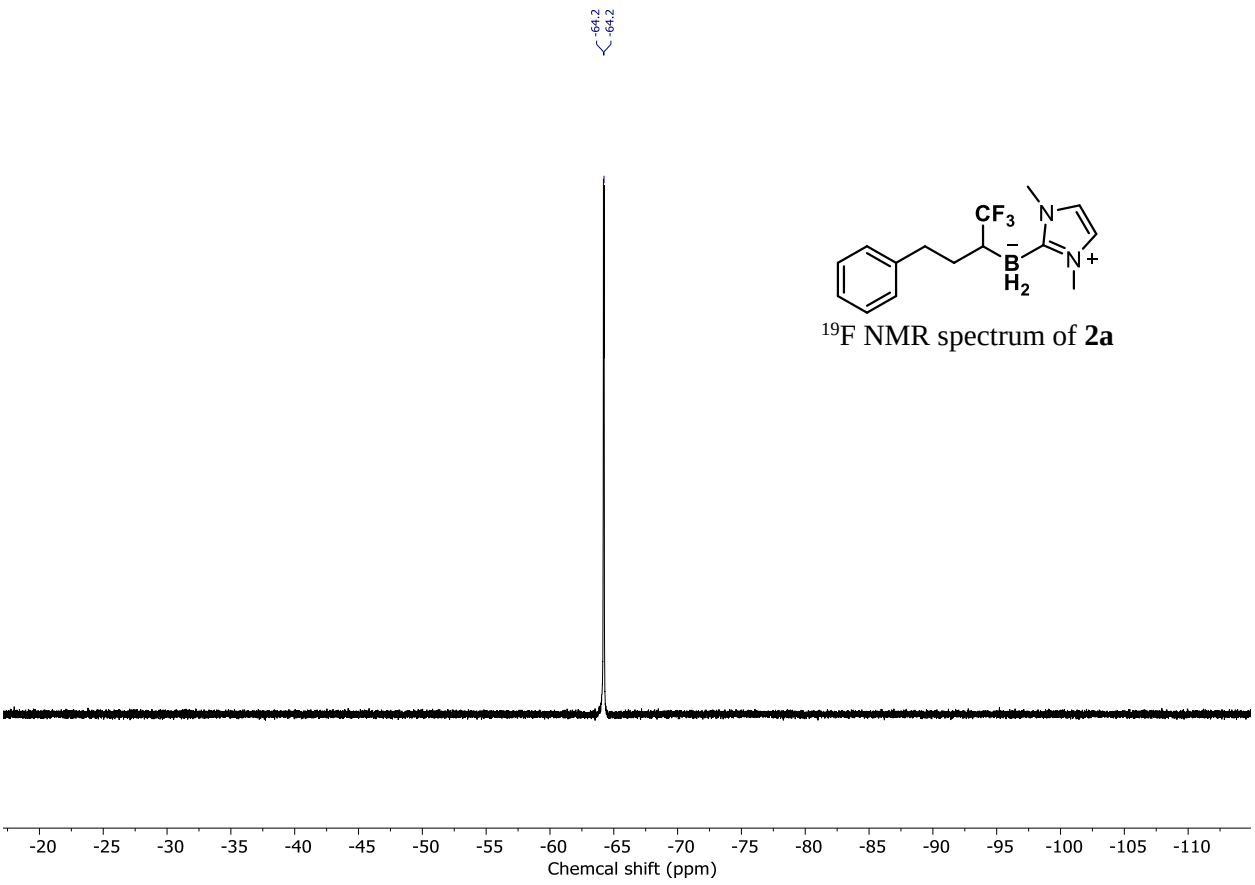

^{19}F NMR spectrum of **2a**

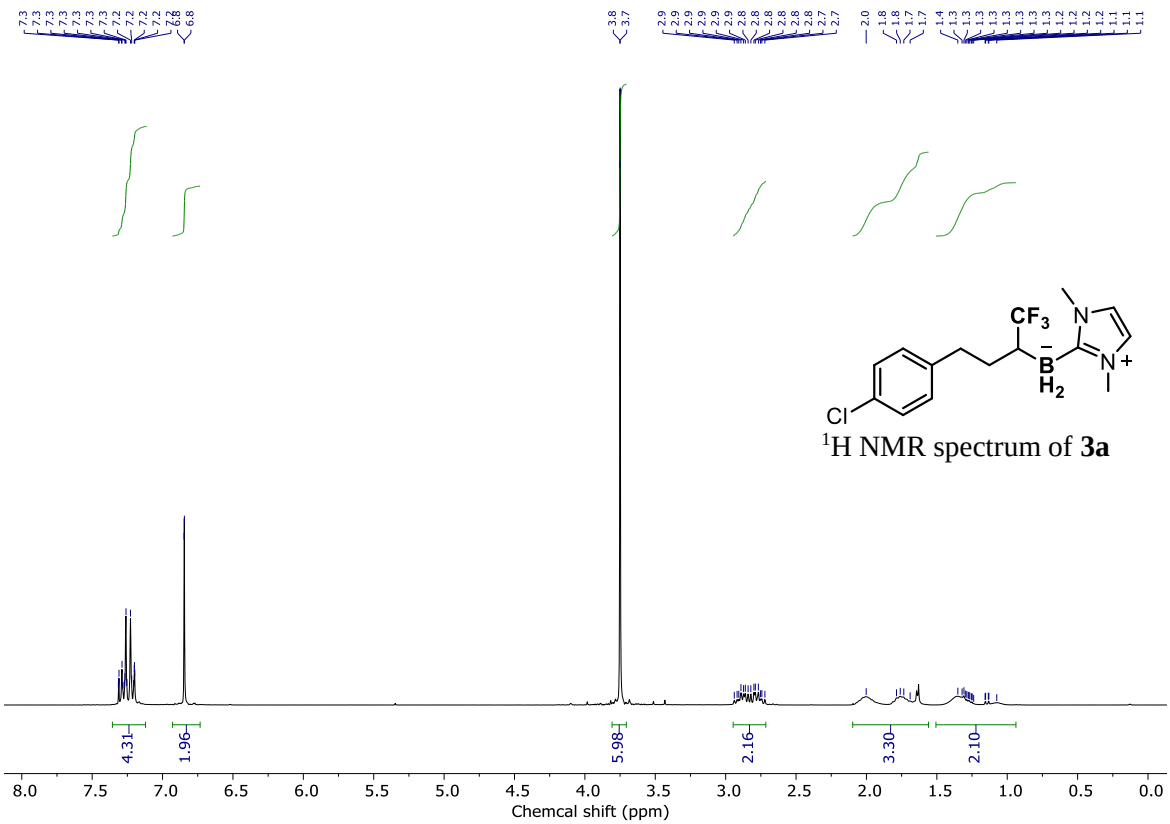

^{1}H NMR spectrum of **3a**

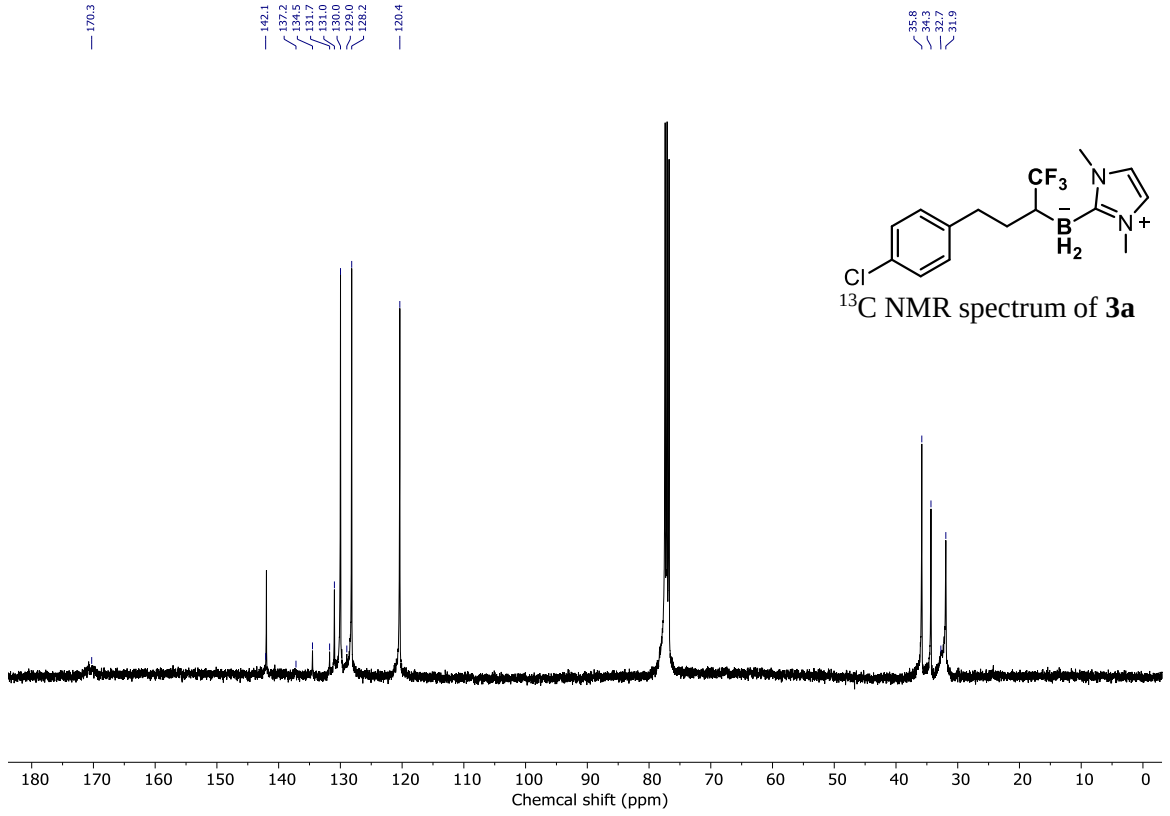

^{13}C NMR spectrum of **3a**

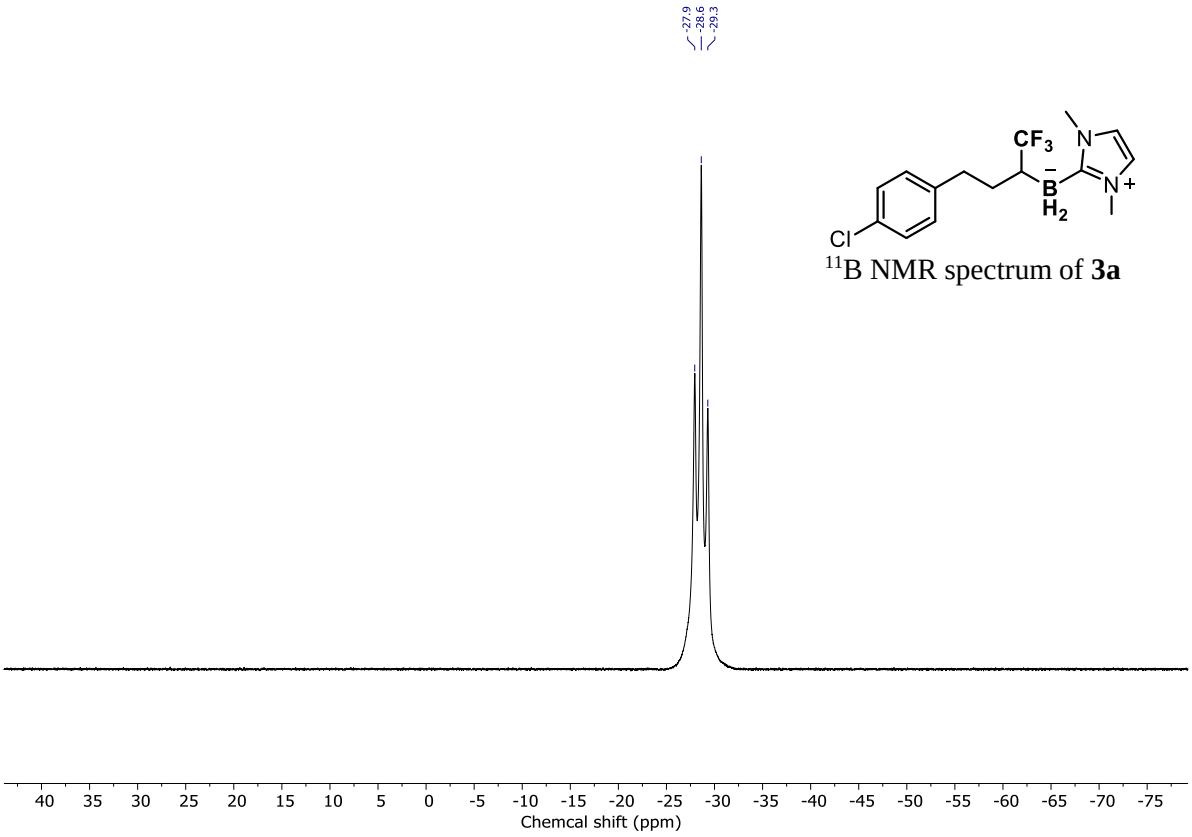

^{11}B NMR spectrum of **3a**

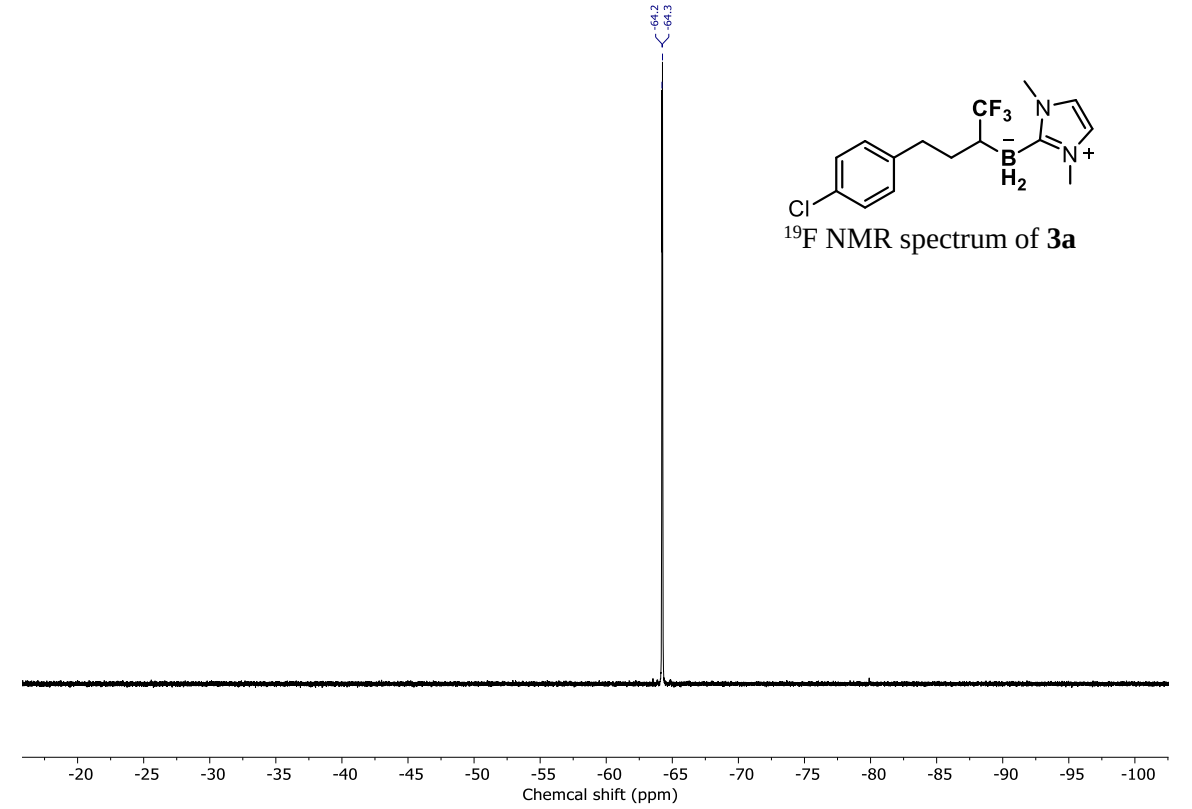

^{19}F NMR spectrum of **3a**

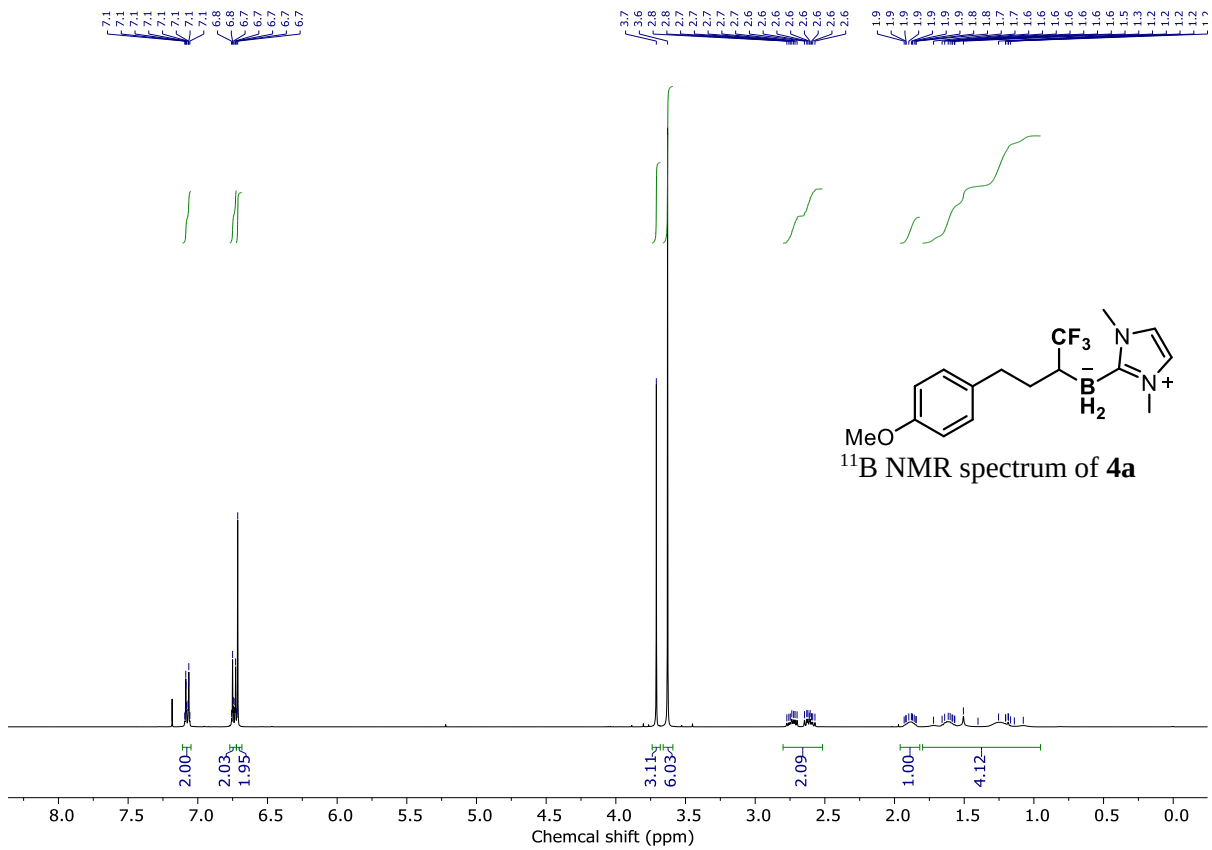

^{11}B NMR spectrum of **4a**

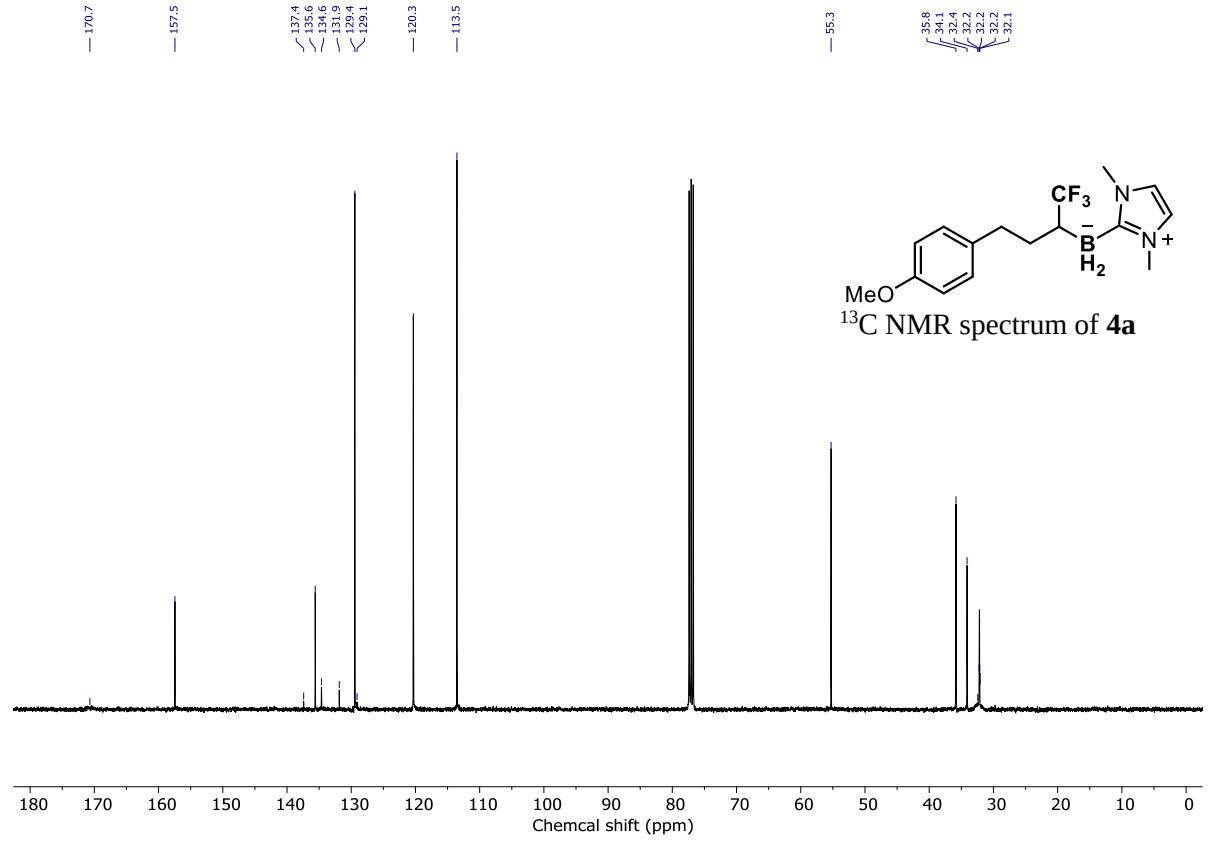

^{13}C NMR spectrum of **4a**

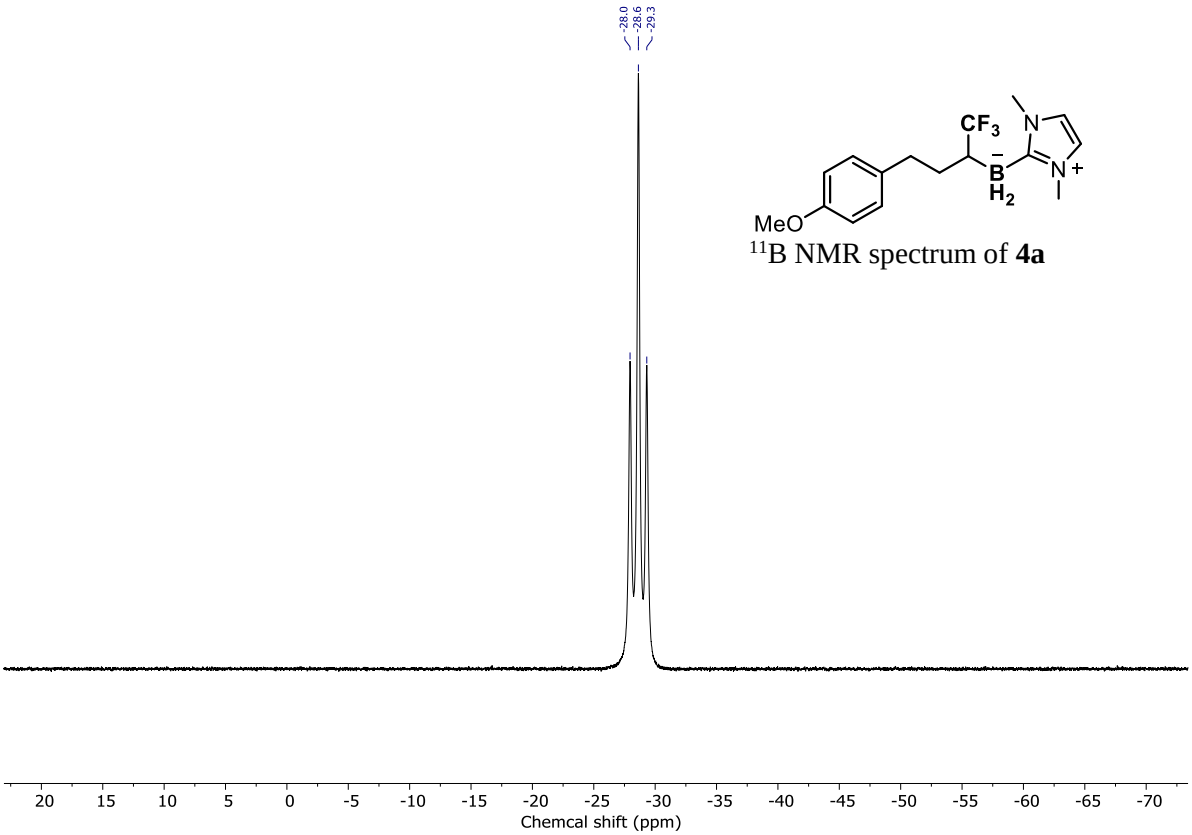

^{11}B NMR spectrum of **4a**

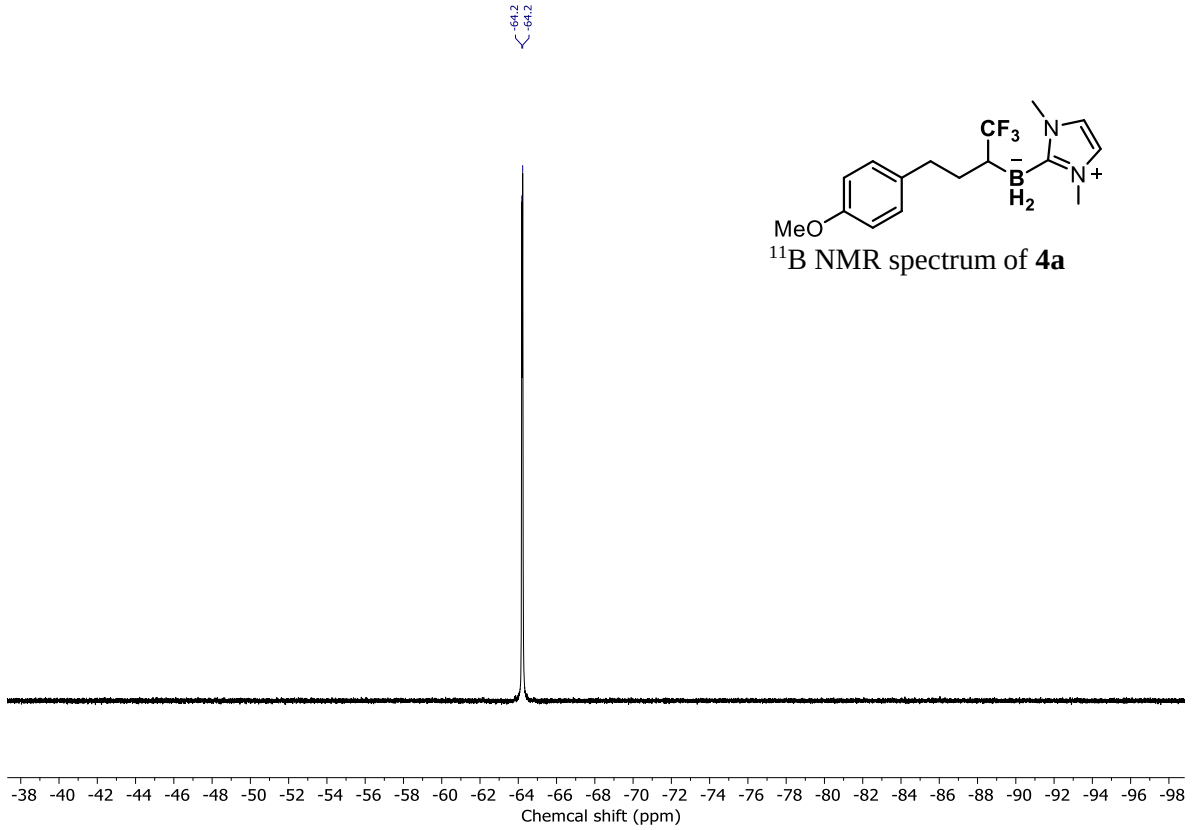

^{11}B NMR spectrum of **4a**

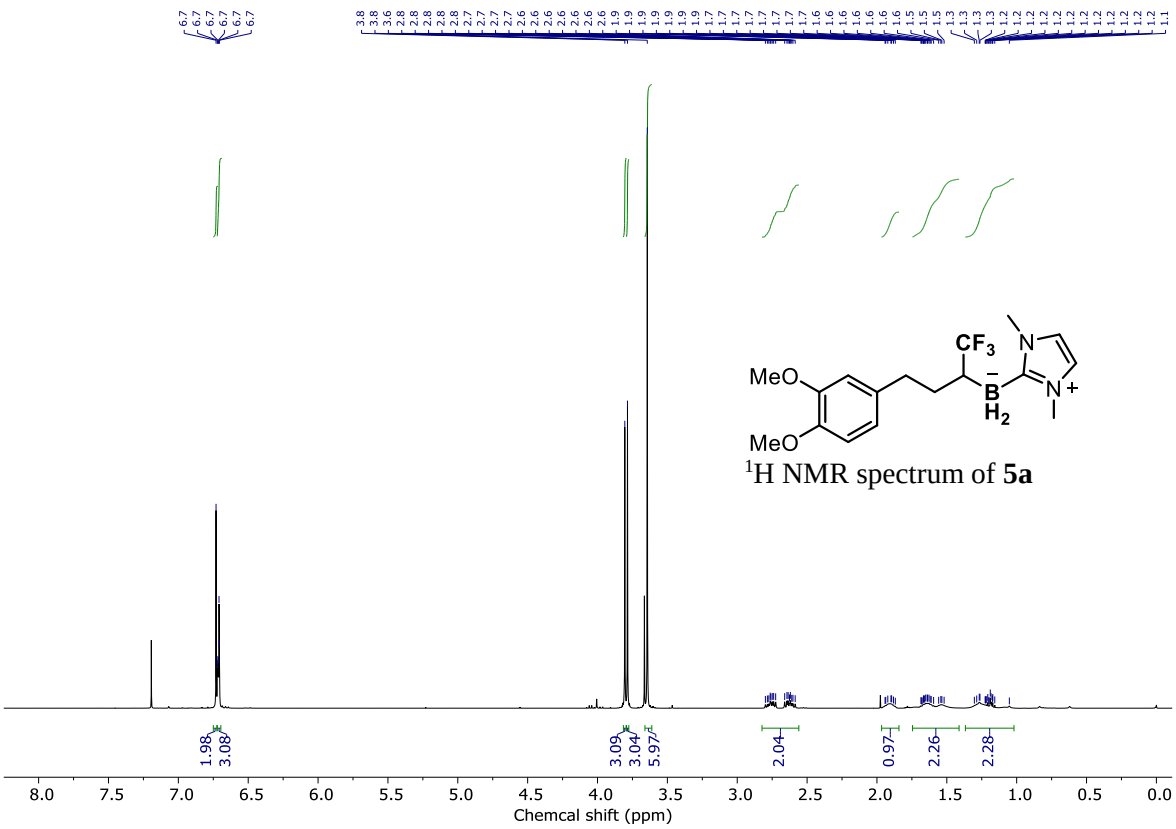

^{1}H NMR spectrum of **5a**

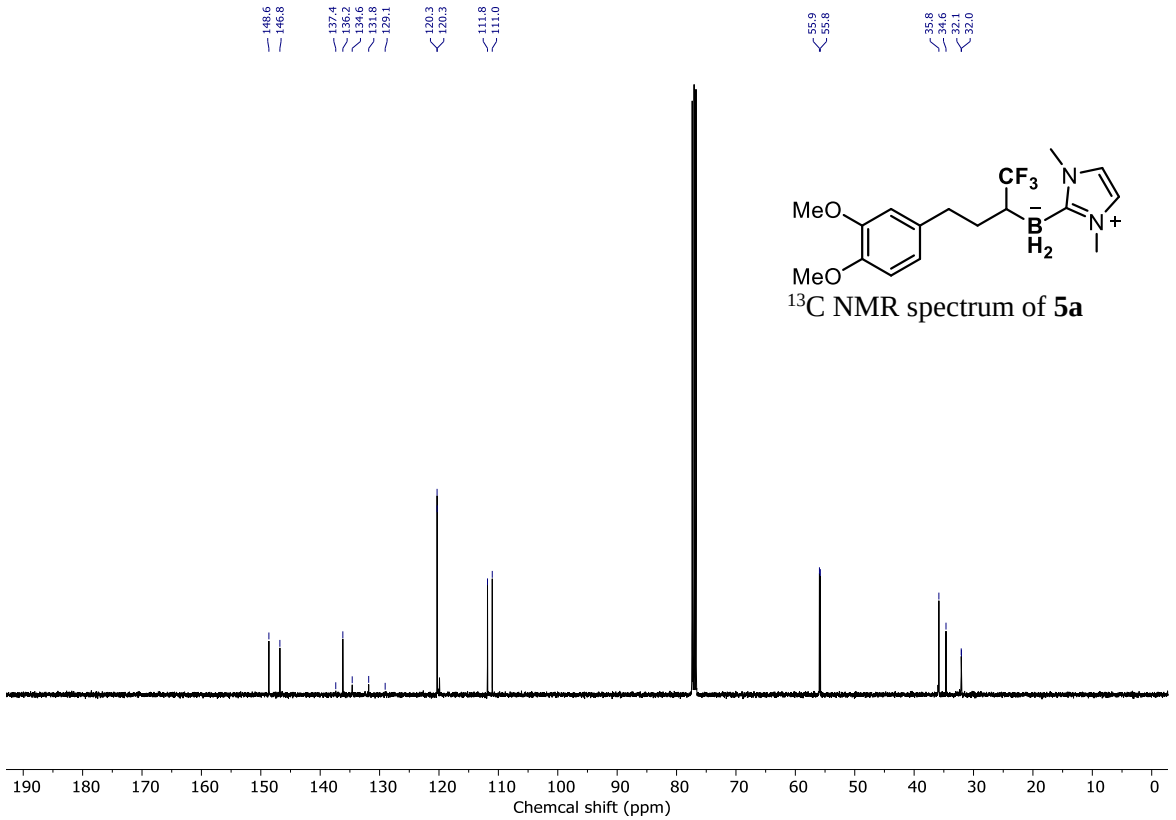

^{13}C NMR spectrum of **5a**

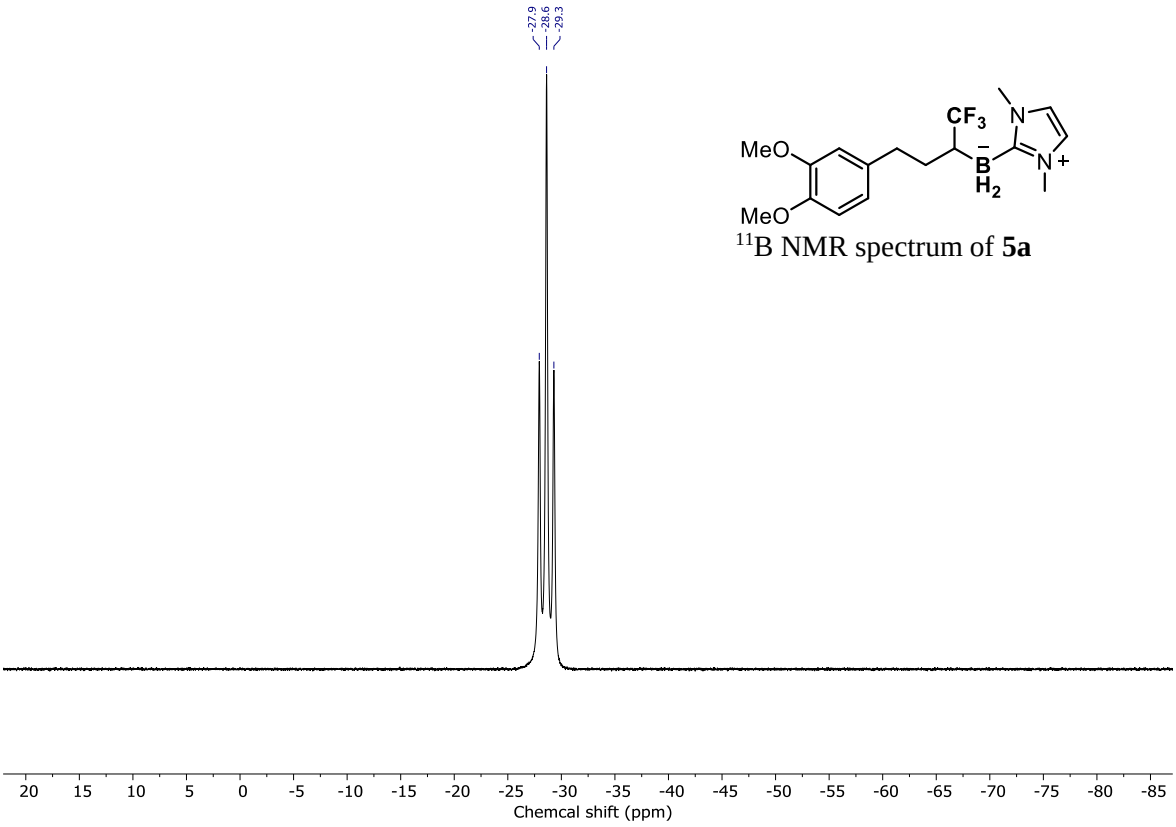

^{11}B NMR spectrum of **5a**

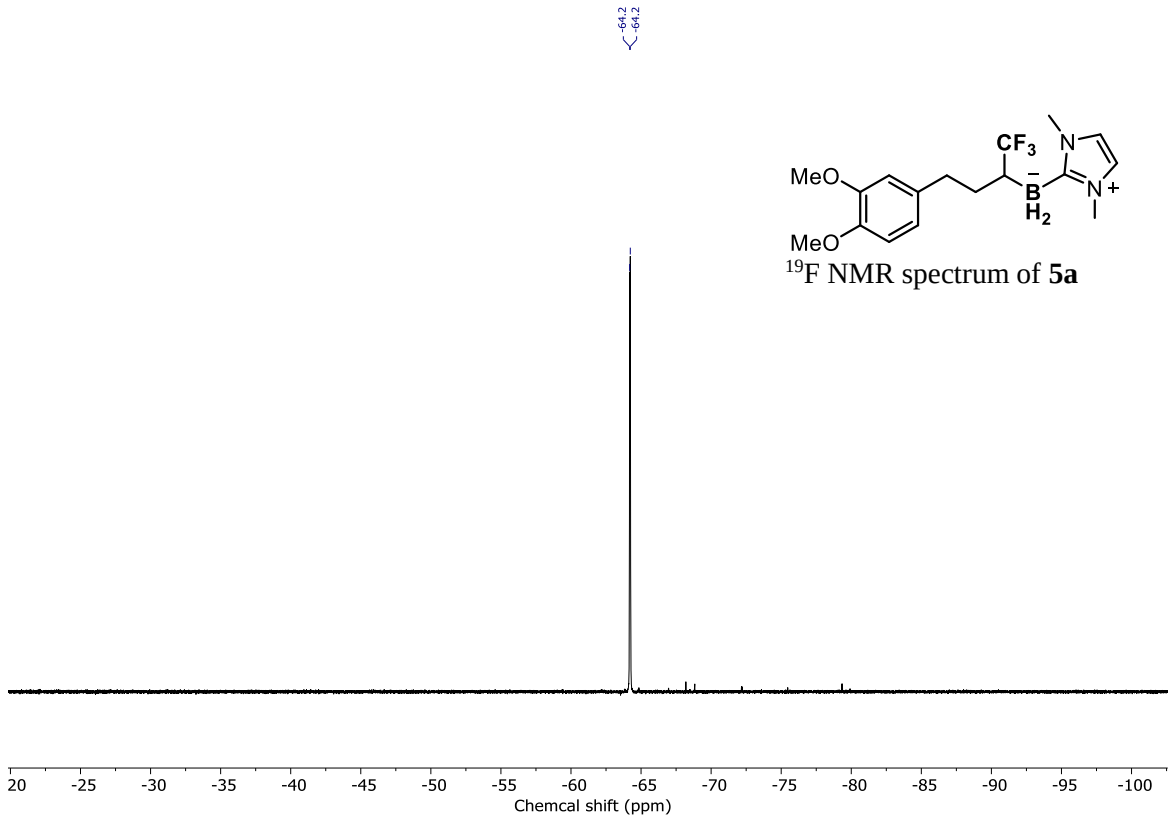

^{19}F NMR spectrum of **5a**

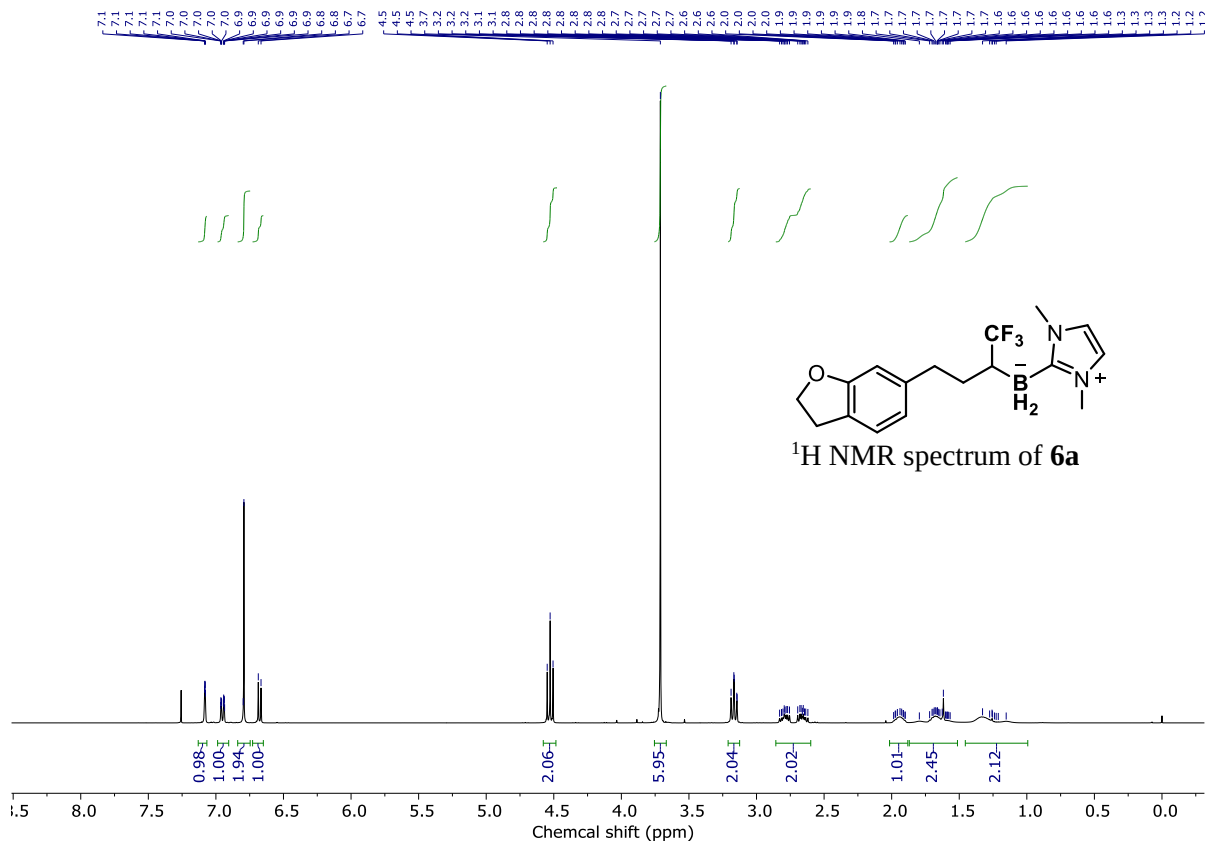

^{1}H NMR spectrum of **6a**

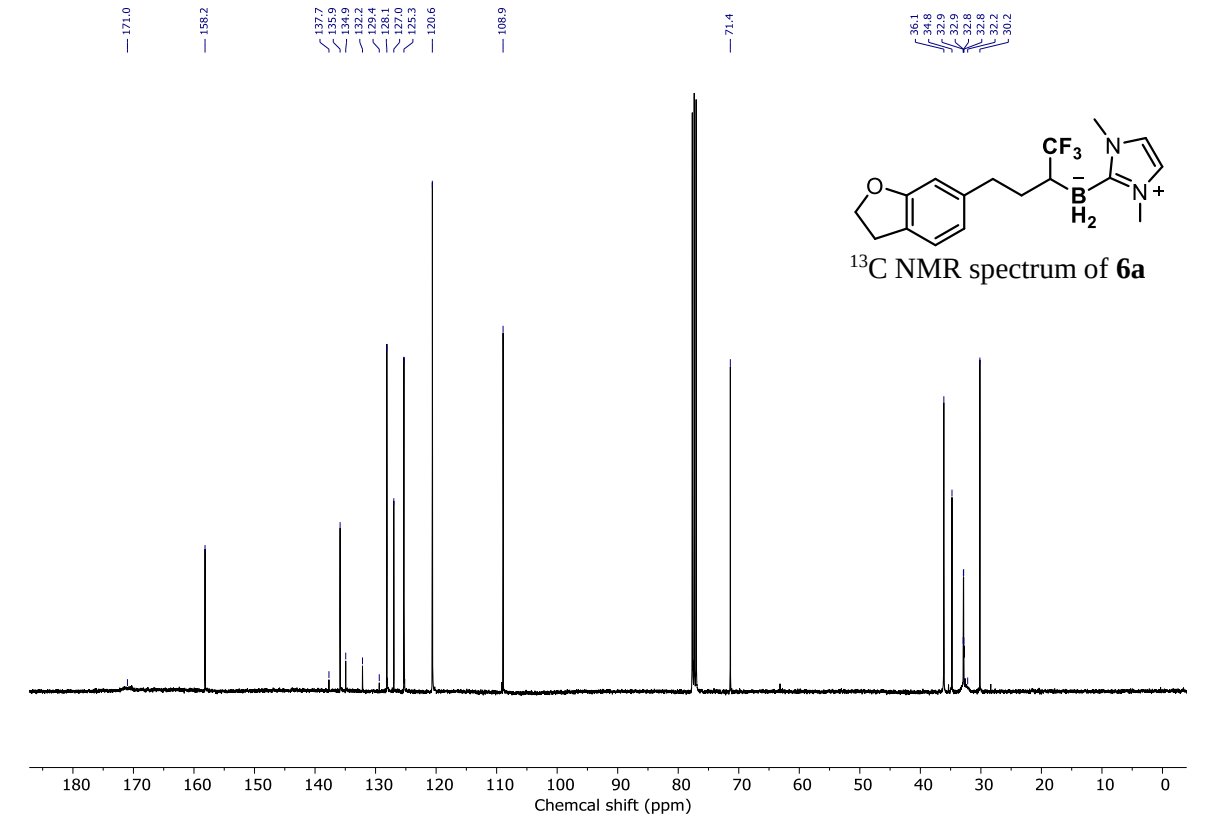

^{13}C NMR spectrum of **6a**

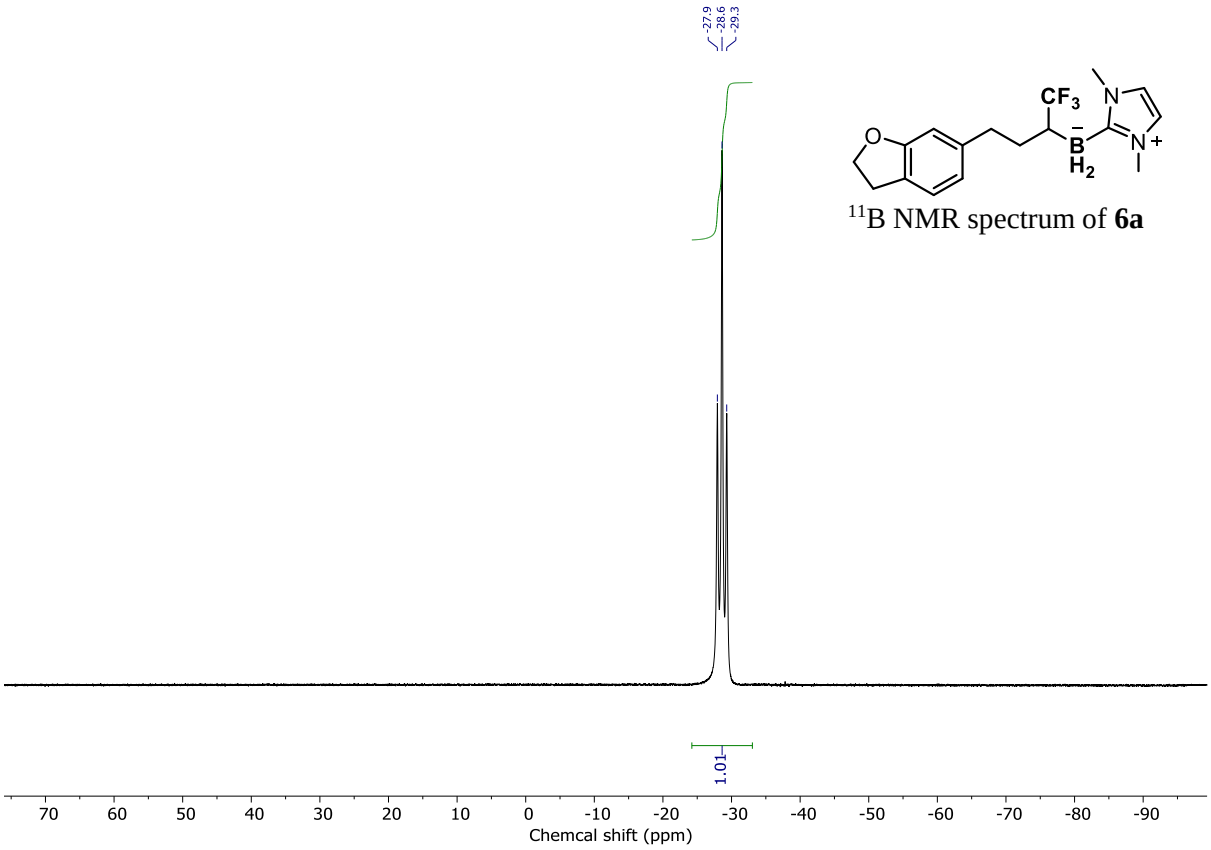

^{11}B NMR spectrum of **6a**

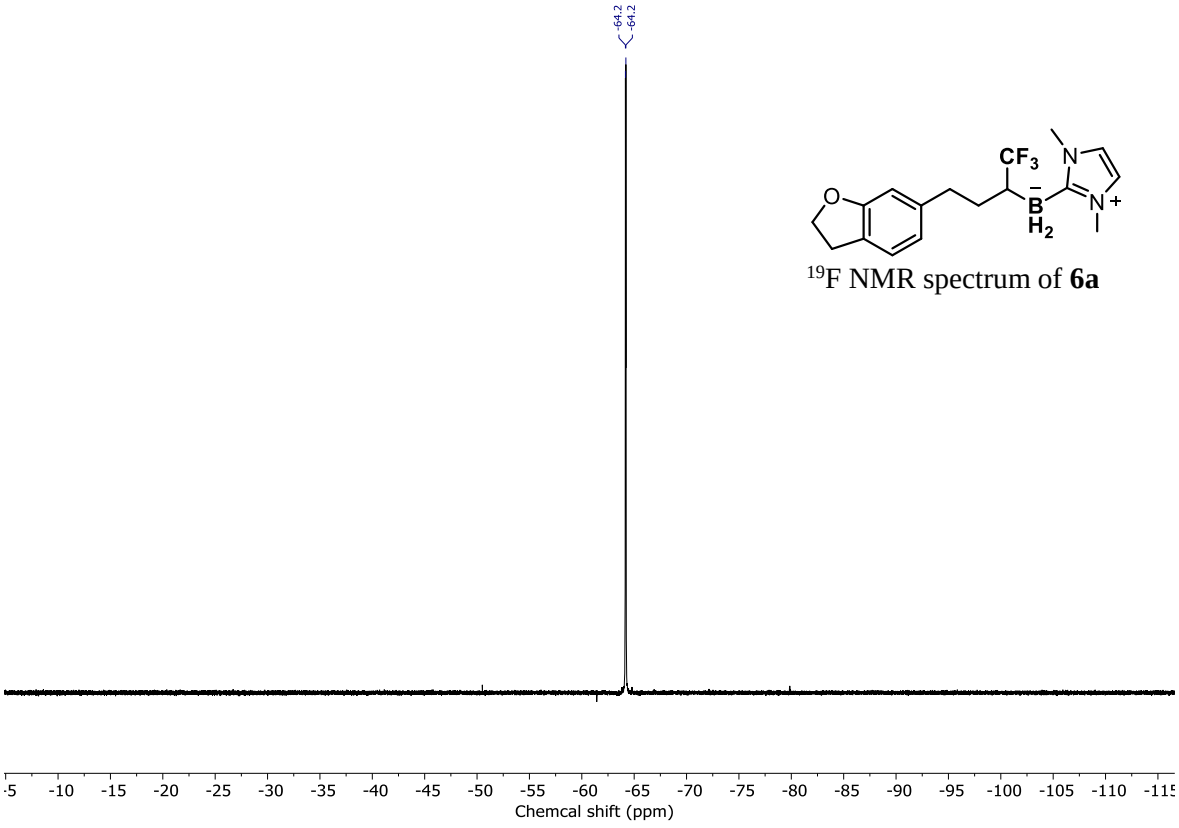

^{19}F NMR spectrum of **6a**

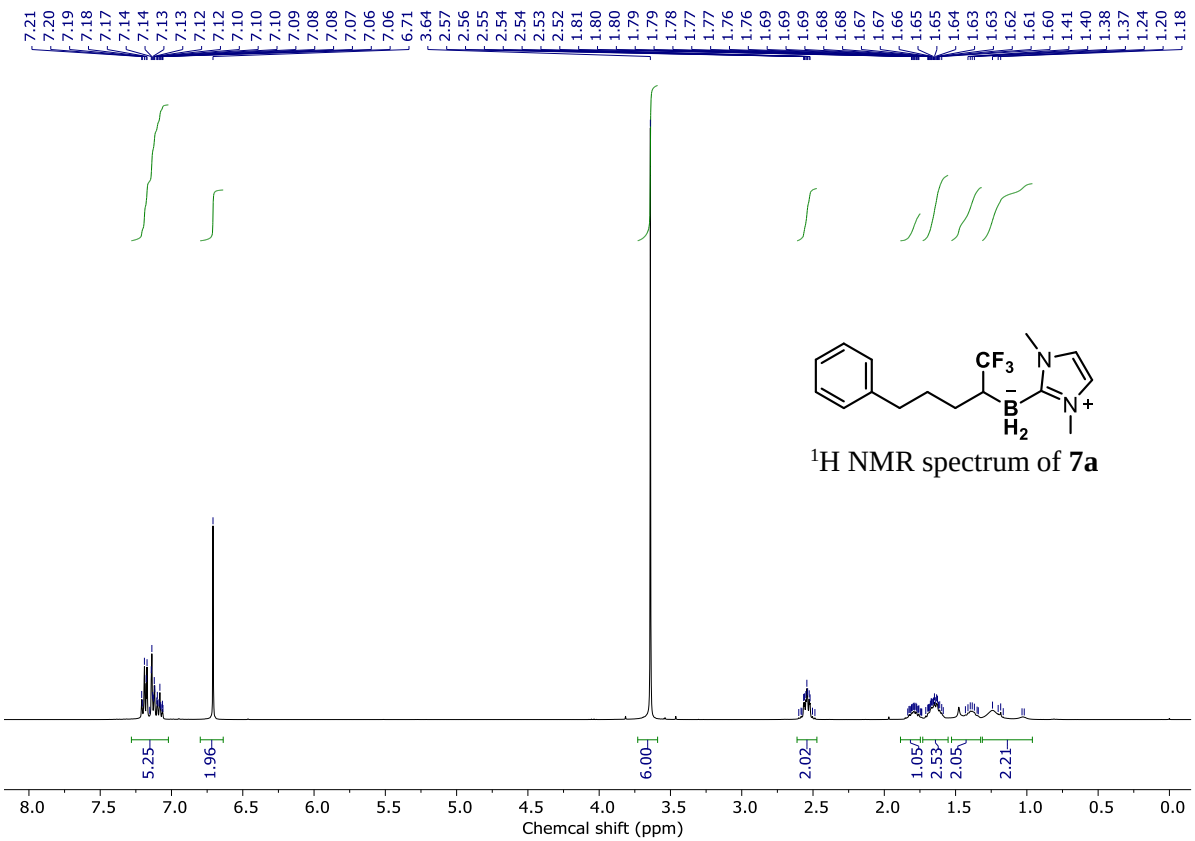

^{1}H NMR spectrum of **7a**

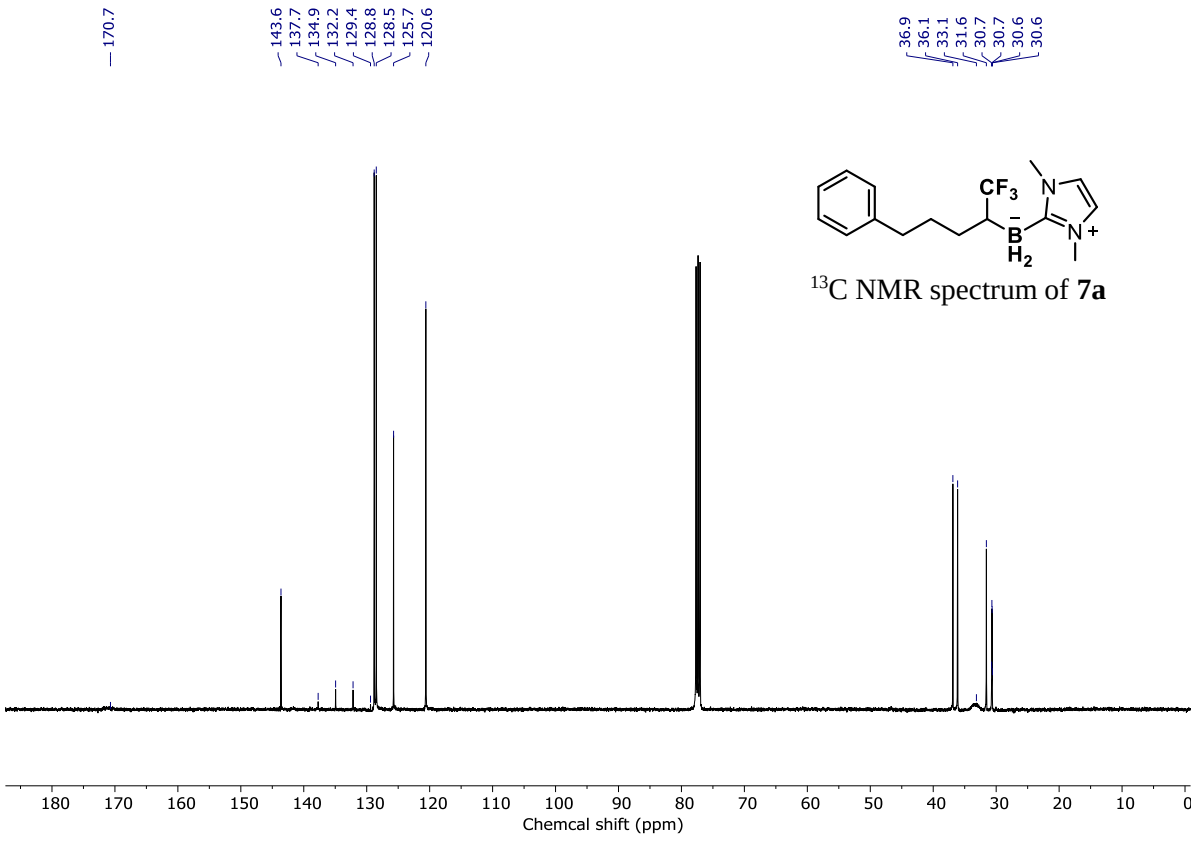

^{13}C NMR spectrum of **7a**

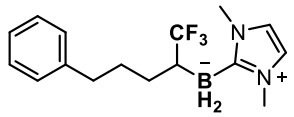

^{11}B NMR spectrum of **7a**

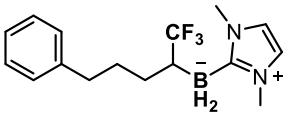

^{19}F NMR spectrum of **7a**

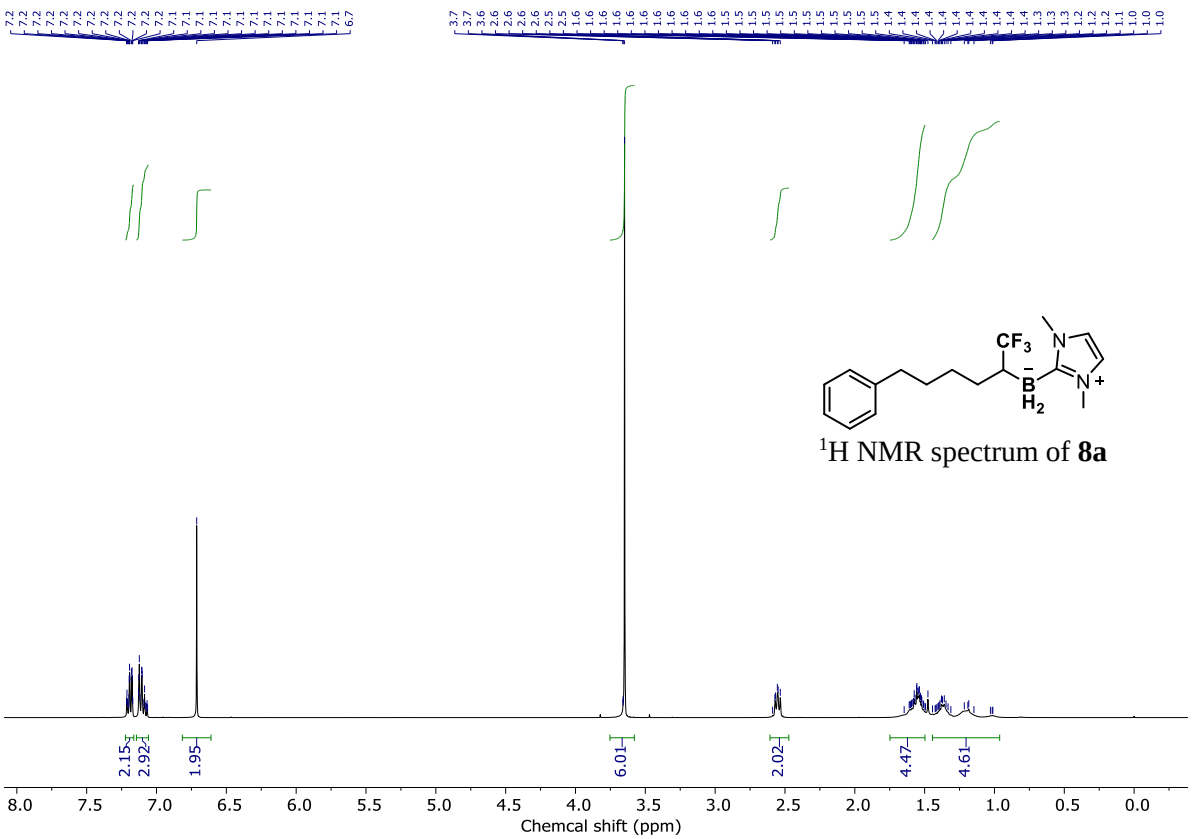

^{1}H NMR spectrum of **8a**

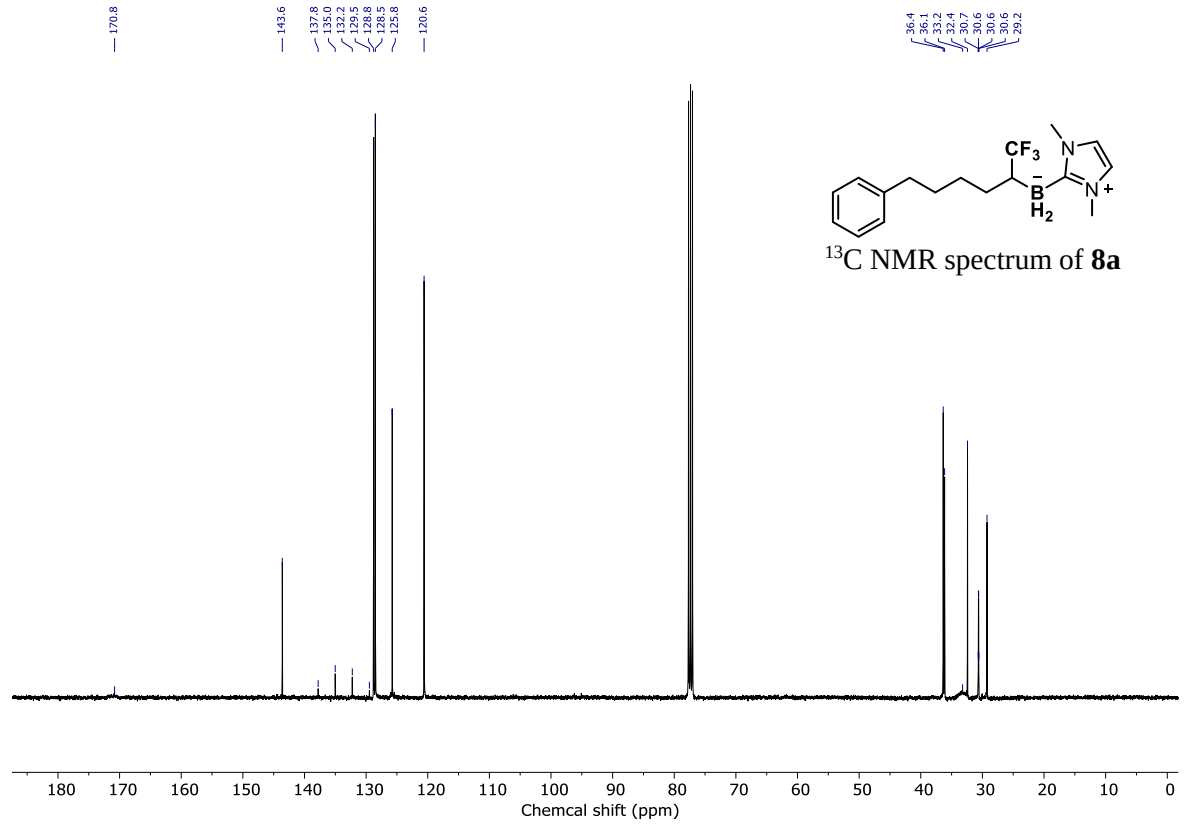

^{13}C NMR spectrum of **8a**

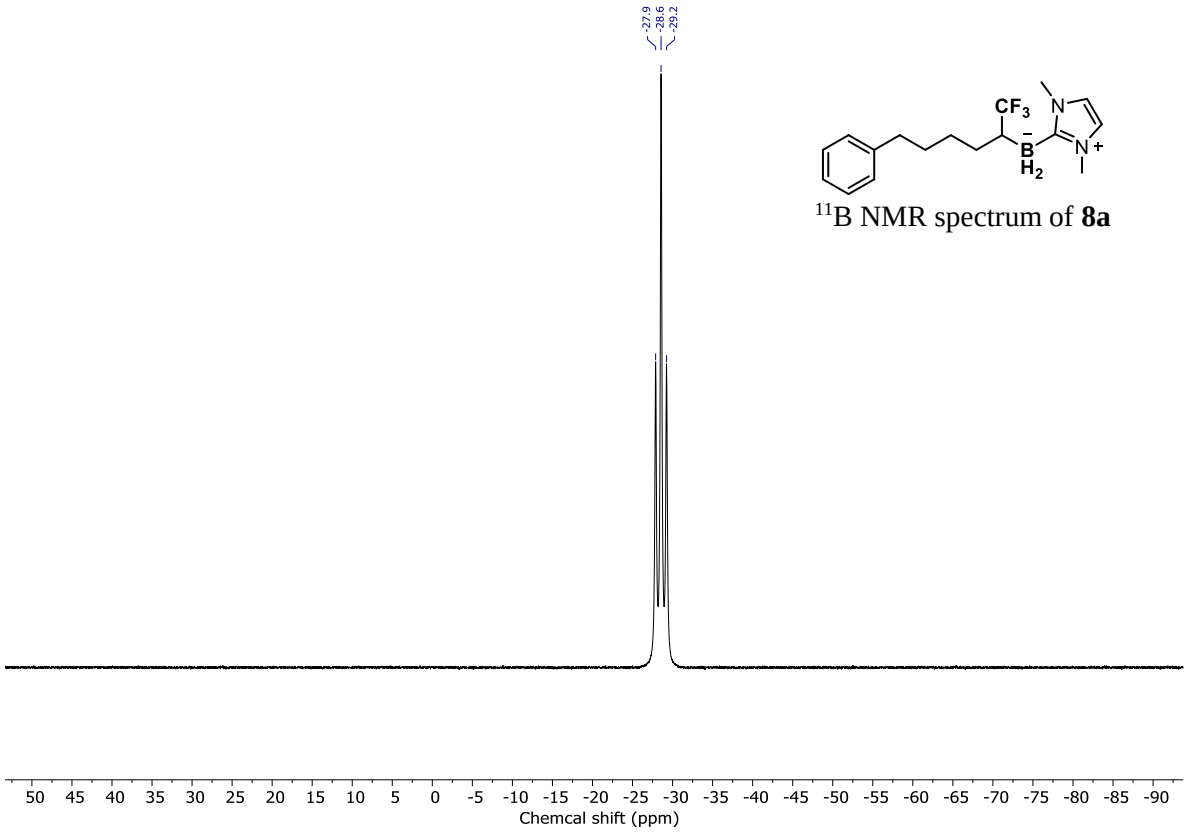

^{11}B NMR spectrum of **8a**

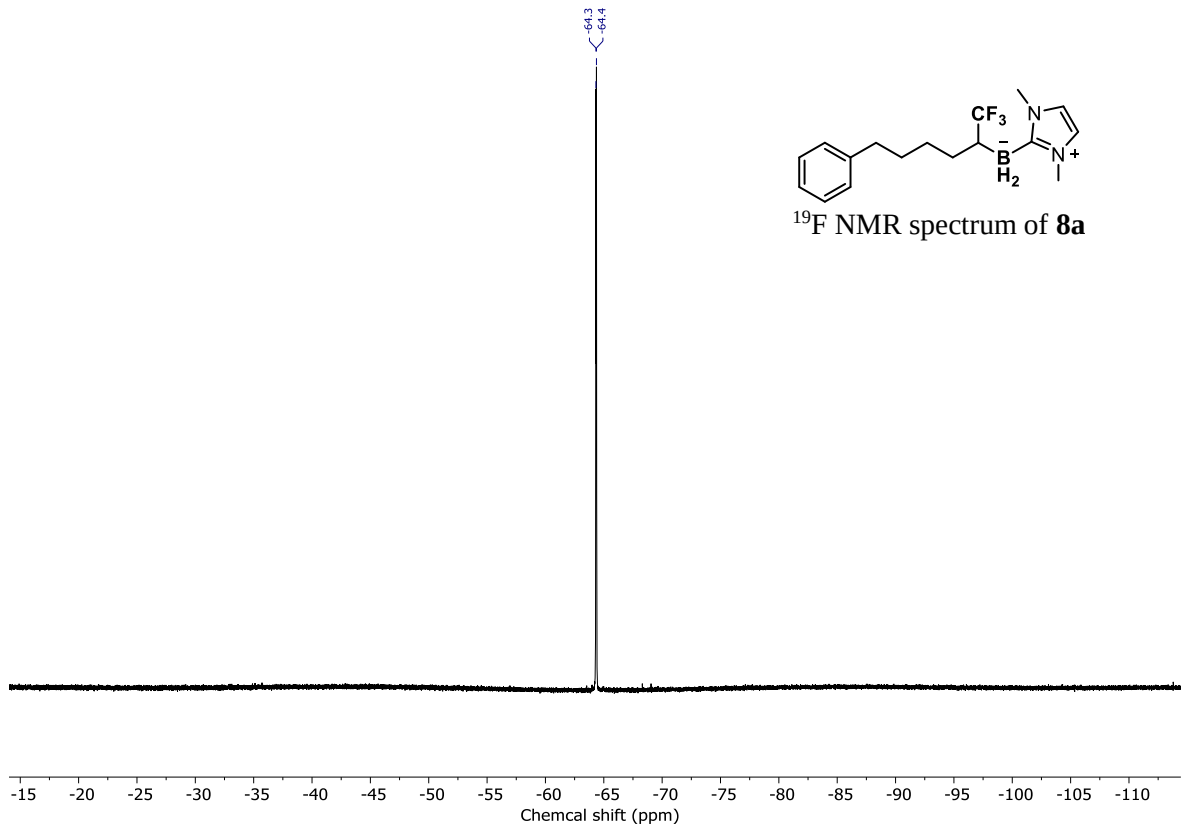

^{19}F NMR spectrum of **8a**

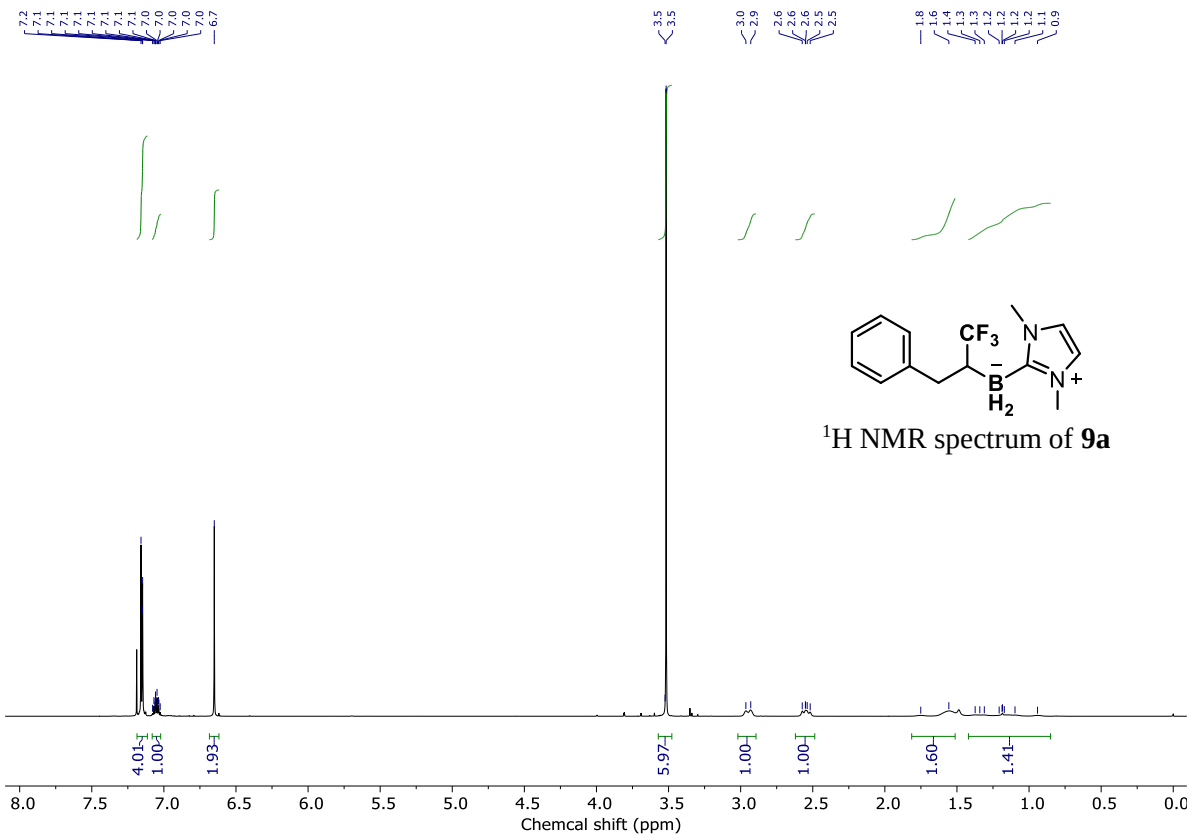

^{1}H NMR spectrum of **9a**

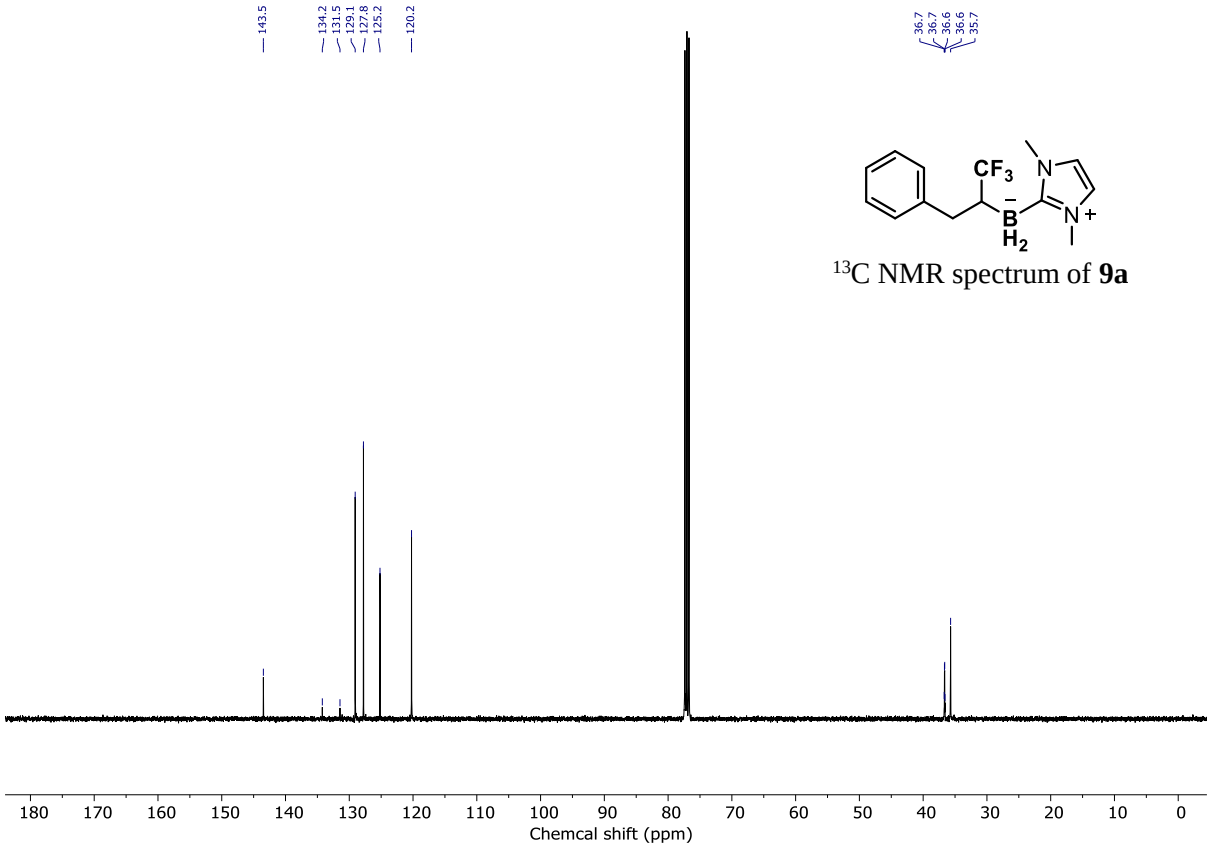

^{13}C NMR spectrum of **9a**

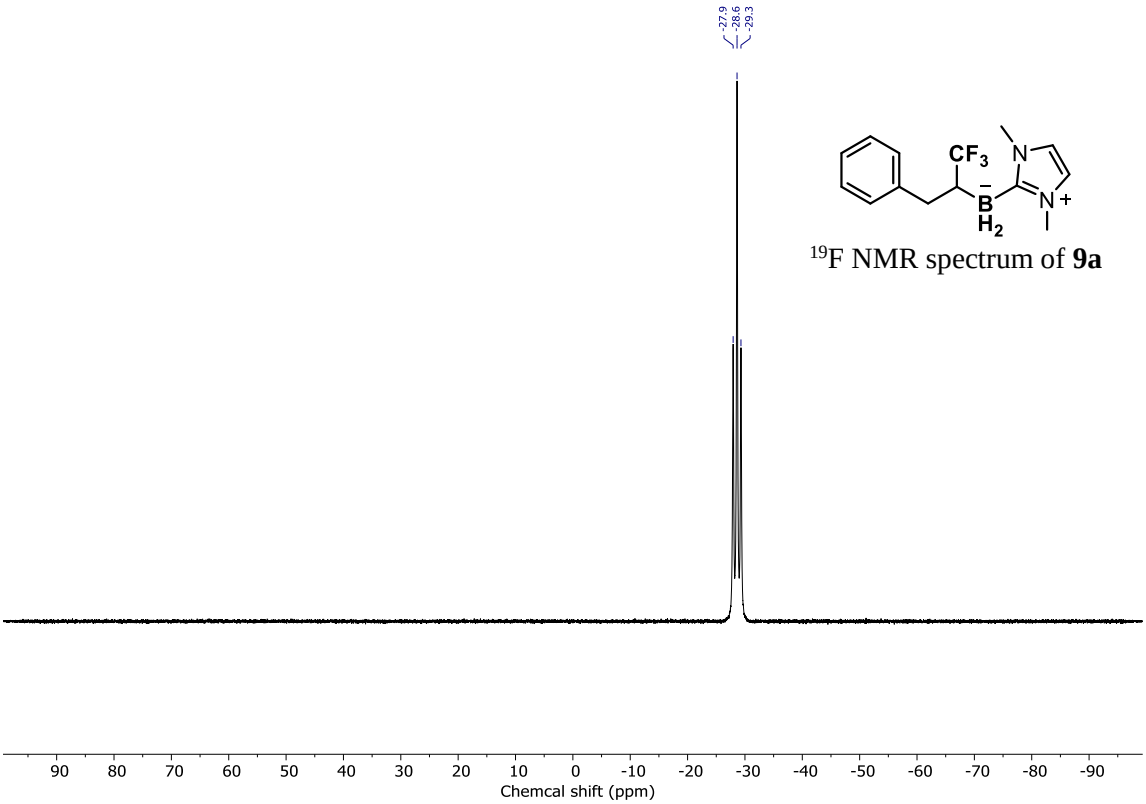

^{19}F NMR spectrum of **9a**

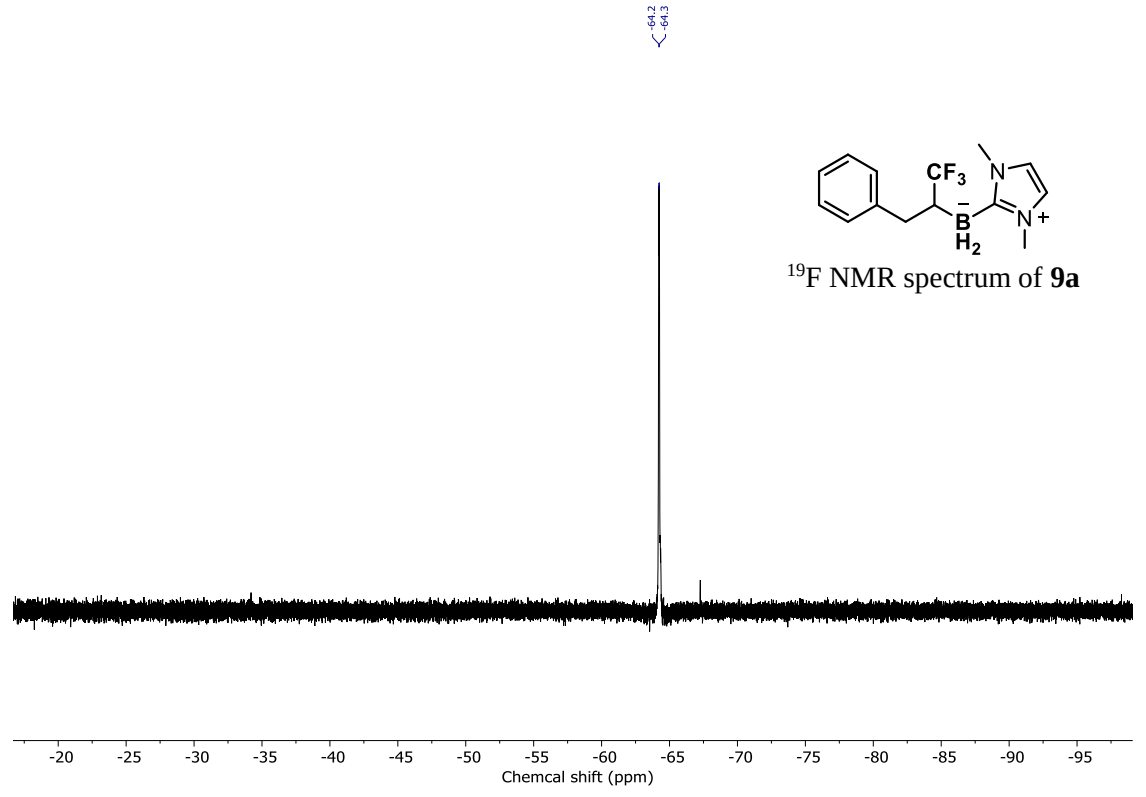

^{19}F NMR spectrum of **9a**

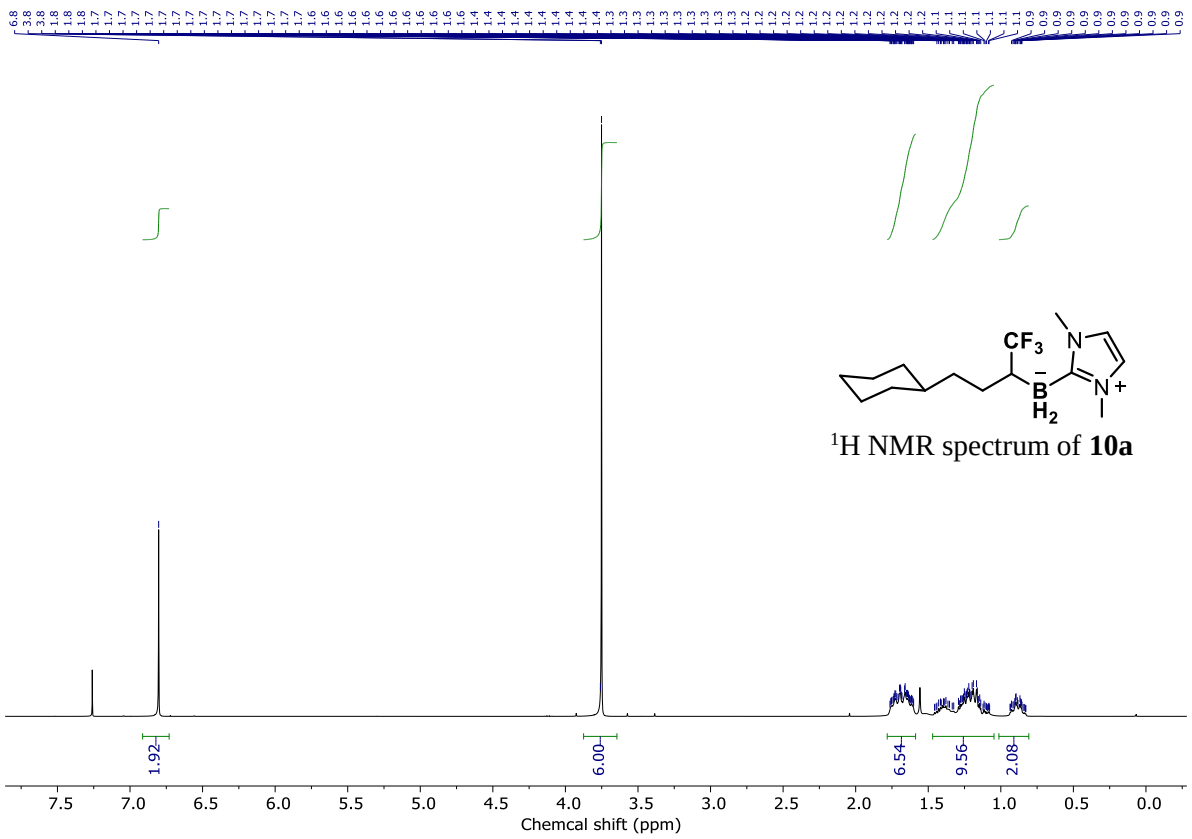

^{1}H NMR spectrum of **10a**

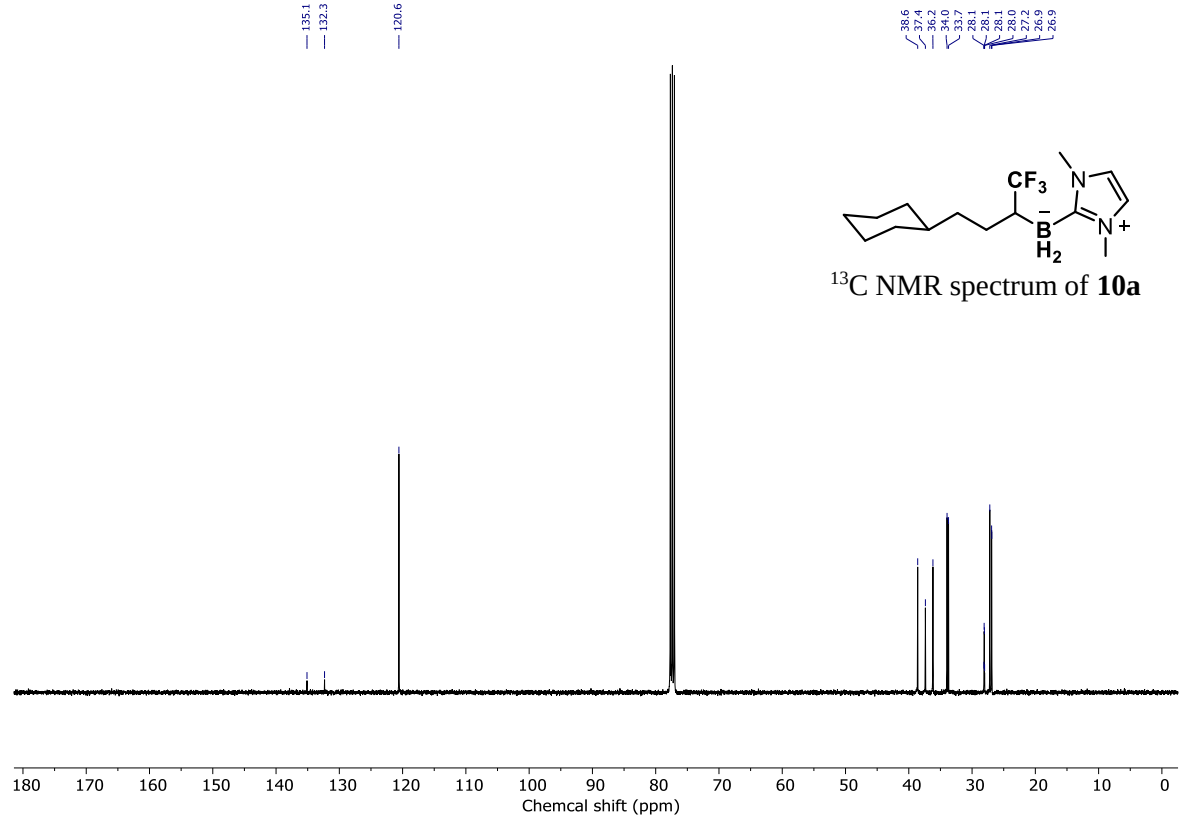

^{13}C NMR spectrum of **10a**

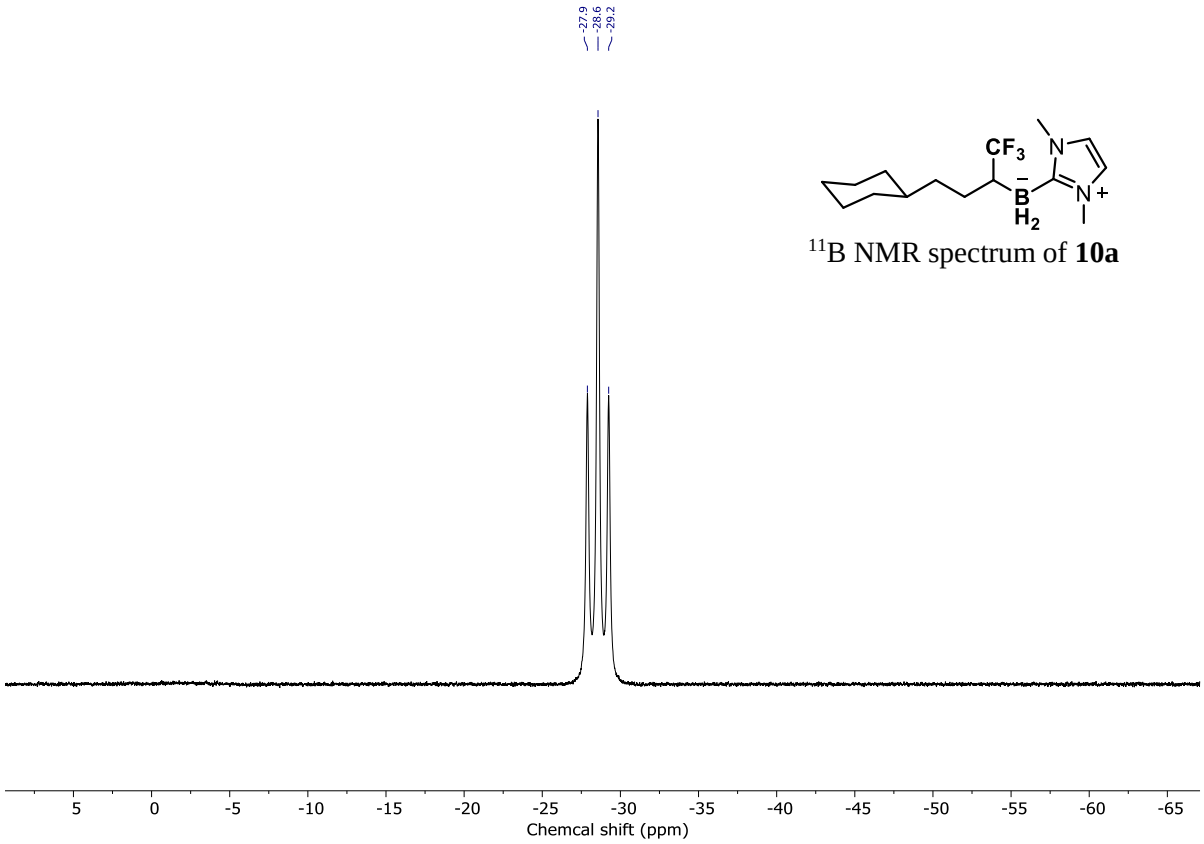

^{11}B NMR spectrum of **10a**

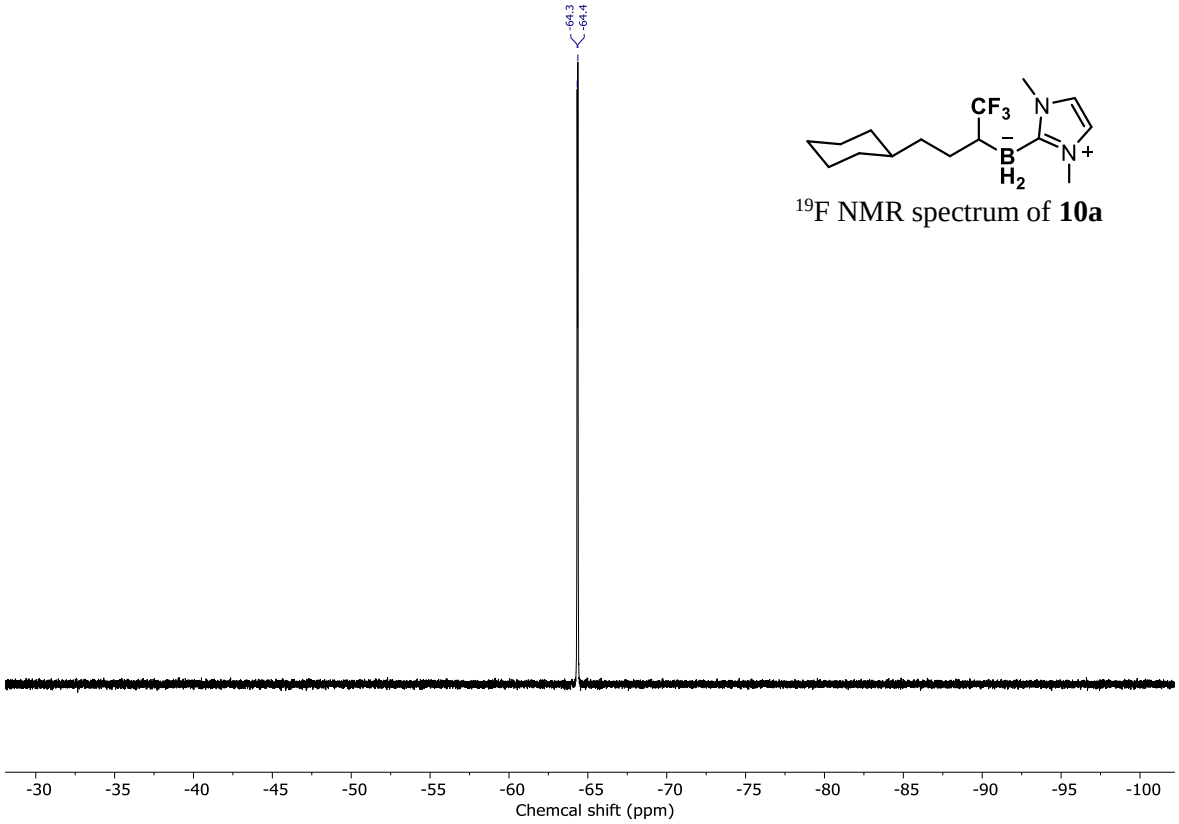

^{19}F NMR spectrum of **10a**

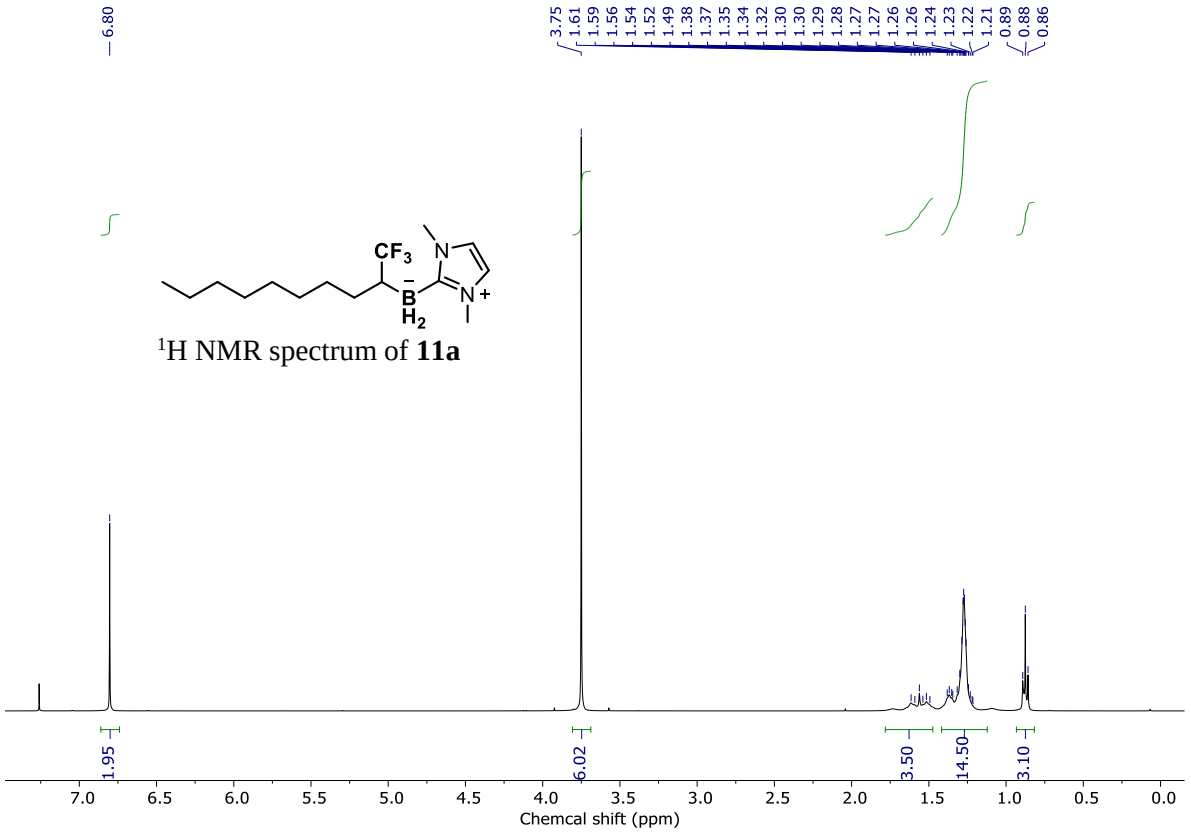

^{1}H NMR spectrum of **11a**

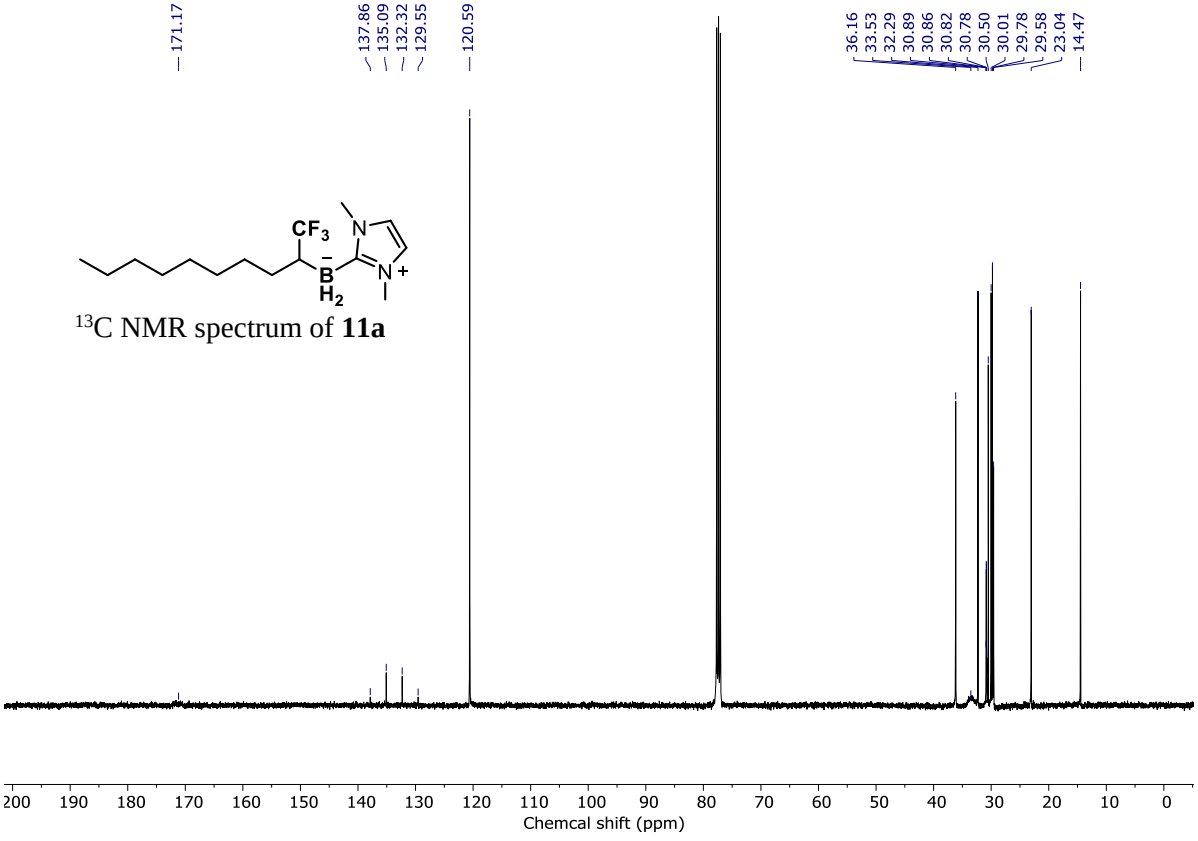

^{13}C NMR spectrum of **11a**

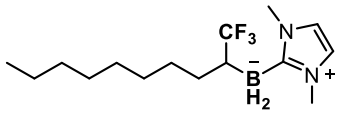

^{11}B NMR spectrum of **11a**

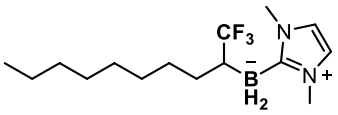

^{19}F NMR spectrum of **11a**

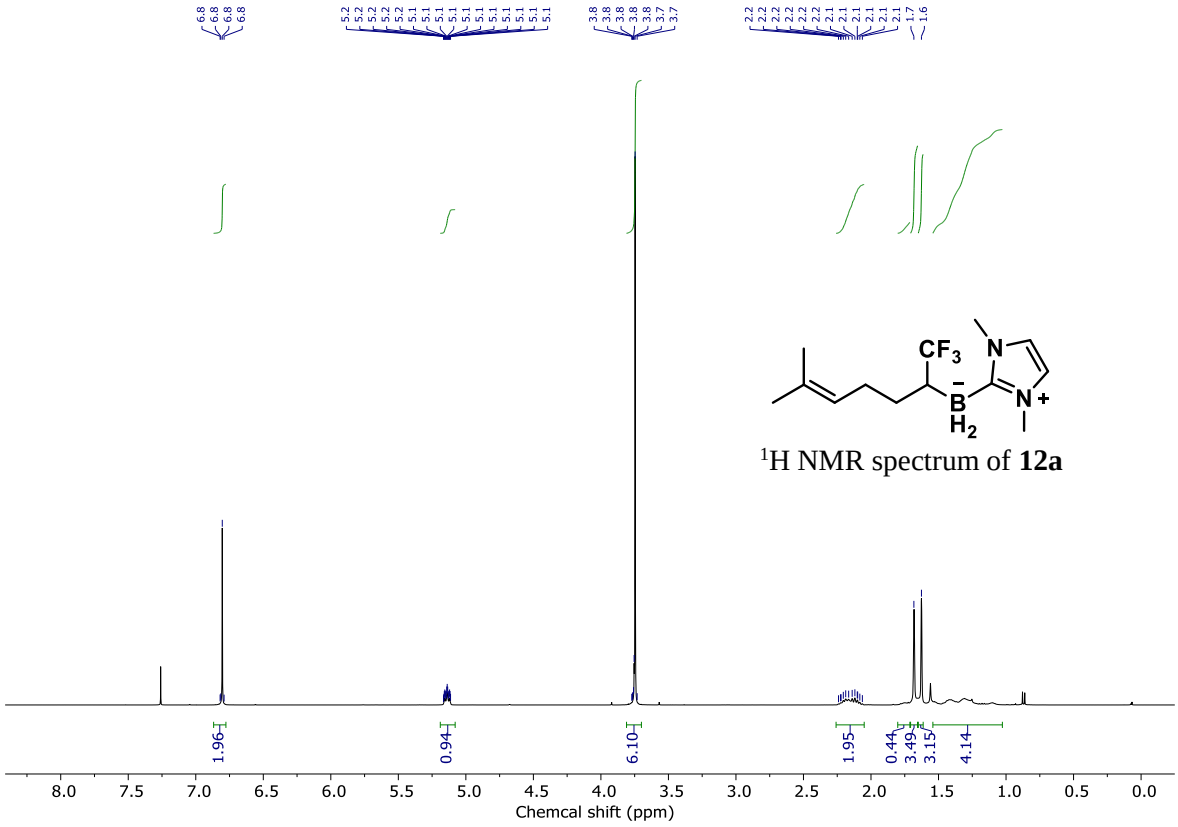

^{1}H NMR spectrum of **12a**

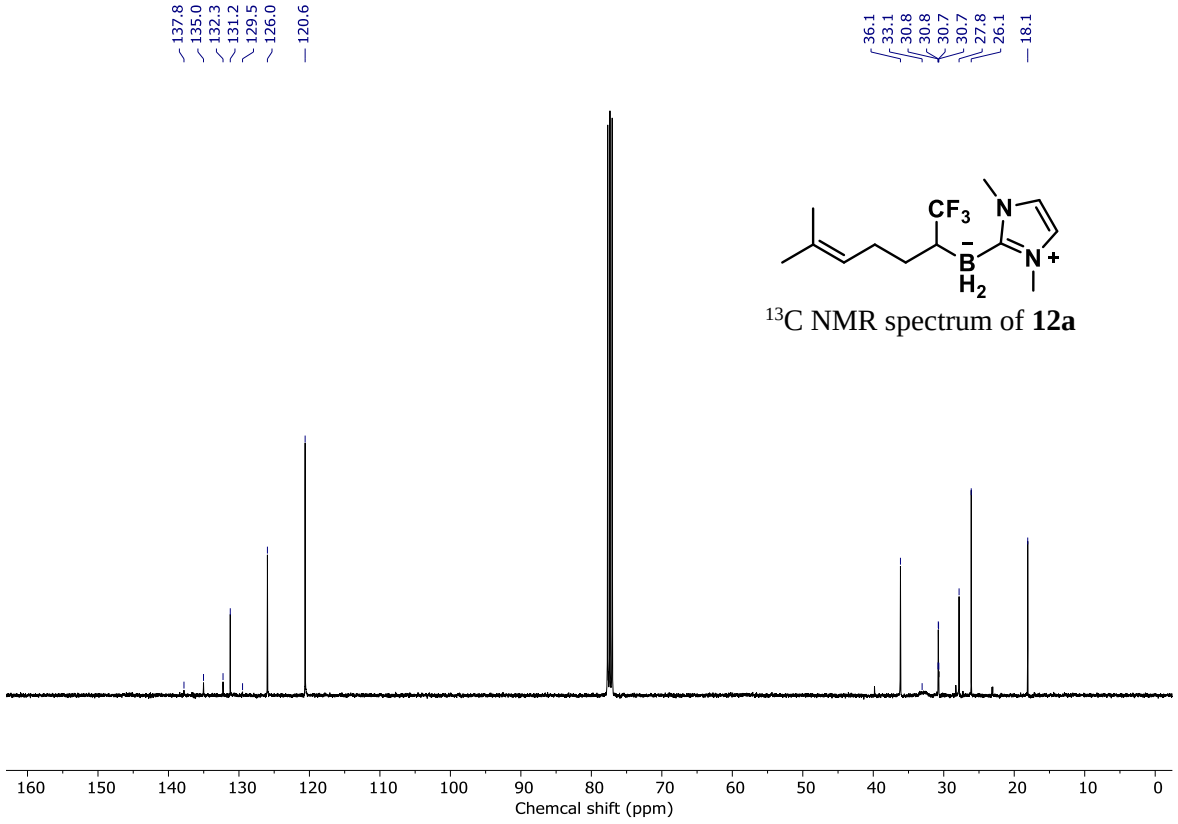

^{13}C NMR spectrum of **12a**

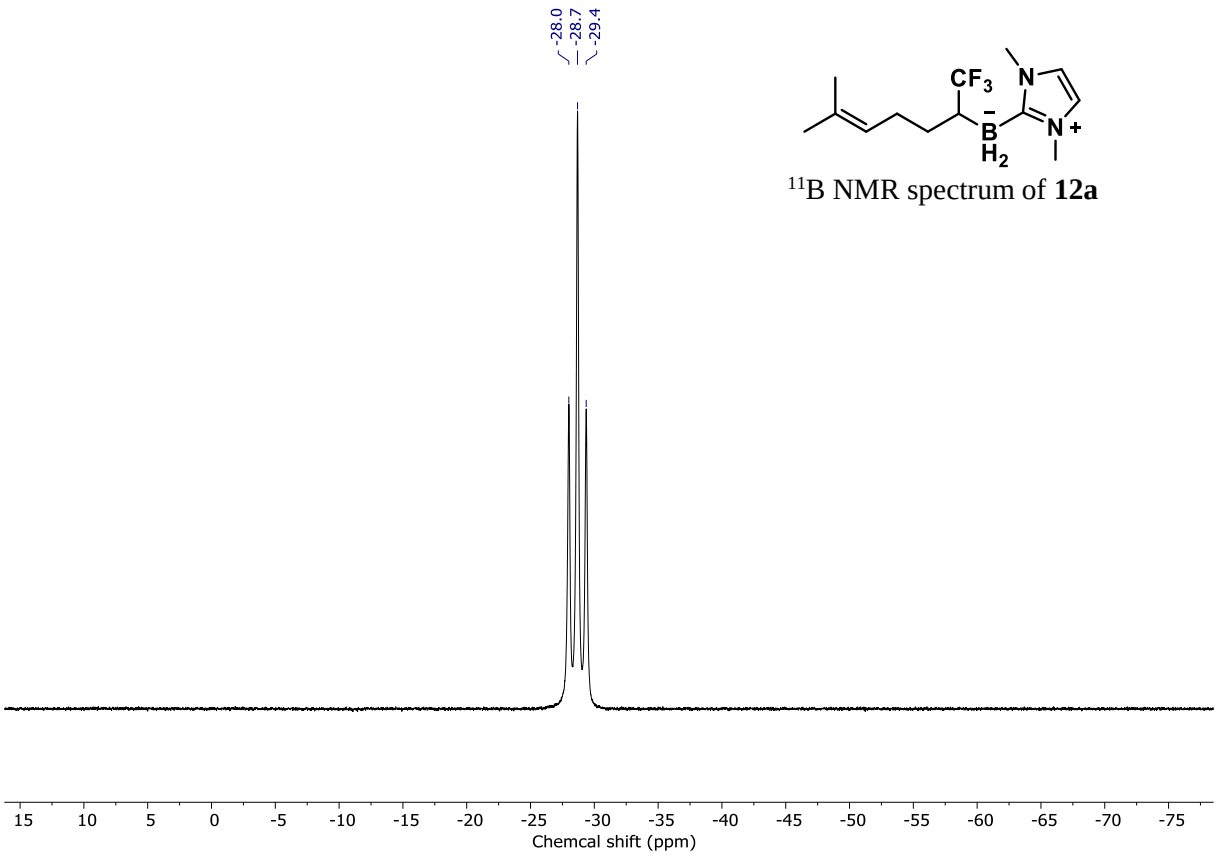

^{11}B NMR spectrum of **12a**

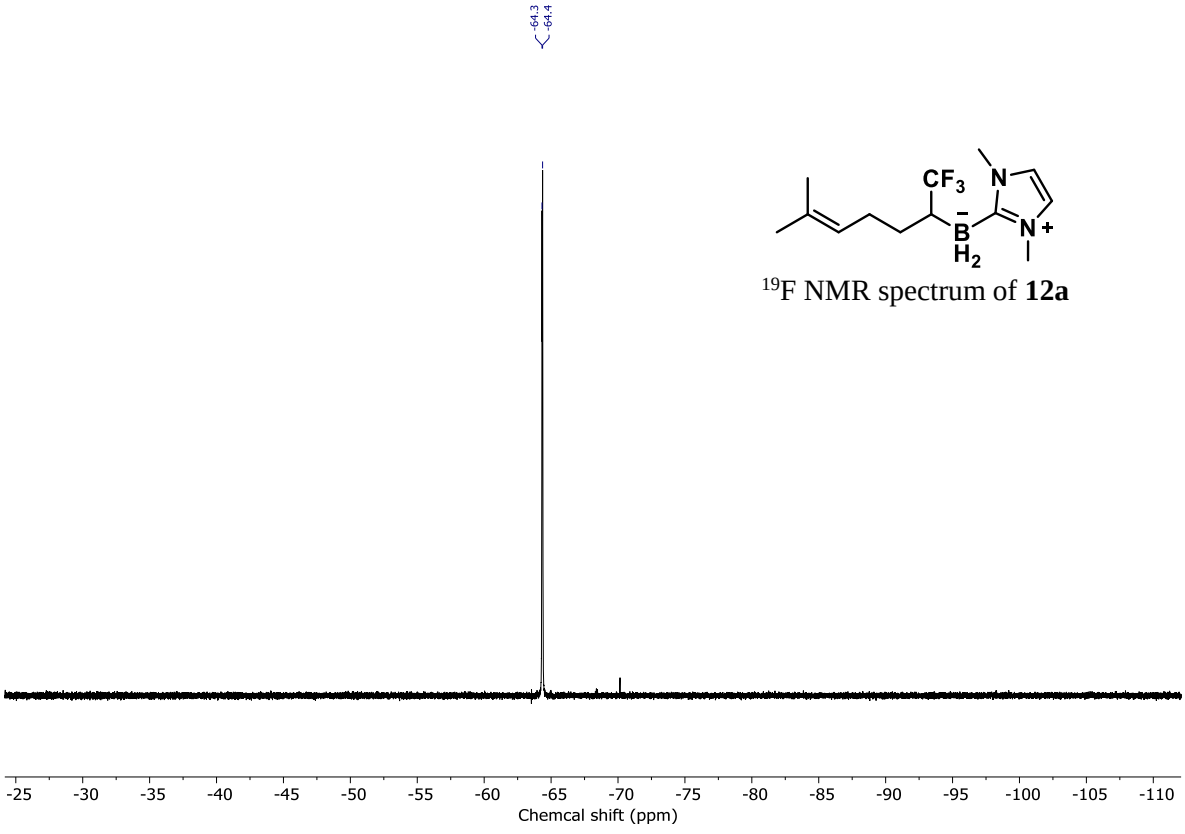

^{19}F NMR spectrum of **12a**

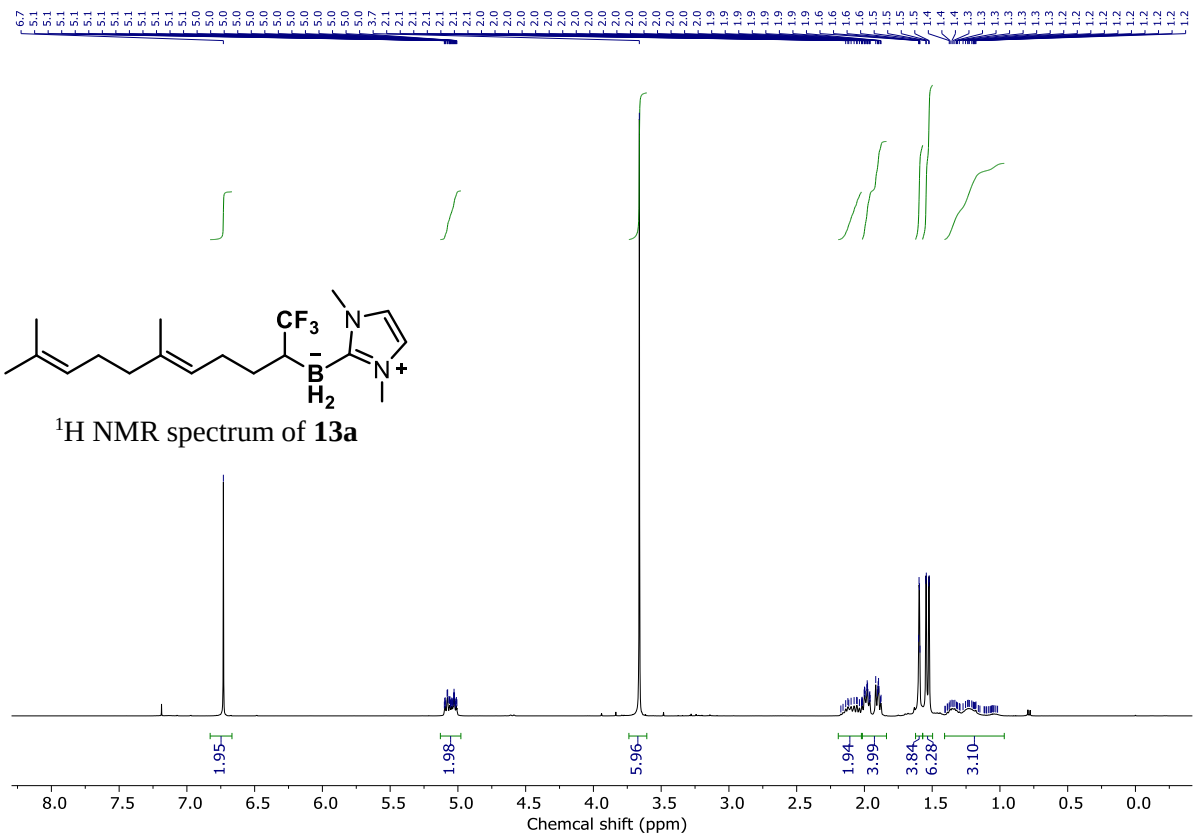

^{1}H NMR spectrum of **13a**

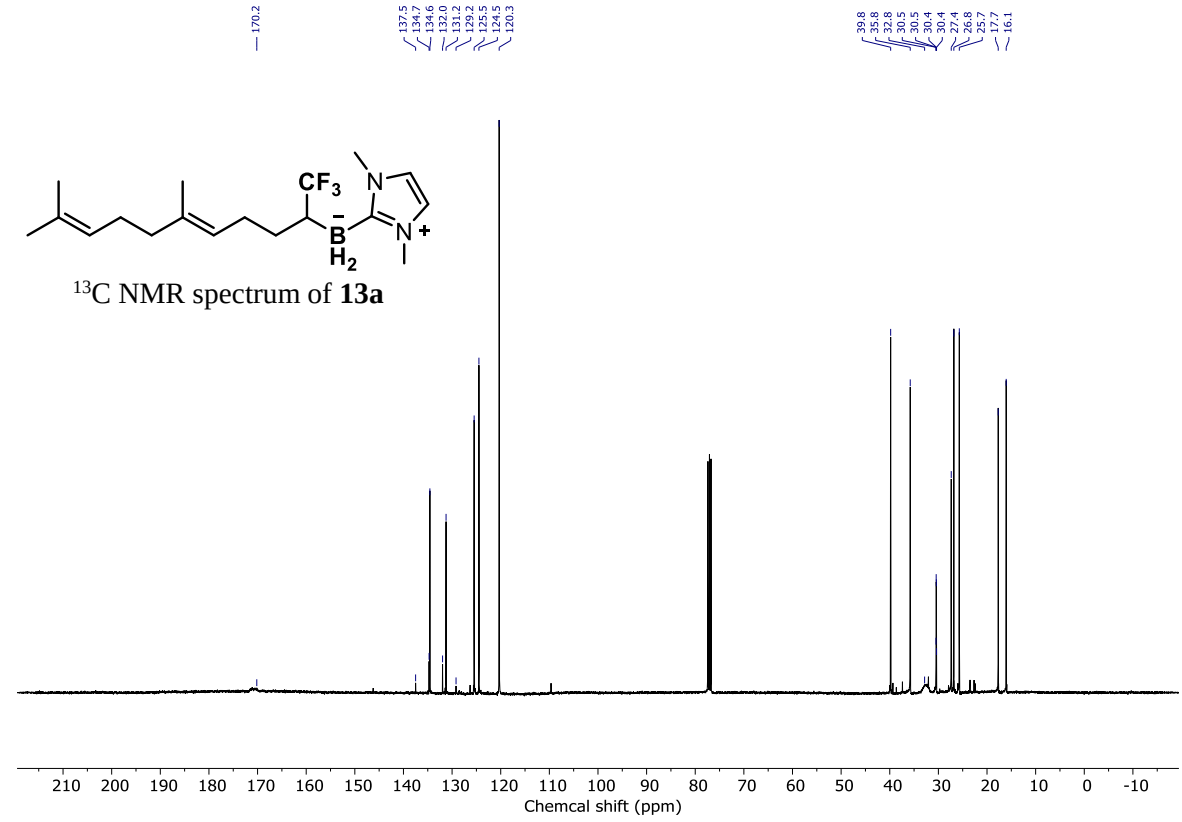

^{13}C NMR spectrum of **13a**

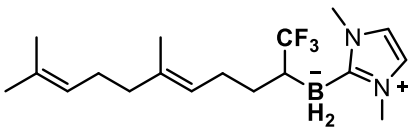

^{11}B NMR spectrum of **13a**

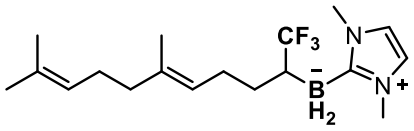

^{19}F NMR spectrum of **13a**